2

X-646-72-384

PREPRINT

NASA TM X- 66065

A SYNOPTIC STUDY OF THE NATURE AND EFFECTS OF FIELD ALIGNED LOW ENERGY ELECTRON PRECIPITATION IN THE AURORAL REGIONS

FREDERICK W. BERKO

OCTOBER 1972

GSFC — GODDARD SPACE FLIGHT CENTER
GREENBELT, MARYLAND

A SYNOPTIC STUDY OF THE NATURE AND EFFECTS OF FIELD ALIGNED LOW ENERGY ELECTRON PRECIPITATION IN THE AURORAL REGIONS

Frederick W. Berko

NASA-Goddard Space Flight Center
Greenbelt, Maryland 20771

October 1972

A dissertation submitted to the Faculty of the Graduate School of Arts and Sciences of the Catholic University of America in partial fulfillment of the requirements for the Degree Doctor of Philosophy

ACKNOWLEDGMENTS

It is with great pleasure that I acknowledge the advice and encouragement given me by Dr. Robert A. Hoffman, who suggested the topic of this thesis and gave me free access to the OGO-4 data. His assistance and guidance throughout my period of graduate study were a great source of encouragement to me; his personal interest and professional guidance were exceeded in value only by his friendship. I would also like to thank Drs. J. L. Burch, Y. C. Whang, H. L. Crannell, and A. D. Johnstone for many beneficial discussions and helpful criticisms. Most important, I wish to thank my wife Rayzella, who has persevered with me throughout my years of graduate study, and without whose encouragement and unswerving moral support I would never have been able to complete this dissertation.

PREFACE

This dissertation will present new information on the nature of field-aligned low energy electron precipitation in the auroral regions and the relationships between this phenomenon and other geophysical phenomena. The data presented herein were obtained by the Auroral Particles Experiment on the fourth Orbiting Geophysical Observatory satellite (OGO-4), a highly successful experiment which obtained auroral zone measurements from July 1967, through January 1969.

The citations in this dissertation follow the style of the Journal of Geophysical Research.

TABLE OF CONTENTS

		Page
	Acknowledgements	iii
	Preface	iv
	Table of Contents	v
	List of Tables	vi
	List of Figures	vii
I.	Introduction	1
II.	Background and Current Status of Field-Aligned Precipitation Measurements	4
III.	Theories Concerning Field-Aligned Currents	8
IV.	Presentation of Data	12
V.	Spatial Distributions	35
VI.	Phenomena Influencing Field-Aligned Precipitation	48
VII.	Comparisons with Observations of Other Phenomena	72
VIII.	Field-Aligned Particles and Field-Aligned Currents	80
IX.	Summary and Conclusions	90
	Appendix A	92
	References	93

TABLES

Page

1. Counts per readout to differential flux conversion factors 36
2. Distribution of all 2.3keV precipitation events considered for this study 37
3. Number of times each element was sampled during the time period covered in this study 39
4. Normalized distribution of all 2.3keV precipitation events 40
5. Normalized distribution of all field-aligned events 42
6. Seasonal effects on field-aligned precipitation occurrence 62
7. Variations in field-aligned precipitation event occurrence with altitude, by season 64
8. Published values of field-aligned currents 84

FIGURES

Page

1. A portion of Pass 3393, showing differential fluxes of 0.7 and 2.3 keV electrons, plus the ratio of 0° pitch angle 2.3keV electron flux to 60° pitch angle 2.3keV electron flux. One-second averages are displayed 14
2. Same as Figure 1 for Pass 4011 16
3. Same as Figure 1 for Pass 4225 17
4. Same as Figure 1 for Pass 4351 19
5. Same as Figure 1 for Pass 3031 21
6. Same as Figure 1 for Pass 5771 22
7. Same as Figure 1 for Pass 5829 23
8. Same as Figure 1 for Pass 6617 25
9. Same as Figure 1 for Pass 6677 27
10. Same as Figure 1 for Pass 6419 28
11. Same as Figure 1 for Pass 2710 30
12. Same as Figure 1 for Pass 6558 31
13. Same as Figure 1 for Pass 5696, except 1/4-second averages are displayed 33

Page

14. Normalized distribution of field-aligned 2.3keV electron precipitation events in a magnetic local time-invariant latitude polar projection . . . 43

15. Distribution of field-aligned events as a function of magnetic local time 45

16. Percent of field-aligned events as a function of invariant latitude: a. for 2-1/2° wide intervals; b. for 5° wide intervals 46

17. Energy spectrums for four periods during Pass 4351 (Figure 4). Spectrums 1 and 2 were obtained during field-aligned precipitation events. Spectrums 3 and 4 were obtained during times of isotropic fluxes 49

18. Average three point energy spectrums for all field-aligned and non-field-aligned precipitation events used in this study 50

19. Probability of 2.3keV precipitation being field-aligned as a function of 0° particle flux at 0.7 and 2.3keV 52

20. Percent of precipitation which was field-aligned above given 2.3 keV fluxes, as a function of the 0° pitch angle 2.3keV flux 53

21. Probability of precipitation being field-aligned as a function of the one-hour average AE value 56

22. One-second average fluxes of 0.7, 2.3, and 7.3keV near 0° pitch angle electrons, and the ratio of 0° - 2.3keV to 60° - 2.3keV electron fluxes, for a midnight pass during substorm expansion. Periods of field-aligned precipitation are indicated by cross hatching. Three magnetograms for the time period are shown with a heavy vertical line indicating the time when Pass 2590 occurred 58

Page

23. Latitudinal distribution of auroral electron precipitation at three energies for 38 passes in the dusk-to-midnight sector. The orbit number is given for each pass 60

24. Winter and summer universal time modulation of field-aligned precipitation 63

25. Schematic representation of two possible parallel electric field configurations: top - probable summer, fully sunlit situation; bottom - possible winter, nighttime situation 70

26. Polar projection of the regions of high numbers of field-aligned events in the nighttime hours in comparison with the region of high probability of all auroral forms (Stringer and Belon, 1967) during the same hours 74

27. Comparison of the regions of observing field-aligned precipitation events with the location of 200kHz centers (Laaspere et al., 1971) . . . 76

28. Comparison of the regions of observing field-aligned precipitation events with the "maximum" region of transverse magnetic disturbances (Zmuda et al., 1970) 78

29. Representation of two models of magnetospheric field-aligned current systems: top - line current model; bottom - double sheet current system 82

30. Average field-aligned pitch angle distribution 86

I. INTRODUCTION

Dissertation Objectives

Much attention has been given recently to the electric fields and currents from charged particles flowing within the magnetosphere. Special concern has been given to the study of how such magnetospheric currents might be related to magnetic field-aligned Birkeland currents in the ionosphere. A large number of individual observations of precipitating low energy electrons and protons with near 0° pitch angles (i.e. moving essentially parallel to the direction of the local magnetic field) have been reported in the literature, as well as reports of observed magnetic fluctuations indicative of the presence of currents aligned in the direction of the local magnetic field. Several models of field-aligned current flow have been proposed to explain the varying observations, but no unified theory has emerged which is able to satisfactorily explain all of the measurements. Equally important is the fact that there has never been any long term, systematic study of field-aligned particle precipitation and of the geophysical phenomena which may influence the occurrence or properties of field-aligned precipitation.

Early results from the OGO-4 Auroral Particles Experiment indicated the first direct satellite measurements of field-aligned precipitation in the auroral zone (Hoffman and Evans, 1968). In that paper, Hoffman and Evans presented observations

of field-aligned particles made during the first several days of satellite operation. This dissertation presents a synoptic study of field-aligned precipitation events observed during a 16-month period by this experiment, representing a full 4π precession of the satellite orbital plane in magnetic local time (MLT). The morphology of this type of precipitation, its nature, and relationships between this phenomenon and other geophysical events will be discussed in the context of this 16 month data base.

Experiment Description

The OGO-4 Auroral Particles Experiment (Hoffman and Evans, 1967) consisted of an array of 8 detectors, each comprised of an electrostatic analyzer for species and energy selection and a Bendix channel electron multiplier as the particle detector (Evans, 1965). Four of the detectors, (the "energy detectors"), were positioned to point radially away from the earth and measured either electrons or protons in narrow energy bands centered at 0.7, 2.3, 7.3, and 23.8 keV. Three other detectors (the "angle detectors"), which measured charged particles at 2.3 keV were positioned 30°, 60°, and 90° from the earth-spacecraft vector; the eighth detector served as a background detector.

Each of the "energy" and "angle" detectors had bandpasses of -13% and +19% about their center energy. At the high latitudes where almost all of the data used for this study were taken, the energy detectors were oriented approximately parallel to the local magnetic field, and thus primarily measured particles with pitch angles near 0°. Henceforth, these four detectors will also be referred to as the "0°" detectors. The background count rates and geometric factors for the 0° and 60° 2.3 keV detectors were almost identical, allowing a direct comparison of outputs from these two detectors.

Launch of the OGO-4 satellite occurred on 28 July 1967. The satellite achieved a nearly circular low-altitude polar orbit with an apogee of 908 km and a perigee of 412 km. This orbit had an initial inclination of 86°, which, combined with the motion of the earth around the sun, caused a precession of the orbital plane from its initial dusk-dawn orientation through all local times at the rate of about 1-1/2° per day. Thus the satellite passed through all local times every 120 days, so that by 20 November 1968 two complete 360° precessions (i.e. a 4π precession) in local time had been achieved.

II. BACKGROUND AND CURRENT STATUS OF FIELD-ALIGNED PRECIPITATION MEASUREMENTS

Measurements of field-aligned fluxes of electrons at high latitudes have been made by both satellite and rocket-borne experiments. In addition to the direct particle measurements, such as those reported by Hoffman and Evans (1968), indirect evidence of field-aligned particles has been obtained from magnetometer measurements. Transverse magnetic disturbances observed at 1100km altitude in the auroral region by a satellite-borne magnetometer were reported by Zmuda et al. (1966). In later work (Zmuda et al., 1967; Armstrong and Zmuda, 1970), these high latitude disturbances were shown to be likely manifestations of the effects of field-aligned sheet currents. Armstrong and Zmuda reported transverse magnetic disturbances of as much as 800γ, from which they computed field-aligned current intensities of 0.64 A/m, and postulated that particle fluxes greater than 5×10^{10} electrons/cm^2-sec at energies greater than $\sim$1keV were the electric current carriers.

Measurements of 1keV electron precipitation obtained during rocket flights by Chase (1970) revealed ratios of fluxes at 0° pitch angle to 90° pitch angle ranging from 2.77 at 250km altitude to 4.34 at 180km. Chase proposed that he had observed what was an initially isotropic electron flux (at greater than 1500km altitude), which

by rocket altitudes of less than 300km, had become peaked in the direction of the local magnetic field primarily by interactions with the upper atmosphere.

Using a rocket equipped with both particle detectors and a vector magnetometer, Cloutier et al. (1970) detected field-aligned sheet currents associated with a visible auroral arc. Precipitated electrons in the energy range from 2 to 18keV were observed with 0° to 90° flux ratios of about 3 (Vondrak et al., 1971). These electrons are credited with carrying a significant fraction of the total upward field-aligned sheet current, postulated to be about 0.26 A/m. Existence of such geomagnetically aligned current sheets is also necessary to explain the magnetometer fluctuations which they observed (Park and Cloutier, 1971).

Field-aligned currents with an average strength of 5×10^{-7} A/m^2 were observed by a rocket flown into an auroral band by Choy et al. (1971). One maximum in their observed field-aligned current coincided with the rocket moving through a bright auroral fold coincident with a peak in the electron spectrum from 3 to 7keV, but the maximum current was observed when the spectrum was much softer, and was due mostly to 500 eV to 1keV electrons. This latter, intense current, which occurred just as the rocket crossed the northern edge of an auroral form, Choy et al. called a sheet current. They postulate that the particles constituting the current sheet originate in the center of a compressed plasma sheet in the magnetotail. Although their magnetometer was aligned properly to measure any transverse magnetic disturbances which are associated with field-aligned currents, Choy et al. found no evidence for the existence of any such disturbances during this flight.

Using two separate payloads launched by a single rocket, O'Brien and Reasoner (1971) measured enhanced fluxes of precipitated electrons at altitudes up to 800km.

They observed the flux of 5keV electrons at 750km to be enhanced by a factor of ~10 at pitch angles less than about 10°, with no enhancement in 4 - 7keV electrons in the 30° - 60° pitch angle range. These enhancements were short-lived or burst-like, lasting from < 0.1sec to several seconds. Although they found no consistent pattern of burst growth, duration and decay, they were able to deduce that the source of these field-aligned bursts was at an altitude $\lesssim 1\ R_E$. Since they could not pose a meaningful, coherent explanation for their observations, especially when considered in relation to the other work cited above, they concluded there are at least two or more mechanisms involved. The separation between their two payloads enabled them to perform simultaneous, spatially separate measurements which supported the hypothesis of Hoffman and Evans (1968) that the observed bursts of electrons are temporal in nature.

Electrons with 0.55keV energy were observed to be peaked at near 0° pitch angles by Whalen and McDiarmid (1972) in an experiment flown aboard a sounding rocket. The rocket was launched into an aurora during a moderate substorm in the early morning hours, and enhancements of near 0° pitch angle electrons were observed at energies from 0.55keV to 9keV. At the time of maximum observed 0.55 keV field-aligned flux, they estimate the field-aligned current from electrons with energies less than 1keV to be about 2×10^{-4} A/m^2. Whalen and McDiarmid attribute the 0° peak in the electron pitch angle distribution to a local acceleration mechanism that increases the particle energy parallel to the magnetic field. Such a mechanism, they hypothesize, could consist of a parallel electric field confined to altitudes less than about 1 R_E.

Measurements by Haerendel et al. (1971) on the HEOS I satellite at 12.4 R_E during a substorm revealed changes in the declination of the near tail magnetic field in phase with auroral zone magnetic perturbations. These observations, at 0400 local time on field lines which map to latitudes above the auroral oval, were interpreted as field-aligned currents flowing from the plasma sheet to the morning hour auroral oval, and tend to support the current system model of Akasofu and Meng (1969). From the data collected, they estimated a total field-aligned current of $\sim 5 \times 10^5$ A, of the same magnitude as the auroral electrojet.

III. THEORIES CONCERNING FIELD-ALIGNED CURRENTS

Perhaps the earliest reference to field-aligned currents at high latitudes was the proposal by Birkeland (1908) that some of the magnetic fluctuations observed in the polar regions by ground-based magnetometers could be caused by closely spaced field-aligned currents. A direct connection between auroral phenomena and particle precipitation into the high latitude upper atmosphere was proposed at least as early as 1940 by Alfvén. Alfvén (1940) theorized that auroral arcs were caused by charged particles which travelled along the earth's geomagnetic field lines.

The classic model of magnetospheric convection put forth by Axford and Hines (1961) provided a coherent mechanism for the connection of magnetospheric plasma flow and high latitude auroral phenomena. Chamberlain (1961) presented a model in which the acceleration of particles parallel to geomagnetic field lines was associated with the recovery of the particle's original kinetic energy in motion along the direction of $\vec{B}$, and applied the model to the production of rayed auroral forms. Elaborating on these two models, Kern (1962) proposed a model in which charge separation of trapped radiation leads to polar electrojet current systems. The charge separation created regions of excess charge in Kern's model, and particles with small magnetic moments were accelerated from these regions along magnetic

field lines in two current sheets which connected with the westward auroral electrojet in the near midnight hours.

Taking into account the height variation of auroral ionization and conductivity, Boström (1964) presented a model to account for auroral electrojet flow. This model consisted of two cases: one which assumed current flow between the auroral ionosphere and the outer magnetosphere is limited; and a second which assumed perfect conductivity along magnetospheric field lines. The first case consisted of a line current, closing in the ionosphere via the electrojet and driven by an electric field of $\sim 1.5 \times 10^{-3}$ V/m. The second case consisted of two current sheets driven by an electric field of $\sim 1.8 \times 10^{-3}$ V/m produced by a longitudinal plasma motion in the magnetosphere. This latter sheet current model required the field-aligned sheet currents to consist mainly of electrons, and a primarily ion carried Pedersen current in the ionosphere flowing from the northern to southern edges of the (Hall current) electrojet (Boström, 1968). Bonnevier et al. (1970) found fairly good agreement between Scandinavian and Soviet ground station magnetic perturbations and the perturbations predicted by a line current system similar to Boström's first case.

Field-aligned currents (also known as Birkeland currents - see e.g. Schield et al., 1969) flowing during substorms may be so intense as to form space-charge regions in the ionosphere, which Carlqvist and Boström (1970) have likened to a vacuum diode. High potential drops along field lines can arise in space charge regions, and account for considerable auroral particle acceleration. Electrostatic double layers in the ionosphere, which give rise to parallel electric fields like a capacitor, have been proposed by Albert and Lindstrom (1970) as a mechanism to explain auroral particle precipitation. Such electrostatic double layers, they

proposed, could account for a shifting of particle pitch angles to lower values by increasing the parallel (to the local geomagnetic field) energy of precipitating particles. This mechanism was used to explain enhanced particle precipitation at pitch angles lower than 90°, which they observed in a 1966 rocket flight.

Vasyliunas (1968) found that during magnetic bays (depressions in the horizontal component of the earth's magnetic field measured at high latitude ground stations in the midnight sector), the plasma sheet moves inward to $6 R_E$ at the equator, and suggested that particles from this region could then be guided along field lines into auroral latitudes. Commenting on the findings of Vasyliunas and noting the similarity in magnitude and spectrums of plasma sheet and auroral zone electron fluxes, Chase (1969) suggested that the plasma sheet is the source of auroral electrons.

Plasma waves are amplified under certain conditions and move along magnetic field lines. Perkins (1968) has proposed that energy can be transferred, through wave-particle interactions, to electrons of energy greater than 1 keV, in such a fashion as to impart particle velocities parallel to the direction of the earth's magnetic field. These particles would then travel along field lines and precipitate in the auroral regions.

Under the assumption of weak electric field acceleration, Chamberlain (1969) noted that such an electric field would not precipitate particles without accelerating them. But for relatively large potential differences, he notes that particles would preferentially emerge with small pitch angles. O'Brien (1970) argues that electric fields parallel to the geomagnetic field cannot be the dominant acceleration mechanism for 1-10 keV particles, since electrons and protons with comparable energies are precipitated simultaneously at the same locations in many auroras. He cites

the results of Reasoner et al. (1968), who measured alpha particles in the auroral zone, to assert that the solar wind is the ultimate source of auroral particles. However, both Chamberlain and O'Brien concede that parallel electric fields could be responsible for the field-aligned electrons observed by Hoffman and Evans, (1968).

Localized low-frequency transverse magnetic disturbances observed by Zmuda et al. (1966) from the low altitude polar orbiting satellite 1963-38C, and some of the localized magnetic fluctuations observed on the earth's surface were explained by Cummings and Dessler (1967) to be the result of currents flowing along magnetic field lines. They proposed a field-aligned double sheet current system flowing through magnetic tubes of flux and driven by a charge separation mechanism in the magnetosphere. This model called for current to flow down one set of field lines, across the ionosphere, and back up another set of field lines, achieving intensities of the order of 10^5 A. Conductivity of the lower ionosphere is sufficiently high to allow the required transverse currents, and their field-aligned currents were confined to flow within a tube of flux to account for the localized nature of the observed magnetic fluctuations. Schield et al. (1969) have suggested that there should be a gap in the field-aligned currents on the dayside, displaced from noon slightly towards earlier hours due to asymmetries introduced by the DS current system, but Zmuda et al. (1970) performed a survey in which no such gap or displacement was observed in the locations of the transverse magnetic distrubances.

IV. PRESENTATION OF DATA

All of the data to be presented in this dissertation were acquired by the OGO-4 spacecraft at invariant latitudes (Λ) greater than 60°. In all cases any background present has been subtracted from the raw count rates, which have, in turn, been converted into differential number fluxes. Although the fluxes are plotted as time-continuous histograms, data were collected (i.e. counts accumulated) over only one-half a main telemetry frame, so that to be precise, each vertical bar in a histogram should be separated from the next by a blank space equal (in time) to one-half a telemetry frame. Along the bottom of each histogram is shown the universal time (UT) at which the measurements were made, as well as the satellite position in both Λ (in degrees) and magnetic local time (MLT), in hours and minutes.

Generally, when the geomagnetic field is disturbed, more intense fluxes of precipitated particles are observed. As an indication of the degree to which the geomagnetic field was disturbed during the time of each data example, the value of the one-hour average AE index at the time of each data acquisition will be shown on each data example. The AE index will be more completely defined in Section VI, but in general, higher values of AE indicate more unsettled, or magnetically disturbed, conditions in the high latitude regions of interest in this dissertation. AE is expressed in units of gammas (γ), where $1\gamma = 10^{-5}$ gauss.

As a first example, we consider a portion of Pass 3393 presented in Figure 1. Fluxes of 0° 2.3keV and 0.7keV electrons are plotted here as functions of time, along with the ratio of 2.3keV flux at 0° to that at 60° (the bottom curve), using averages of the counts accumulated during 1-second intervals. Let us first consider the correlations (or non-correlations) between the 0.7keV and 2.3keV fluxes. From about 20:05:28 to 20:06:13, there are appreciable fluctuations observed in the 0.7keV flux, while the 2.3keV flux remains fairly constant. A simultaneous short duration burst occurs at both energies (and also at 7.3keV and 23.8keV) at 20:06:14. Rapid large fluctuations in 0.7keV flux began at 20:06:25, with somewhat similar fluctuations at 2.3keV appearing about 1 second later. Flux increases at 0.7keV generally are coincident with or precede by about one second those at 2.3keV; the decreases are usually simultaneous. This creates a situation where the 0.7keV flux histogram seems to form an "envelope" about the 2.3keV flux histogram during such periods of large amplitude, rapid fluctuations at fairly high fluxes levels. If we also consider the fluxes measured by the two higher energy 0° detectors, the situation is much like the "inverted V" type of precipitation reported by Frank and Ackerson (1971).

Of greater interest for this dissertation is the degree of isotropy in the observed fluxes of 2.3keV electrons, as evidenced by the bottom curve in Figure 1. We note that during only 21 of the 132 seconds of data shown was the ratio of 0° to 60° flux greater than 2. Thus, the observed flux at 2.3keV was essentially isotropic, or at least non-field-aligned, during 84% of that portion of data shown. In fact, data from this pass continued at low flux levels to higher latitudes for almost 9-1/2 additional minutes, to 20:17:00, and no further anisotropies were observed during that period.

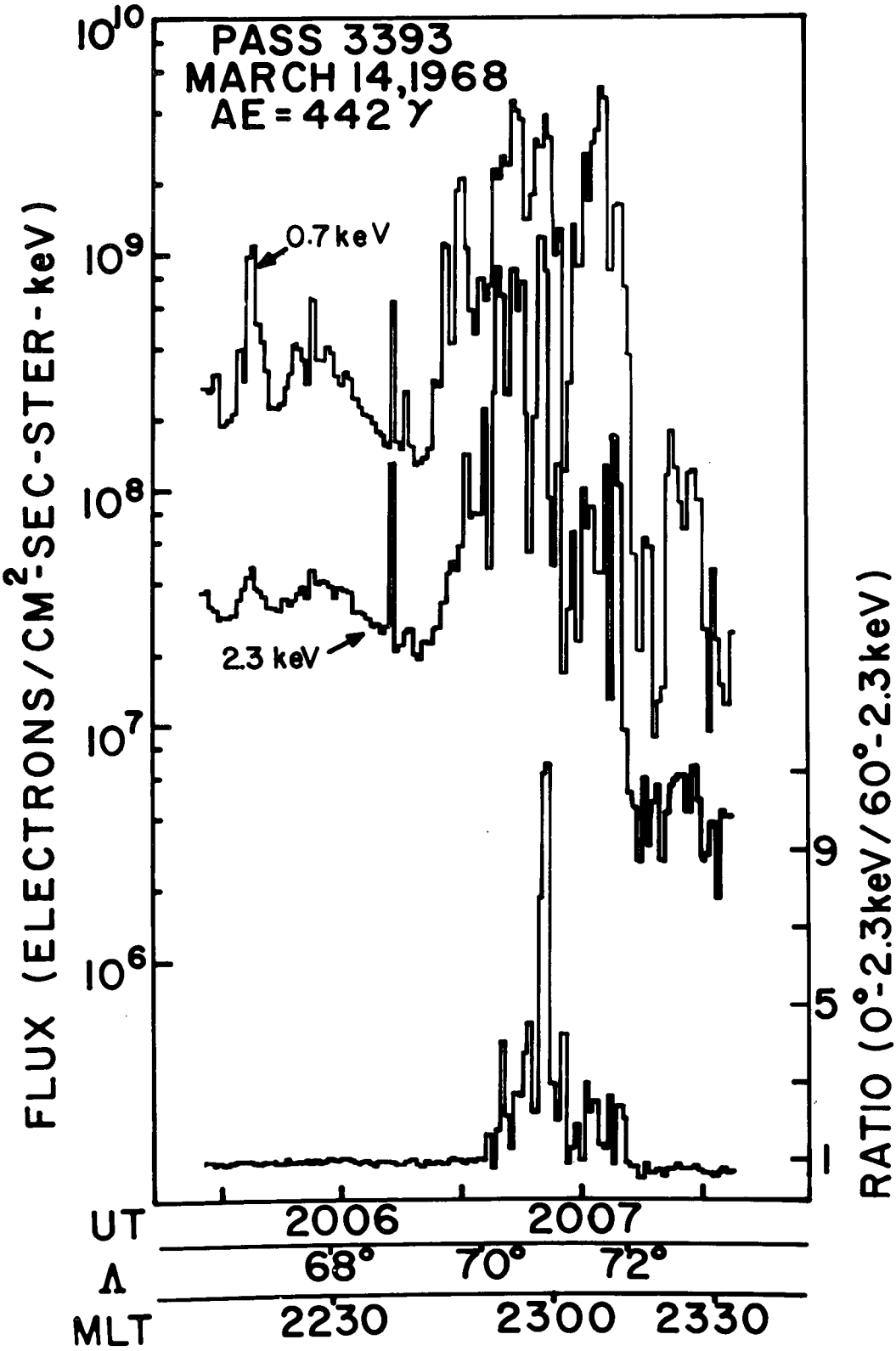

Figure 1. A portion of Pass 3393, showing differential fluxes of 0.7 and 2.3 keV electrons, plus the ratio of 0° pitch angle 2.3 keV electron flux to 60° pitch angle 2.3 keV electron flux. One-second averages are displayed.

Pass 3393 displays several other important features. First, the principal anisotropic period, centered around 20:06:50, coincides with the period of high 2.3keV flux. Secondly, the greatest anisotropy, where the ratio of 0° to 60° flux reaches a value greater than 11, is coincident with the peak in the 2.3keV flux. Finally, although this pass occurred during what was a rather intense geomagnetic substorm (the hourly average value of AE was 365γ during this pass), the precipitation observed at 2.3keV was primarily non-field-aligned, as mentioned earlier. The relationships between substorms and field-aligned precipitation will be discussed further in a later chapter.

Pass 4011 (Figure 2) shows an example of a pass with an appreciable amount of field-aligned precipitation during only a moderately disturbed time. During the higher latitude portion of this pass, i.e., prior to 16:06:00, the 2.3keV flux generally decreased by more than an order of magnitude and some moderate anisotropy was evident. At the time of the first rapid increase of 2.3keV flux (16:06:07), anisotropy again appears, which gradually disappears, except for a brief period at 16:06:41. Then the field-aligned nature of the precipitation during this pass becomes evident again in coincidence with the flux increase at 16:06:58, but more noticeably with the large peak in the flux centered at 16:07:06. The ratio of 0° to 60° 2.3keV flux during this latter peak reached a value of approximately 24. It is unfortunate that data acquisition was lost at 16:07:42, as the observations might have shown additional interesting phenomena as the satellite moved towards lower latitudes during the remainder of this orbit.

In contrast to Pass 4011, the portion of Pass 4225 displayed in Figure 3 shows a much lower degree of anisotropy. The one-second averaged fluxes plotted for

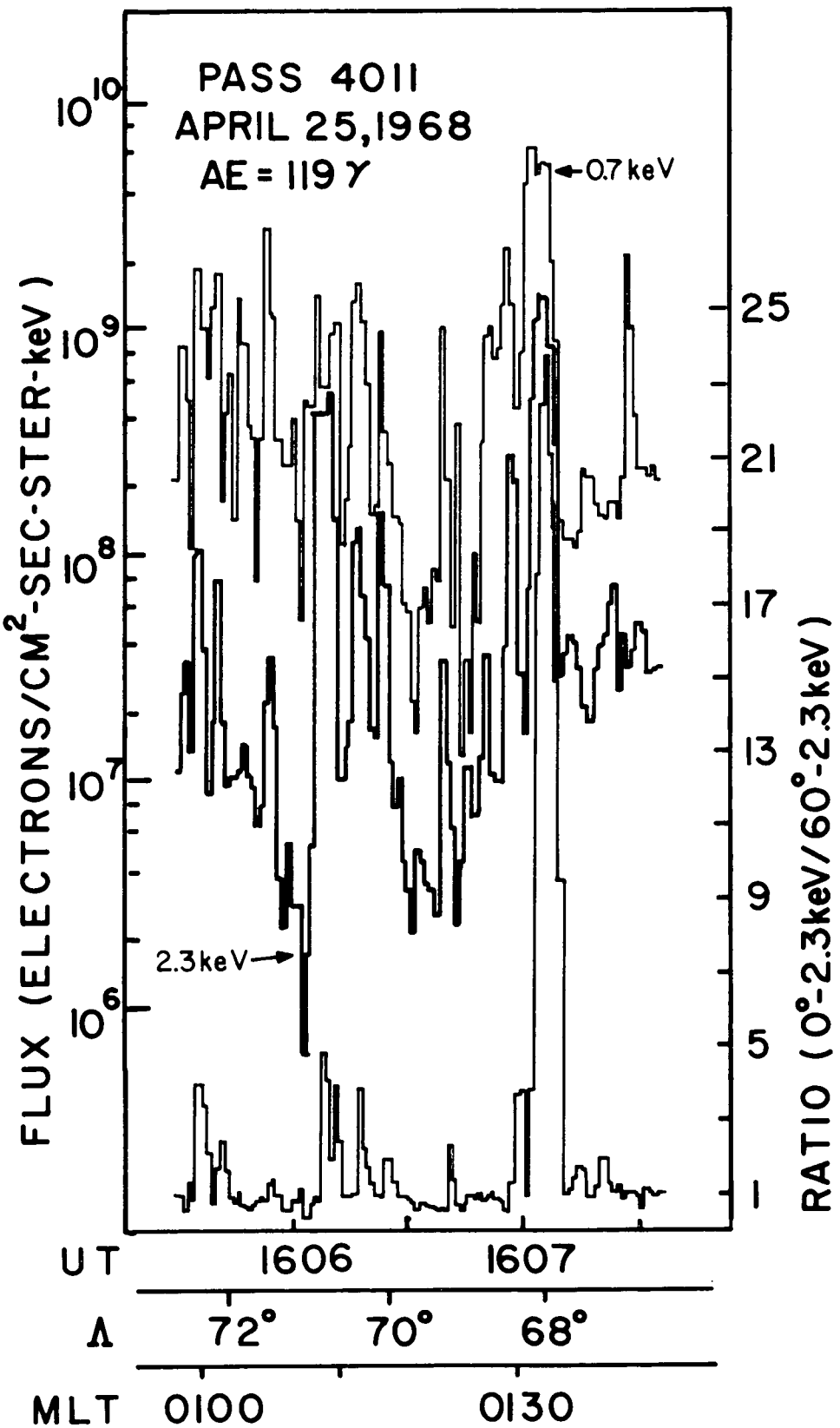
PASS 4011
APRIL 25,1968
AE = 119 γ
0.7 keV
2.3keV
FLUX (ELECTRONS/CM²-SEC-STER-keV)
RATIO (0°-2.3keV/60°-2.3keV)
10¹⁰
10⁹
10⁸
10⁷
10⁶
25
21
17
13
9
5
1
UT
1606
1607
Λ
72°
70°
68°
MLT
0100
0130

Figure 2

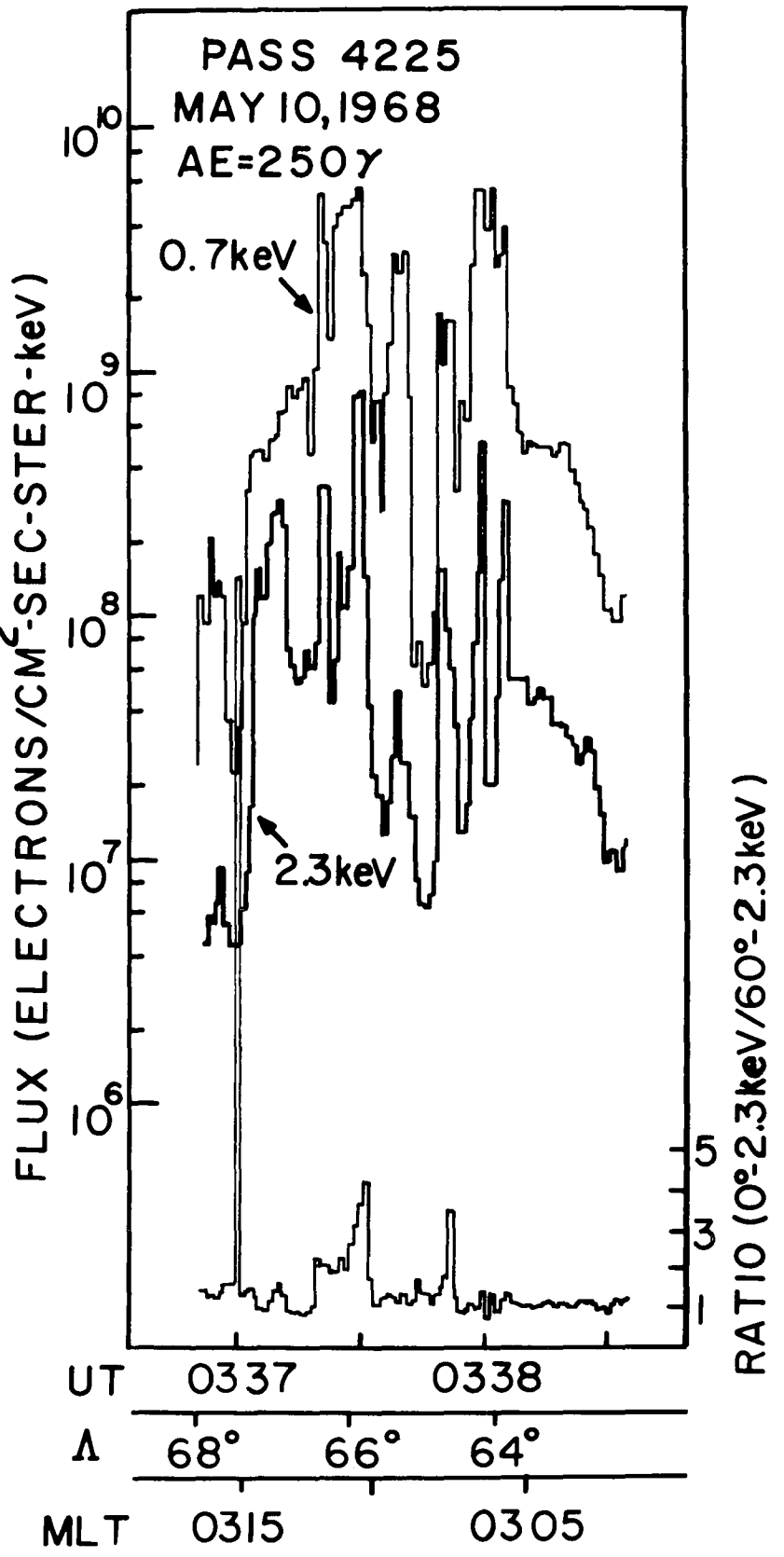
PASS 4225
MAY 10, 1968
AE=250γ
0.7keV
2.3keV
FLUX (ELECTRONS/CM²-SEC-STER-keV)
10¹⁰
10⁹
10⁸
10⁷
10⁶
RATIO (0°-2.3keV/60°-2.3keV)
1
3
5
UT 0337 0338
Λ 68° 66° 64°
MLT 0315 0305

Figure 3

both 2.3keV and 0.7keV do indeed show both rapid fluctuations and high peak values, but except for the high 0° to 60° 2.3keV flux ratio at 03:37:00, which is entirely attributable to the very low ($\sim 4 \times 10^6$) 2.3keV flux at that time, none of the several other anisotropies present are even as great as 5. One would usually expect relatively high fluxes at these latitudes ($63° < \Lambda < 68°$) during such moderately disturbed geomagnetic conditions (i.e., AE = 250γ), and these are indeed observed here. But the lack of appreciable periods of field-aligned precipitation, in particular during the high flux periods centered about 03:38:00, (albeit these are at $\Lambda \lesssim 64°$), and the relatively low degree of anisotropy during these few times when field-aligned precipitation is evident, may be due to the local time of this pass, around 3 hours MLT. The connection between MLT and field-aligned 2.3keV precipitation will be discussed further in a later chapter.

An interesting example of data collected during a strong magnetospheric disturbance is the portion of Pass 4351 shown in Figure 4. In the high latitude portion of this near-midnight pass the fluxes at 0.7keV and 2.3keV are fairly low and structureless, and very isotropic. The fluxes begin increasing and fluctuating at 16:04:16, but the first appreciably anisotropic period does not begin until 16:04:36, coinciding with a moderate peak in the 2.3keV flux. Small, short duration anisotropies appear from 16:04:54 to 16:06:37, where a large peak in the 2.3keV flux begins in coincidence with the beginning of a seven second period of anisotropy. The ratio of 0° to 60° 2.3keV flux attains a peak value just greater than 5 during this time interval. This data transmission continued after 16:07:13 with substantially the same levels of isotropic fluxes until 16:07:56, at which time the satellite was just south of Λ = 61°.

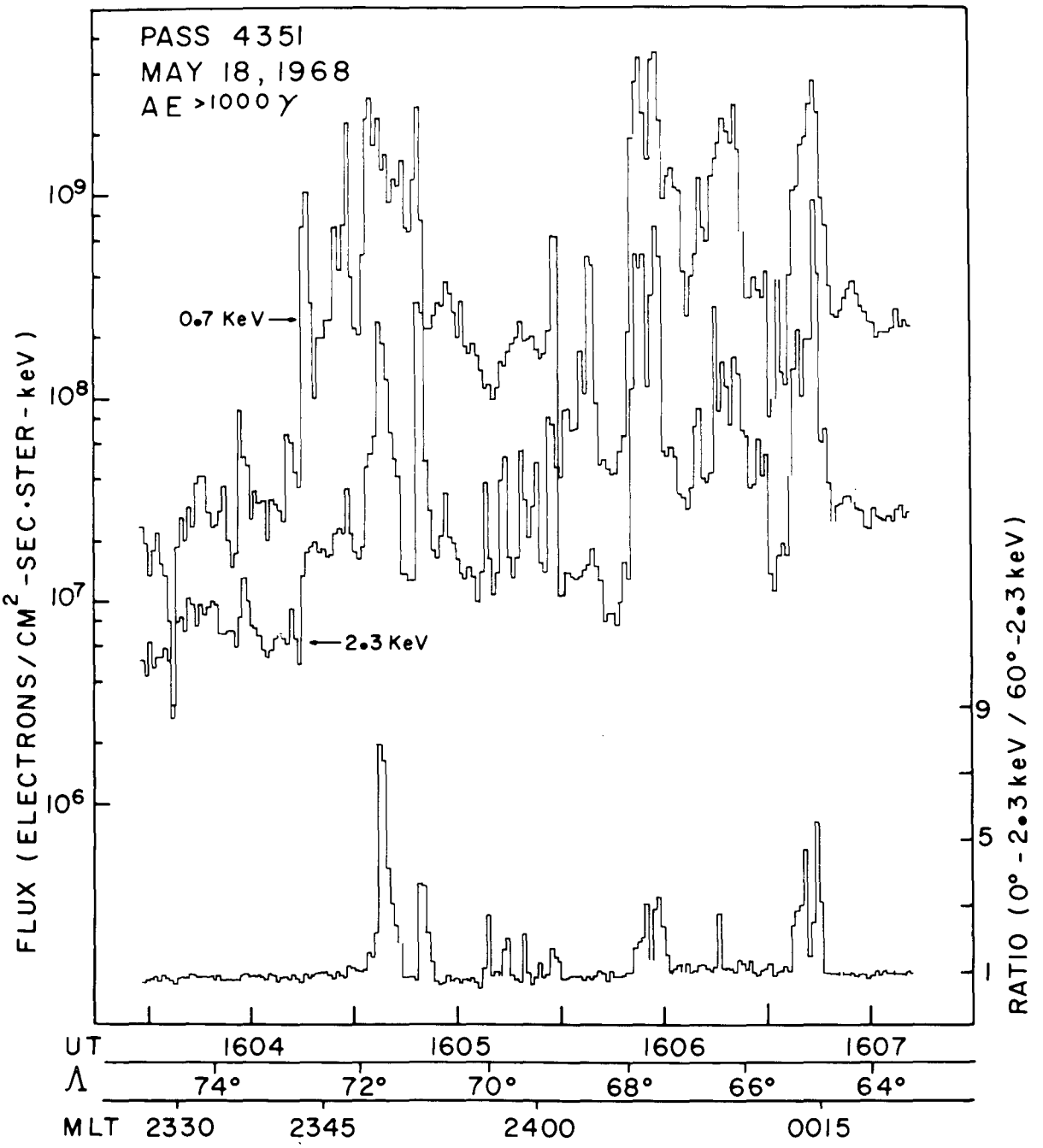
PASS 4351
MAY 18, 1968
AE >1000 γ
0.7 KeV
2.3 KeV
FLUX (ELECTRONS/CM²-SEC·STER-keV)
RATIO (0° - 2.3 keV / 60° - 2.3 keV)
UT
Λ
MLT
1604
1605
1606
1607
74°
72°
70°
68°
66°
64°
2330
2345
2400
0015

Figure 4

The portion of Pass 3031 displayed in Figure 5 shows several short duration bursts of highly anisotropic precipitation, where the ratio of 0° to 60° 2.3keV flux exceeds a value of 30. This pass occurred during a period of only moderate magnetic activity as indicated by the hourly AE value of 133, which was higher than that for the two hours before and after this time period. Although this pass displays an unusually high degree of anisotropy, it displays some features which are also fairly typical. All of the field-aligned precipitation occurs during high intensity bursts of 2.3keV electrons, and during those periods of relatively lower 2.3keV fluxes, the precipitation is quite isotropic. In addition, the bursts at 2.3keV occur simultaneously with or during bursts of 0.7keV electrons. For purposes of future discussion, we note that this pass occurred at about 21 hours MLT, with $69° < \Lambda < 74°$.

Pass 5771, a portion of which is shown in Figure 6, occurred during a period of extremely low geomagnetic activity (AE = 11γ), which is also evident from the plotted data. Although short duration bursts are present for most of the time at 0.7 keV, they are not especially intense, and the few bursts which occur at the 2.3keV energy are also of relatively low intensity. The several seconds of anisotropic precipitation between 15:08:15 and 15:08:50 are correlated with those few, relatively weak 2.3keV bursts appearing during that time, and the anisotropies are not very pronounced, with the ratio of 0° to 60° 2.3keV flux just exceeding 4 for only one of the several events. In general, this quiet-time early morning pass can be characterized as being one with low intensity fluctuations in the low energy electron flux and generally isotropic fluxes at 2.3keV.

Another example of data collected during a geomagnetically very quiet period is the portion of Pass 5829 shown in Figure 7. Unlike Pass 5771, which, although a

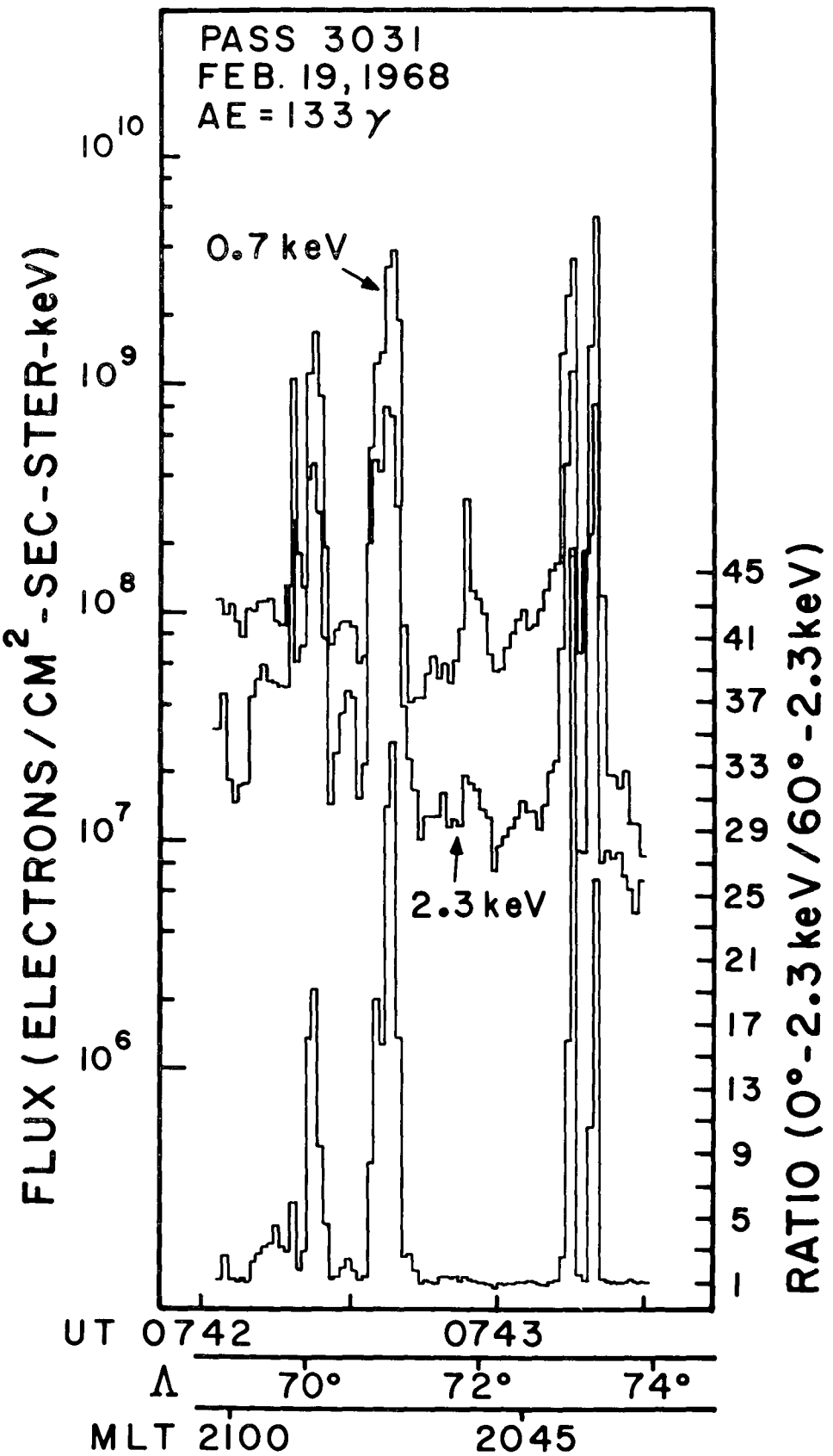
PASS 3031
FEB. 19, 1968
AE = 133 γ
0.7 keV
2.3 keV
FLUX (ELECTRONS/CM²-SEC-STER-keV)
RATIO (0°-2.3 keV/60°-2.3keV)
UT 0742
0743
Λ
70°
72°
74°
MLT 2100
2045

Figure 5

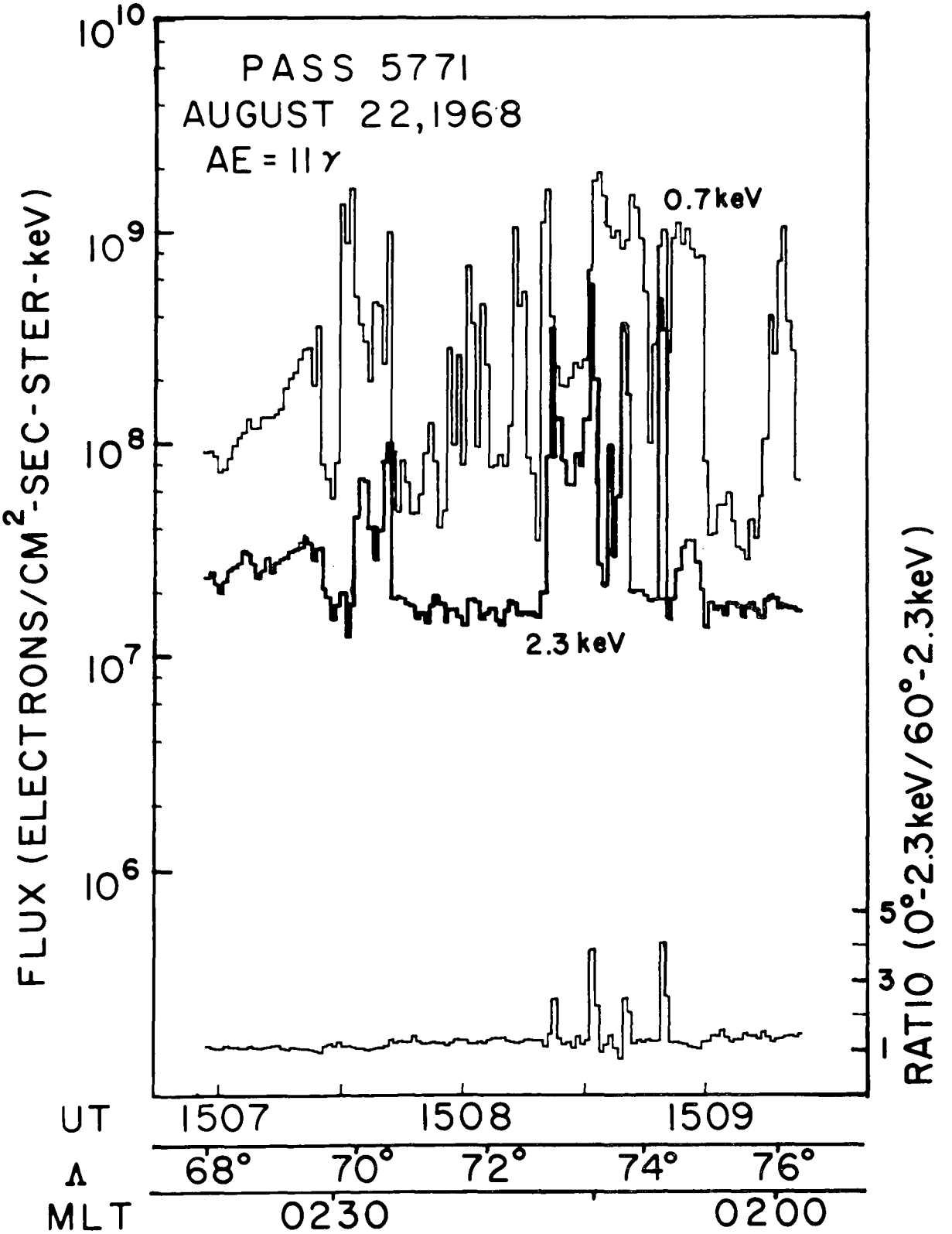
PASS 5771
AUGUST 22,1968
AE = 11γ
0.7keV
2.3 keV
FLUX (ELECTRONS/CM²-SEC-STER-keV)
RATIO (0°-2.3keV/60°-2.3keV)
UT
1507
1508
1509
Λ
68°
70°
72°
74°
76°
MLT
0230
0200

Figure 6

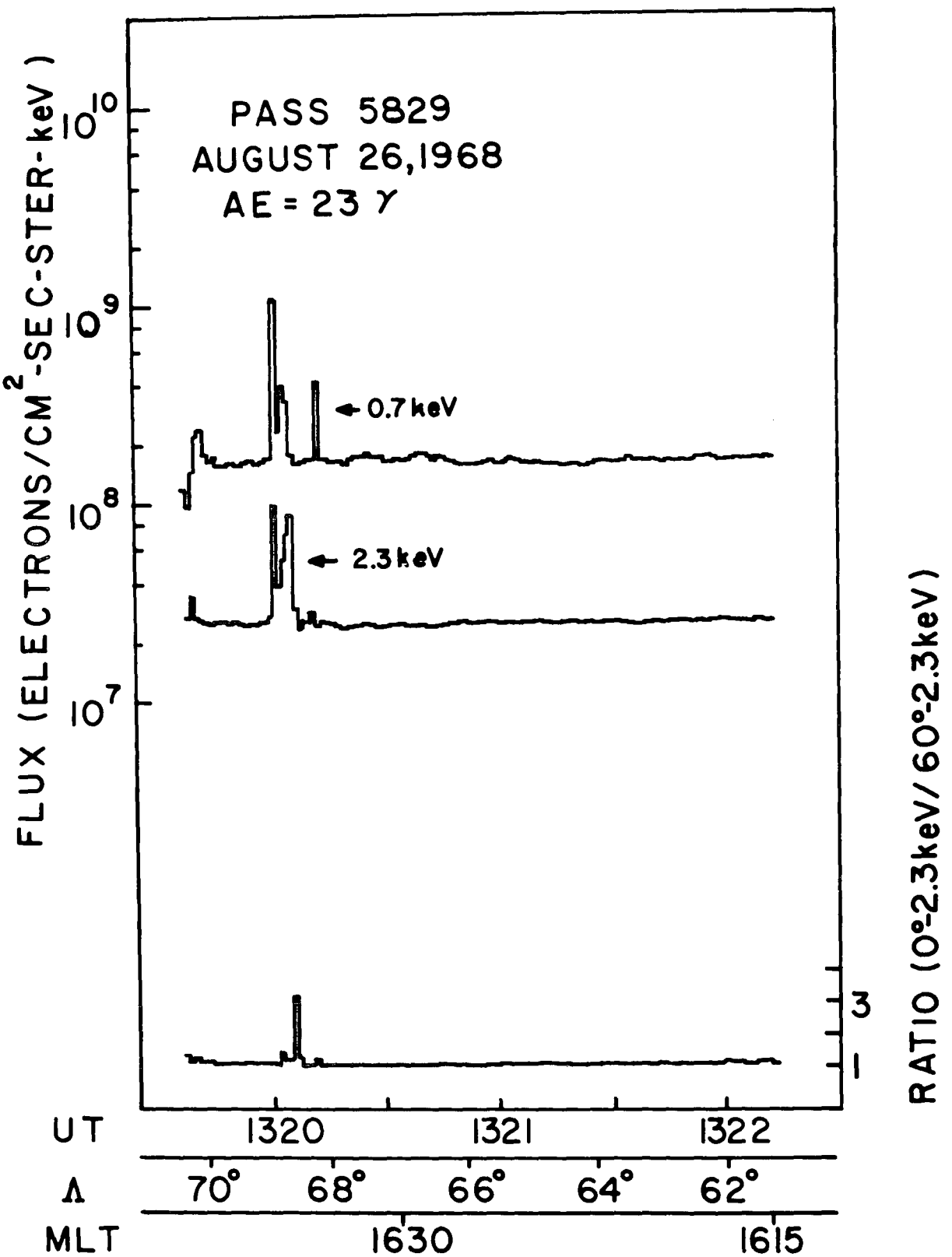
PASS 5829
AUGUST 26,1968
AE = 23 γ
FLUX (ELECTRONS/CM²-SEC-STER-keV)
10¹⁰
10⁹
10⁸
10⁷
0.7 keV
2.3 keV
RATIO (0°-2.3keV/ 60°-2.3keV)
3
UT
1320
1321
1322
Λ
70°
68°
66°
64°
62°
MLT
1630
1615

Figure 7

quiet-time pass, displayed some structure in the 0.7 and 2.3keV fluxes and a small but meaningful degree of anisotropy, this pass shows about 2-1/2 minutes of essentially non-changing isotropic fluxes, except for a 10 second period centered about 13:20:02. During this latter time period, small increases in the fluxes of 0.7 and 2.3keV electrons are present, as well as a single one-second averaged period (13:20:04 to 13:20:05) when the 2.3keV flux at 0° exceeded that at 60° by more than 2. Aside from this single peak in the ratio curve, this pass is completely isotropic in the observed 2.3keV flux. In connection with this isotropy, (or lack of anisotropy), we note for later discussion that these data were collected at $71° > \Lambda > 61°$ and about 16:30 MLT. Generally speaking, then, Pass 5829, like Pass 5771, is one with only a few low intensity fluctuations in the electron fluxes; and the fluxes appear (at 2.3keV) to be quite isotropic throughout the pass.

The portion of Pass 6617 shown in Figure 8, when the hourly averaged value of AE was 32γ is another example of data collected during a geomagnetically quiet period. This morning hour pass shows appreciable structure in the 0.7keV electron flux, with fluxes at this energy exceeding 2×10^9 electrons/cm^2-sec-ster-keV for several of the one-second averaged accumulation periods shown. At 2.3keV, the flux also shows some fluctuations, but only the peak at 18:03:45 barely exceeds 10^9 electrons/cm^2-sec-ster-keV. Aside from the slightly anisotropic bursts at this time, the pass is predominantly isotropic, with the exception of a ten-second period of anisotropic 2.3keV fluxes near the beginning of the pass at $\Lambda \gtrsim 79°$. The anisotropies around 18:02:30 never exceed a value of 3 in the ratio of 0° to 60° 2.3 keV fluxes, so this pass can be considered to be generally isotropic.

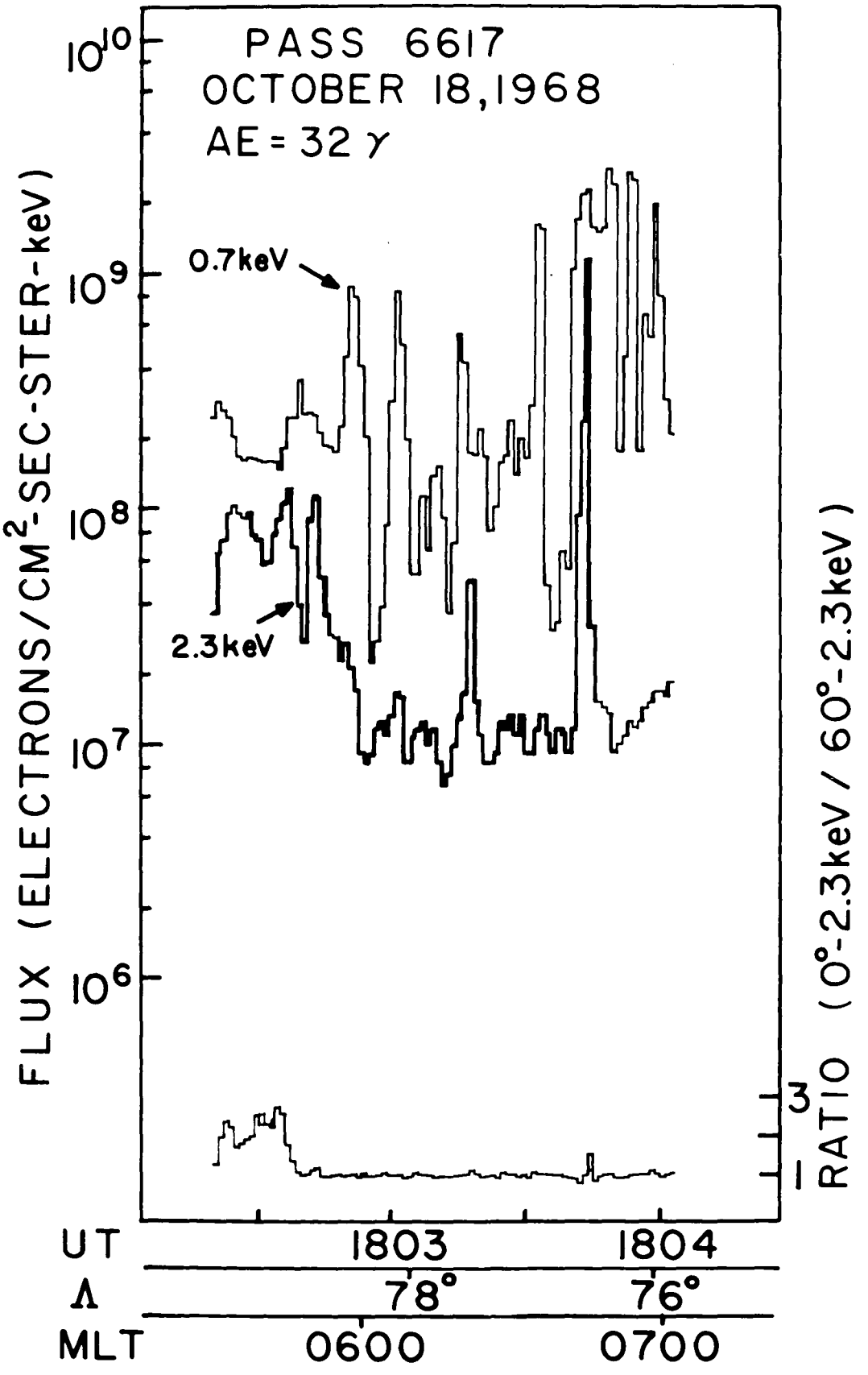
PASS 6617
OCTOBER 18,1968
AE = 32 γ
0.7keV
2.3keV
FLUX (ELECTRONS/CM²-SEC-STER-keV)
10¹⁰
10⁹
10⁸
10⁷
10⁶
RATIO (0°-2.3keV / 60°-2.3keV)
3
UT
1803
1804
Λ
78°
76°
MLT
0600
0700

Figure 8

The portion of Pass 6677 shown in Figure 9 again displays data collected during a relatively quiet period. Fluxes of both 0.7keV and 2.3keV electrons were quite high at the beginning of this data acquisition period, but the 2.3keV fluxes fell to a fairly low level more than 10 seconds before the large decrease occurred in the 0.7 keV electron flux. Between $\Lambda = 76°$ and $\Lambda = 75°$, the fluxes at both of these energies rose and fell gradually, forming what look like "bumps" in the plotted curves. Essentially all the field-aligned 2.3keV precipitation occurred prior to 19:12:00, and the precipitation for the remainder of the pass was very isotropic as the satellite moved to lower latitudes. However, the several seconds of data when Λ was just below 77° are extremely field-aligned, with the ratio of 0° to 60° 2.3keV flux reaching a value greater than 20, and exceeding a value of 2 for at least six seconds. The high degree of anisotropy displayed during the early portion of this pass is somewhat atypical for a quiet-time pass. The field-aligned precipitation events during this pass, occurring in conjunction with high 2.3keV fluxes at 0° pitch angle, follow a general trend which will be discussed in a later chapter.

Another pass which occurred during a period of only moderate geomagnetic activity was the segment of Pass 6419 shown in Figure 10. During this near-midnight pass, large abrupt changes are evident in the flux of 0.7keV electrons, while the relatively few fluctuations in the 2.3keV electron flux are not of very large magnitude. The peak 2.3keV flux occurred at 09:13:09, and had a magnitude of $\sim 3 \times 10^8$ electrons/cm^2-sec-ster-keV. Perhaps because of the generally low peaks in the 2.3keV electron flux, the precipitation observed at this energy is only somewhat field-aligned in nature. The plotted ratio of 0° to 60° 2.3keV flux never exceeded a value of 5, and is greater than 2 for only about nine seconds in this time interval.

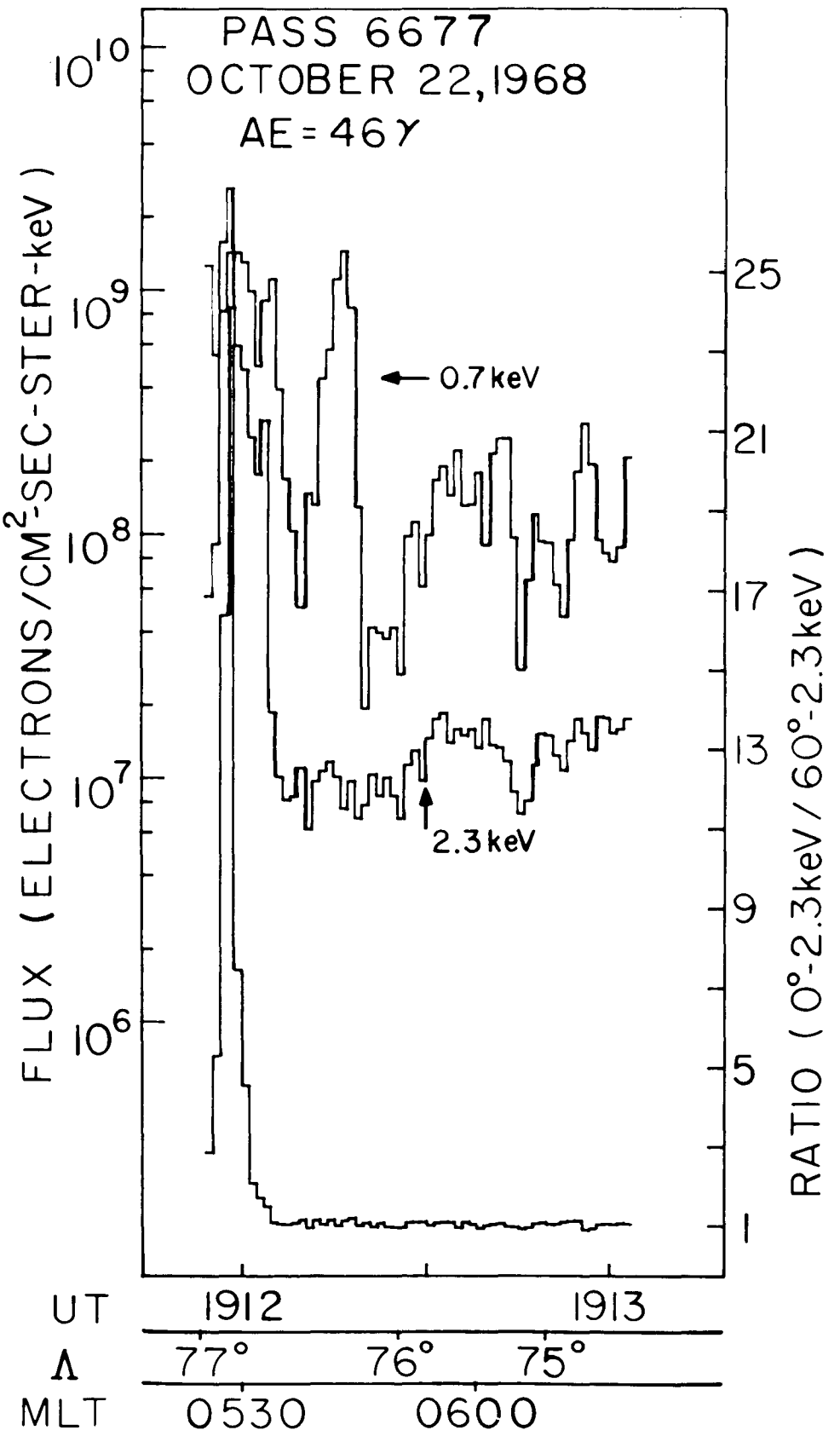
PASS 6677
OCTOBER 22, 1968
AE = 46γ
FLUX (ELECTRONS/CM²-SEC-STER-keV)
RATIO (0°-2.3keV / 60°-2.3keV)
0.7 keV
2.3 keV
UT
Λ
MLT
1912
1913
77°
76°
75°
0530
0600

Figure 9

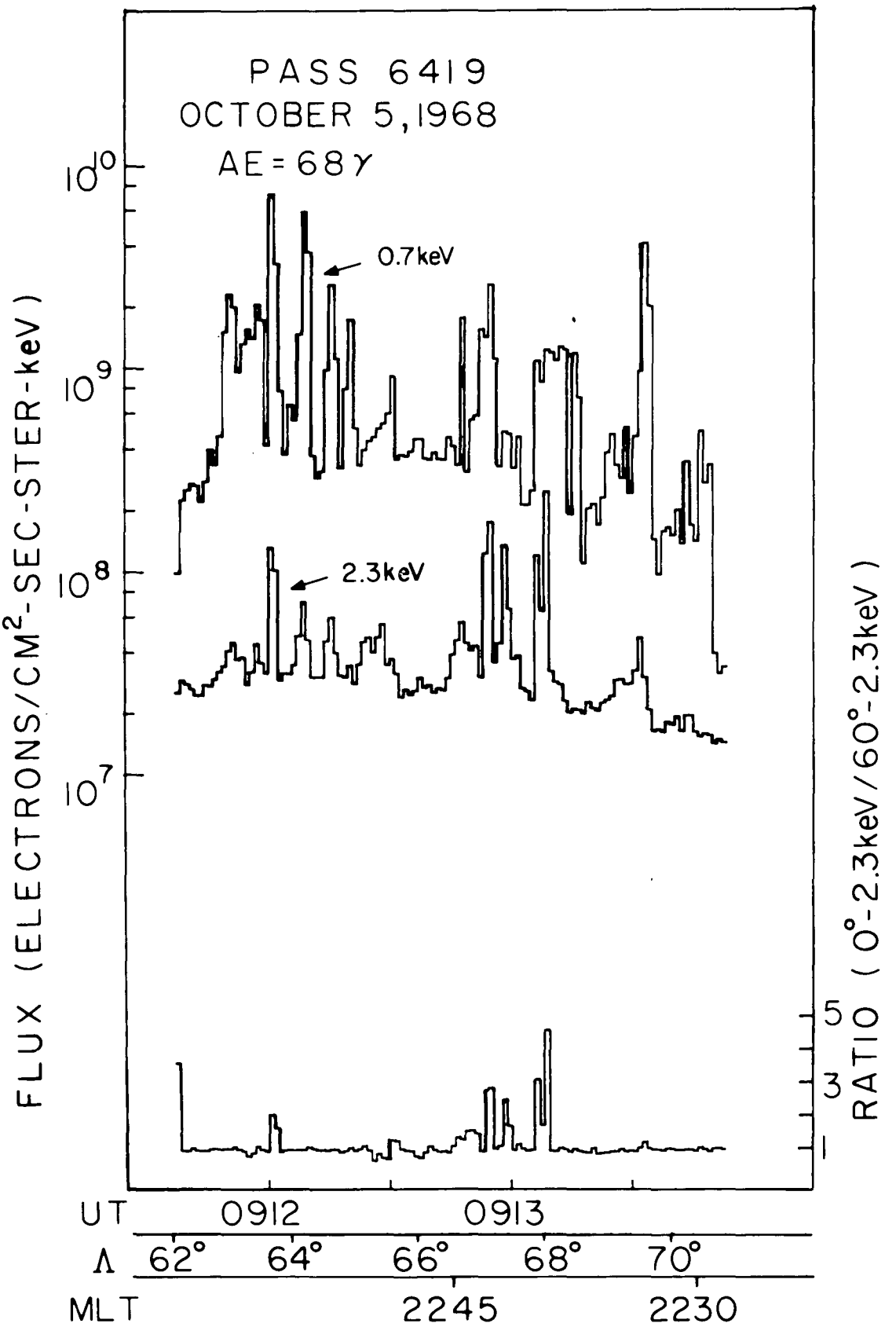
PASS 6419
OCTOBER 5, 1968
AE = 68γ
0.7keV
2.3keV
FLUX (ELECTRONS/CM²-SEC-STER-keV)
RATIO (0°-2.3keV/60°-2.3keV)
UT
0912
0913
Λ
62°
64°
66°
68°
70°
MLT
2245
2230

Figure 10

The relatively large bursts of 0.7keV electrons at $\Lambda \lesssim 65°$ is a rather unexpected feature displayed at the near-midnight local time of this pass (Hoffman and Berko, 1971b).

As will be shown later, more field-aligned 2.3keV electron precipitation was observed within two hours of local midnight than at any other local times. Pass 2710, (Figure 11), shows a portion of data collected in this near-midnight local time sector when the value of the one-hour-averaged AE index was 107γ, indicating a moderate level of magnetic disturbance. We must reject the first several seconds of "apparently" field-aligned precipitation, because the 2.3keV fluxes at that time were $< 2 \times 10^7$ electrons/cm^2-sec-ster-keV, and thus the ratios of 0° to 60° 2.3 keV flux are not meaningful due to the low counting rates. There are two "peaks" in the 0.7keV flux, with the first, at $64° < \Lambda < 66°$, of considerably lower intensity than the second, higher latitude peak. This latter peak in the 0.7keV flux at $68° < \Lambda < 70°$ occurred simultaneously with the peak 2.3keV electron flux. During this same interval of high fluxes, the ratio of 0° to 60° 2.3keV flux rose well above unity, reaching a peak value just greater than 7, and remained at or above a value of 2 during about half of the roughly 25 second time period. The lack of any real anisotropy during the first peak in the 0.7keV flux is not surprising, since there is no correspondingly large flux observed at 2.3keV.

Most field-aligned precipitation occurs when the electron energy spectrum becomes fairly hard (i.e., a larger fraction of the particles detected are at higher energies). A good example of this phenomenon is the highly field-aligned burst of 2.3keV electrons at $\Lambda = 78°$ during Pass 6558 (Figure 12). During this field-aligned burst of 2.3keV electrons, at the time of maximum anisotropy, the ratio of 0° to

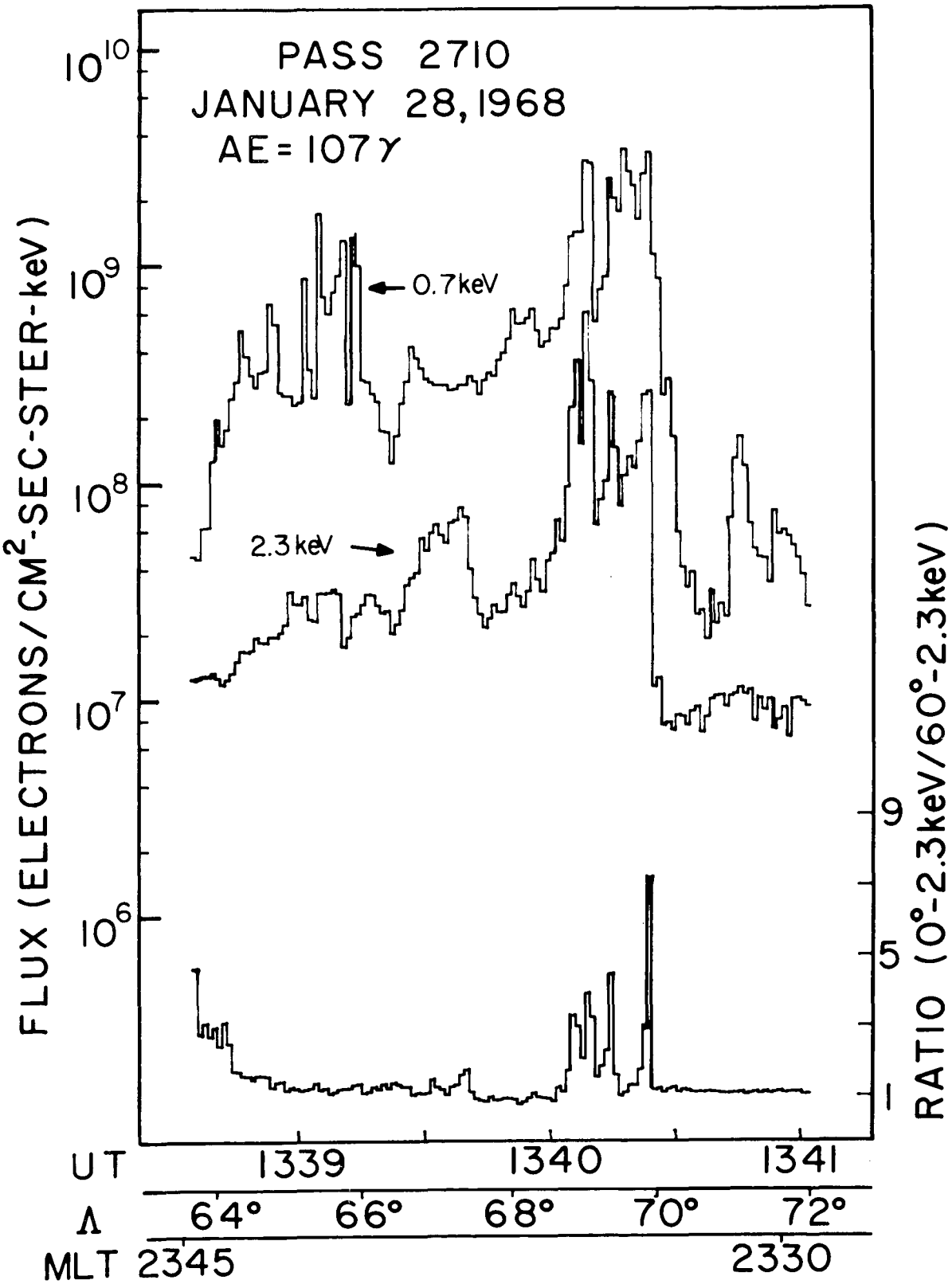
PASS 2710
JANUARY 28, 1968
AE = 107γ
0.7keV
2.3keV
FLUX (ELECTRONS/CM²-SEC-STER-keV)
RATIO (0°-2.3keV/60°-2.3keV)
UT
1339
1340
1341
Λ
64°
66°
68°
70°
72°
MLT 2345
2330

Figure 11

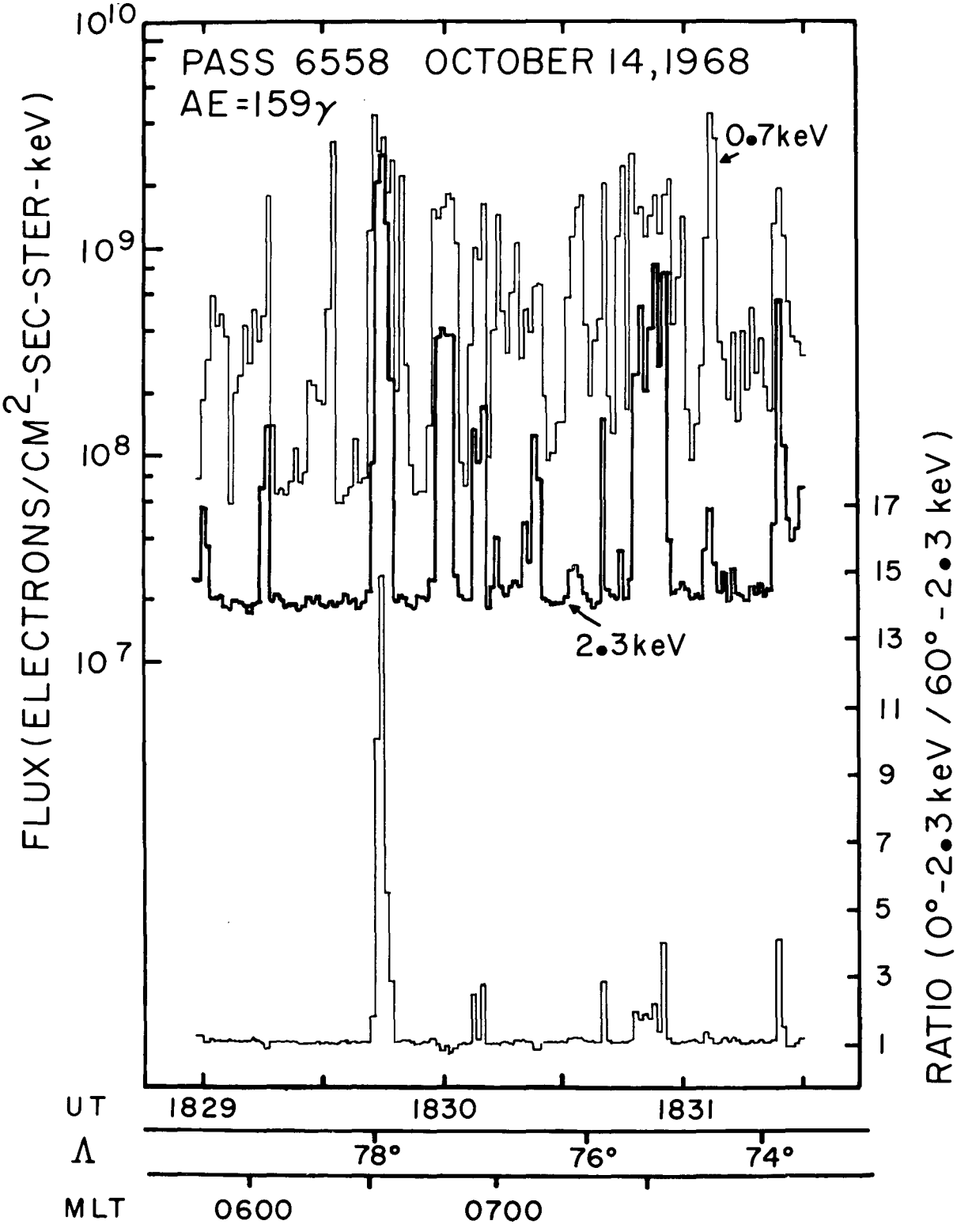
PASS 6558 OCTOBER 14,1968
AE=159γ
0.7keV
2.3keV
FLUX (ELECTRONS/CM²-SEC-STER-keV)
RATIO (0°-2.3keV / 60°-2.3 keV)
UT
1829
1830
1831
Λ
78°
76°
74°
MLT
0600
0700

Figure 12

60° 2.3keV flux was about 15 and the flux of 2.3keV electrons was 2.8×10^9 electrons/cm^2-sec-ster-keV, while the 0.7keV flux was 3.5×10^9 electrons/cm^2-sec-ster-keV. By way of comparison, at 18:30:08, when the ratio of 0° to 60° 2.3 keV flux was 2.5, the 2.3keV and 0.7keV fluxes were 1.35×10^8 and 1.01×10^9 electrons/cm^2-sec-ster-keV, respectively. Not only was the 2.3keV flux more than a factor of 10 higher during the highly anisotropic burst at 18:29:45 than it was at 18:30:08, but at these same two times, the ratios of 0.7keV flux to 2.3keV flux were 1.24 and 7.48, respectively. Thus, the flux of 2.3keV electrons was much higher in magnitude and also much closer in value to the 0.7keV flux during the burst at 18:29:45, indicating that during that highly field-aligned period the electron energy spectrum was considerably harder than it was during other portions of this pass.

We conclude this section with a portion of data collected during a highly disturbed period, when the AE index was well over 1000γ, Pass 5696 (Figure 13). Unlike the prior data examples, 1/4-second averages are shown for this data acquisition. This early morning pass shows a very high degree of anisotropy in the 2.3keV precipitation, with the ratio of 0° to 60° 2.3keV flux greater than 2 for more than 40% of the 1/4-second accumulation periods plotted here. Values of this ratio greater than 5 are prevalent throughout this storm-time pass. Again, we have very anisotropic periods occurring during times of high 2.3keV flux (and when the electron energy spectrum tends to be harder), such as the period of field-aligned precipitation from 13:29:55 to 13:29:58. However, much of the field-aligned precipitation is evident during times of somewhat lower peak fluxes of 2.3keV electrons, such as from 13:30:21 to 13:30:43.

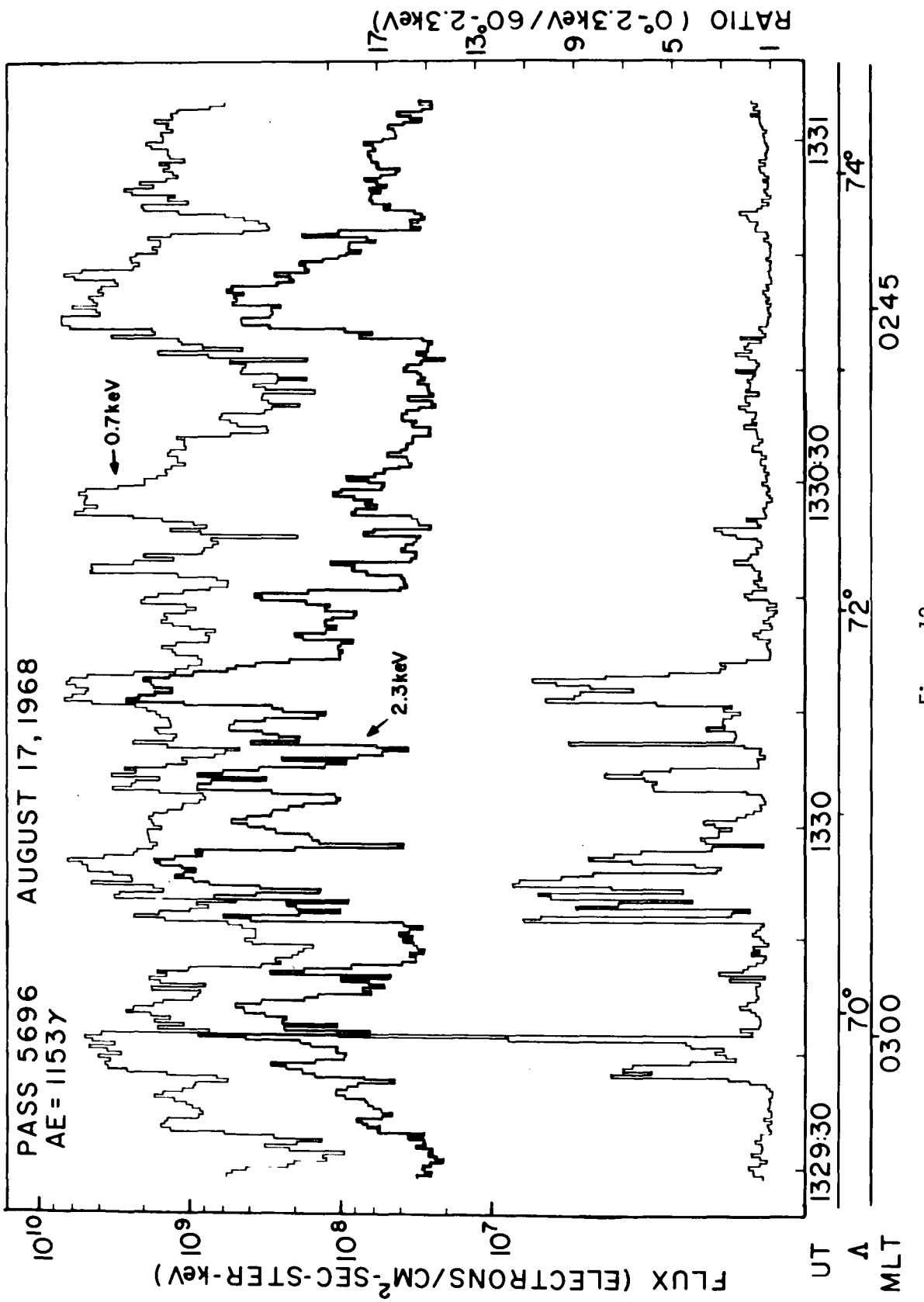
PASS 5696
AE = 1153γ
AUGUST 17, 1968
0.7keV
2.3keV
FLUX (ELECTRONS/CM²-SEC-STER-kev)
RATIO (0°-2.3keV / 60°-2.3keV)
UT
Λ
MLT
1329:30
1330
1330:30
1331
70°
72°
74°
0300
0245

Figure 13

Although the period from 13:29:38 to 13:29:44 contains much field-aligned precipitation, including the most field-aligned event of the pass at 13:29:41, the average 2.3keV flux during this time interval was almost a factor of 2 lower than the average flux from 13:30:43 to 13:30:52, a period of completely isotropic 2.3keV electron precipitation. The most likely explanation for the very different nature of the pitch angle distribution of these two time intervals is the difference in their electron energy spectrums. During the first interval, the average energy spectrum is considerably harder, due to lower average 0.7keV electron fluxes ($\sim 2.72 \times 10^9$ electrons/cm^2-sec-ster-keV), compared with an average 0.7keV flux of 4.04×10^9 electrons/cm^2-sec-ster-keV for the later time interval, but approximately equal average 2.3keV fluxes (2.59×10^8 and 2.56×10^8 electrons/cm^2-sec-ster-keV, respectively). The ratios of average 0.7keV flux to average 2.3keV flux are then 10.48 and 15.78 for the two intervals, respectively, thus yielding a (two-point) electron energy spectrum for the second interval that is $\sim 50\%$ softer than that during the first interval.

V. SPATIAL DISTRIBUTIONS

In order to determine the spatial distribution of high latitude field-aligned electron precipitation, the following scheme was employed. All available electron data from the OGO-4 Auroral Particles Experiment which were taken during the time interval July 30, 1967 through November 20, 1968, (a time period during which the orbital plane of the OGO-4 satellite underwent a complete 4π precession in magnetic local time), were considered as the overall data base. Background count rate values were subtracted from the 0.7 keV - 0°, 2.3 keV - 0°, and 2.3 keV - 60° raw count rates (in counts per readout). The resulting count rates for these detectors, and for the 7.3 keV - 0° detector, for which no background corrections were necessary, were then averaged over several accumulation periods to produce one-second averages. These one-second average count rates were then converted to one-second average particle fluxes, with units of electrons/cm^2-sec-ster-keV, using the factors given in Table 1. Only those sets of one-second averaged data where the 0° - 2.3 keV electron flux exceeded $\sim 2 \times 10^7$ were then kept for further analysis since fluxes less than this value represented as few as 7 counts per second, a statistically insignificant value (see Appendix A). After these several operations, a new data base of $\sim$129,000 one-second averaged "events" had been defined.

COUNTS PER READOUT TO DIFFERENTIAL FLUX CONVERSION FACTORS**

Angle, deg	Center Energy keV	Flux Conversion Factors*		
		4 kbps Rate	16 kbps Rate	64 kbps Rate
0	0.7	6.70×10^5	2.68×10^6	1.07×10^7
0	2.3	2.03×10^5	8.12×10^5	3.25×10^6
0	7.3	8.13×10^4	3.25×10^5	1.30×10^6
60	2.3	2.03×10^5	8.12×10^5	3.25×10^6

*To convert from counts/readout to electrons/cm^2-sec-ster-keV, at the 4, 16, and 64 kilobits/sec telemetry rates.
**From Hoffman and Evans (1968).

TABLE 1

Magnetic local time and invariant latitudes were then computed for each event in this new data base. About 10,000 of these events were found to have occurred at invariant latitudes (Λ) less than 60°, and a decision was made to further consider only those events with $\Lambda \geq 60°$, since these are representative of high-latitude phenomena. The final data base consisted of 118,483 events, each with $\Lambda \geq 60°$. These were sorted into spatial "elements," one hour wide in magnetic local time by 2-1/2° in Λ, except for $\Lambda \geq 85°$, where the latitudinal extent was 5° (see for example Hoffman and Berko, 1971a). The number of events in each element resulting from this sorting is shown in Table 2, where the average number of events per element is 448.8.

It is important, however, to attempt to eliminate any systematic bias in the distribution of data due to uneven satellite coverage of the different elements. Such uneven sampling was due in part to satellite attitude-orientational difficulties and certain other OGO-4 operational procedures which reduced the total possible scientific

DISTRIBUTION OF ALL PRECIPITATION EVENTS

Magnetic Local Time Interval, ΔMLT (hours)	Invariant Latitude Interval, Δ Λ (degrees)										
	60.0-62.4	62.5-64.9	65.0-67.4	67.5-69.9	70.0-72.4	72.5-74.9	75.0-77.4	77.5-79.9	80.0-82.4	82.5-84.9	≥ 85.0
0-1	109	359	607	882	839	724	798	823	666	572	189
1-2	285	568	973	1072	1004	887	690	571	296	426	83
2-3	213	661	1137	1285	903	652	230	255	133	162	95
3-4	202	702	1365	1457	773	588	344	185	87	147	82
4-5	365	717	1031	1004	1069	768	425	104	99	137	76
5-6	115	427	880	1391	1249	972	796	362	77	95	62
6-7	11	112	546	1178	1665	1230	1041	747	64	44	39
7-8	164	313	399	744	996	1026	1054	1337	259	117	21
8-9	7	9	165	301	516	461	712	1474	357	129	58
9-10	7	38	85	258	393	723	612	1256	286	256	78
10-11	39	88	288	419	608	716	1010	1029	232	226	89
11-12	83	171	403	475	686	929	896	606	117	184	146
12-13	93	203	342	620	708	739	520	319	81	161	152
13-14	170	179	258	450	458	441	529	329	141	236	212
14-15	193	166	152	137	226	475	711	656	272	274	149
15-16	470	433	335	258	271	650	716	646	341	260	71
16-17	340	419	554	656	829	725	792	616	419	273	148
17-18	24	22	56	247	535	685	494	434	448	464	219
18-19	86	83	193	423	592	409	181	88	434	532	360
19-20	61	95	245	689	805	518	370	251	96	872	387
20-21	62	87	307	575	533	432	266	400	252	856	360
21-22	76	321	517	686	508	318	250	187	241	725	354
22-23	79	267	396	802	637	480	478	436	223	762	347
23-24	70	270	548	637	406	290	347	561	654	809	269

TABLE 2

data acquisition. Polar-projection plots of all passes during the 16 month period during which usable data were collected were examined to determine weighting factors for normalizing the distribution. It was found that on the average, all elements were sampled for approximately the same number of seconds during each sample, when averaged over all samplings of a given element. Thus, the number of times an element was sampled is the important quantity for normalizing satellite coverage. These latter quantities were determined from the polar plots by simply counting the number of samples per element, and these values are presented in Table 3. Generally, the midnight-to-dawn and noon-to-dusk quadrants were sampled more frequently during the complete 4π precession than were the other two quadrants.

Normalization of coverage was then performed in the following manner. A weighting value of unity was assigned to elements with 100 samples, and weighting factors for each element (WF_N) were computed according to the formula:

$$WF_N = \frac{100}{(\text{number of samples})_N}$$

Applying the weighting factors thus derived to the distribution of all precipitation events shown in Table 2, a normalized distribution of all events was obtained, and is presented in Table 4. This normalized distribution has a considerably higher number of events from about 19 hours MLT, through midnight, to about 10 hours MLT, than in the local time segment from 10 hours, through noon, to 19 hours MLT. Such a general pattern of precipitation is not unexpected, since it has been shown that electron precipitation in the several keV energy range occurs primarily in this type of pattern (Hoffman, 1969; Hoffman and Berko, 1971b).

Having now achieved a final data base with reasonably good statistics at all local times, the next step was to determine the spatial distribution of field-aligned electron

NUMBER OF TIMES EACH ELEMENT SAMPLED, 30 JULY 1967 - 20 NOVEMBER 1968

Magnetic Local Time Interval, ΔMLT (hours)	Invariant Latitude Interval, Δ Λ (degrees)										
	60.0-62.4	62.5-64.9	65.0-67.4	67.5-69.9	70.0-72.4	72.5-74.9	75.0-77.4	77.5-79.9	80.0-82.4	82.5-84.9	≥85.0
0-1	37	52	56	66	74	87	106	93	74	91	49
1-2	54	61	87	97	94	99	84	83	58	94	49
2-3	62	77	87	92	89	82	75	95	57	88	46
3-4	58	79	94	105	90	78	89	85	55	88	46
4-5	59	70	83	85	93	91	81	83	59	78	51
5-6	55	79	91	99	90	90	80	75	62	85	51
6-7	39	56	77	97	105	99	76	84	57	74	58
7-8	52	71	75	76	81	89	87	84	51	69	58
8-9	51	49	59	63	64	58	76	87	61	79	55
9-10	47	55	51	56	64	75	70	93	66	96	55
10-11	42	49	71	74	84	87	88	111	67	78	53
11-12	43	59	64	75	71	82	100	104	83	81	53
12-13	32	49	59	77	81	99	99	113	74	82	43
13-14	46	50	72	81	91	89	98	115	63	69	43
14-15	41	59	68	78	87	89	99	110	57	51	46
15-16	59	65	72	92	88	92	80	84	44	68	46
16-17	58	68	77	103	94	82	78	91	45	74	49
17-18	49	58	72	80	93	79	76	94	54	64	49
18-19	46	59	71	83	78	78	78	81	59	66	64
19-20	32	45	61	70	79	81	89	87	59	91	64
20-21	24	31	42	52	67	70	87	100	69	101	66
21-22	27	38	51	56	68	71	78	103	72	97	66
22-23	32	44	57	68	68	73	82	118	80	86	56
23-24	42	50	53	64	79	88	114	129	82	92	56

TABLE 3

NORMALIZED DISTRIBUTION OF ALL PRECIPITATION EVENTS

Magnetic Local Time Interval, ΔMLT (hours)	Invariant Latitude Interval, ΔΛ(degrees)										
	60.0-62.4	62.5-64.9	65.0-67.4	67.5-69.9	70.0-72.4	72.5-74.9	75.0-77.4	77.5-79.9	80.0-82.4	82.5-84.9	≥85.0
0-1	294	690	1083	1336	1133	832	752	884	900	628	385
1-2	527	931	1118	1104	1068	895	821	687	510	453	169
2-3	343	858	1306	1396	1014	795	306	268	233	184	206
3-4	348	888	1452	1387	858	753	386	217	158	167	178
4-5	616	1024	1242	1181	1149	843	524	125	167	175	149
5-6	209	540	967	1405	1387	1080	995	482	124	111	121
6-7	28	200	709	1214	1585	1242	1369	889	112	59	67
7-8	315	440	532	978	1229	1152	1211	1591	507	169	36
8-9	13	18	279	477	806	794	936	1694	585	163	105
9-10	14	69	166	460	614	964	874	1350	433	266	141
10-11	92	179	405	566	723	822	1147	927	346	289	167
11-12	193	289	629	633	966	1132	896	582	140	227	275
12-13	290	414	579	805	874	746	525	282	109	196	353
13-14	369	358	358	555	503	495	539	286	223	340	493
14-15	470	281	223	175	259	533	718	596	477	537	323
15-16	796	666	465	280	307	706	895	769	775	382	154
16-17	586	616	719	636	881	884	1015	676	931	368	302
17-18	48	37	77	308	575	867	650	461	829	725	446
18-19	186	140	271	509	758	524	232	108	735	806	562
19-20	190	211	401	984	1018	639	415	288	162	958	604
20-21	258	280	730	1105	795	617	305	400	365	847	545
21-22	281	844	1013	1225	747	447	320	181	334	747	536
22-23	246	606	694	1179	936	657	582	369	278	886	619
23-24	166	540	1033	995	513	329	304	434	797	879	480

TABLE 4

precipitation at high latitudes. For every event in the data base, the ratio of 0° - 2.3keV flux to 60° - 2.3keV flux was calculated, and denoted by R. An event was considered to be field-aligned only if its R was greater than or equal to 2.0. Of the more than 118,000 events in the data base, only 2204 events, less than 2%, were field-aligned (i.e. had $R \geq 2.0$).

The normalized distribution of all of these field-aligned precipitation events is tabulated in Table 5 and presented in a magnetic local time-invariant latitude polar coordinate projection in Figure 14. The highest number of field-aligned (FA) events are seen to occur in the element extending from 23 to 24 hours MLT and from $\Lambda = 70°$ to $\Lambda = 72.5°$. Significantly high numbers of FA events occurred in a region extending from 22 hours to 01 hours MLT and 67.5° to 72.5° Λ. A somewhat lower number of FA events were detected in a region roughly symmetric about the meridian plane passing through 23 and 11 hours MLT. The lowest contour shown encloses those sectors which had ≥ 10 FA events. This last contour is also generally symmetric about the 11 hour-23 hour MLT meridian plane, and is wider in latitude near midnight than at either its morning or afternoon terminus. In addition, this contour of lowest number of FA events is seen to enclose higher latitude elements in the morning and afternoon quadrants than near midnight, where it extends from 65° - 77-1/2° Λ, (excluding the pie-shaped region above $\Lambda = 85°$ from 23 hours to 01 hours MLT), while from 09 to 10 hours MLT and also from 13 to 14 hours MLT, it extends from 75° to 77.5° Λ, this time excluding the even higher latitude element also extending from 13 to 14 hours MLT.

The very high latitude sector centered at midnight actually had only 6 and 7 FA events in each element, but when normalized, the values became greater than 10.

NORMALIZED DISTRIBUTION OF ALL FIELD-ALIGNED EVENTS

Magnetic Local Time Interval, ΔMLT (hours)	Invariant Latitude Interval, Δ Λ (degrees)										
	60.0-62.4	62.5-64.9	65.0-67.4	67.5-69.9	70.0-72.4	72.5-74.9	75.0-77.4	77.5-79.9	80.0-82.4	82.5-84.9	≥85.0
0-1	2	5	33	83	62	32	17	3	0	2	12
1-2	1	1	20	45	48	30	11	1	3	0	0
2-3	0	0	18	31	32	41	22	0	7	4	0
3-4	3	2	8	28	28	28	23	22	0	1	0
4-5	3	12	7	12	12	14	6	1	8	1	0
5-6	0	0	5	14	17	30	21	17	0	0	0
6-7	5	0	0	7	13	20	14	7	0	1	0
7-8	7	2	5	13	25	17	14	14	13	1	0
8-9	0	4	1	4	4	5	7	17	8	0	0
9-10	2	0	0	1	4	9	10	1	0	1	0
10-11	0	0	1	2	5	1	7	1	2	1	0
11-12	4	3	4	2	4	1	3	1	0	1	0
12-13	0	2	1	3	0	8	0	7	0	1	0
13-14	0	2	0	3	1	0	10	1	1	10	4
14-15	2	3	2	6	2	23	12	7	1	1	4
15-16	5	0	0	8	6	6	12	16	0	1	2
16-17	1	1	1	4	14	15	10	15	0	0	4
17-18	0	0	0	5	27	27	48	7	12	1	8
18-19	0	11	12	30	28	21	33	3	5	3	9
19-20	0	0	1	32	40	35	29	24	5	0	1
20-21	0	0	14	28	47	47	16	21	4	0	0
21-22	0	10	27	44	36	33	7	7	4	1	0
22-23	3	2	21	63	77	38	15	3	0	0	3
23-24	2	6	22	85	102	47	15	1	0	6	12

TABLE 5

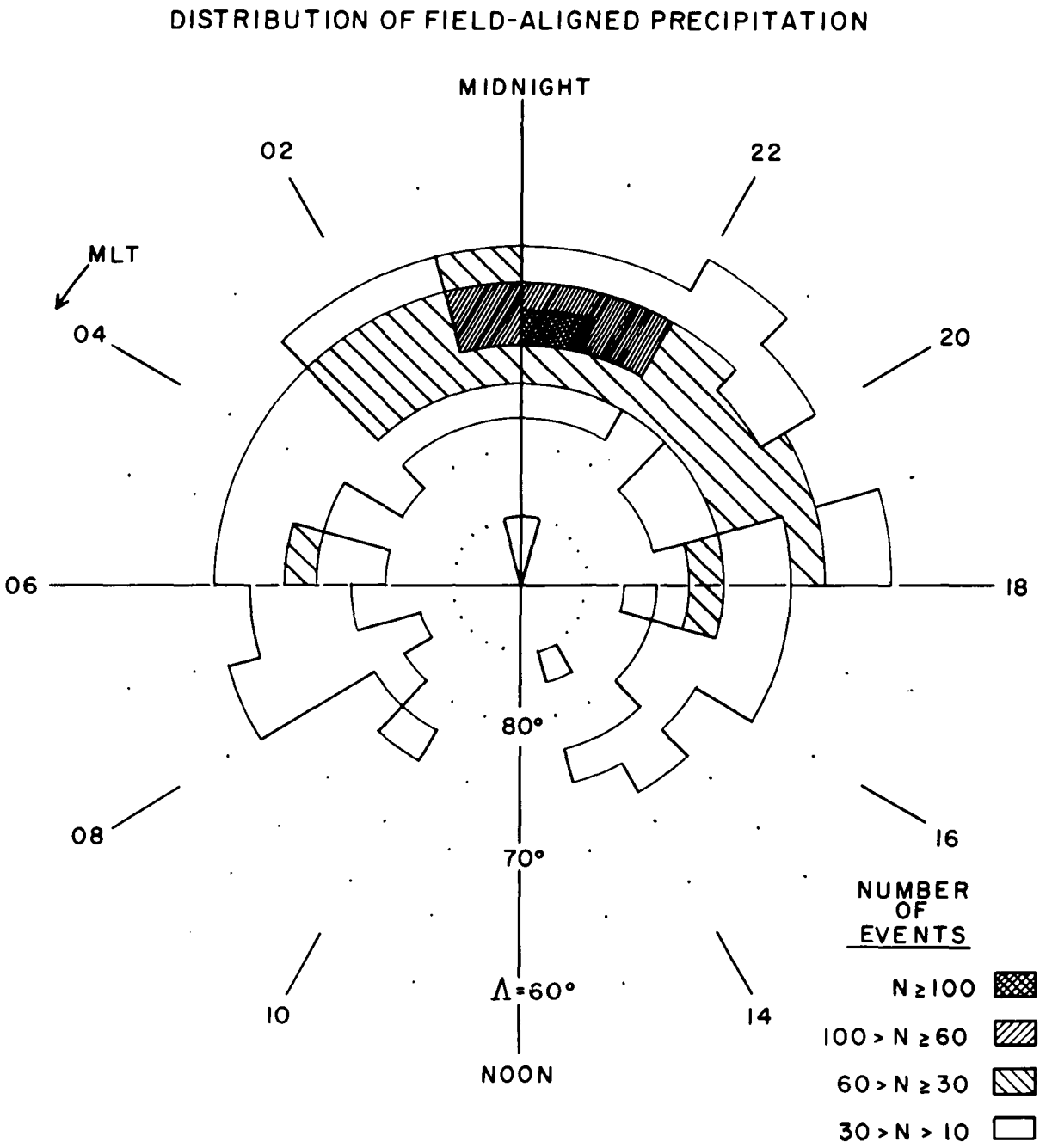

Figure 14. Normalized distribution of field-aligned 2.3 keV electron precipitation events in a magnetic local time-invariant latitude polar projection.

This is not to say that this pie-shaped segment is without meaning, since all the other elements with $\Lambda \geq 85°$ also had about the same high weighting factors. A similar statement is also true for the element from 13 to 14 hours MLT and 82.5° to 85° Λ.

Most of the elements in this figure which are not included in one of the four number-of-event contours had fewer than 5 FA events. Many elements below $\Lambda = 65°$, and below $\Lambda = 75°$ from 08 hours to 14 hours MLT, had no field-aligned events at all. The lack of 2.3 keV field-aligned precipitation around local noon is not unexpected, since one generally does not observe significant fluxes of greater than 1 keV electrons at these local times (Burch, 1968; Hoffman, 1969; Heikkila and Winningham, 1971).

In Figure 15, the predominance of FA events around local midnight is easily seen, as well as the generally low number of events around local noon. This figure also shows a higher number of FA events in the pre-midnight quadrant (18 to 24 hours MLT) than in the post-midnight quadrant (24 to 06 hours MLT). Of the total of all FA events, 43.3% occurred in the dusk-to-midnight quadrant and 32.3% in the midnight-to-dawn quadrant. Slightly more events were observed in the noon-to-dusk quadrant than in the dawn-to-noon quadrant, 13.6% and 10.9%, respectively, of all FA events. The nightside hemisphere as a whole was the locus of 75.6% of all FA events, more than three times as many field-aligned events as were observed in the 12 hours from dawn, through noon, to dusk.

Just as field-aligned events occur primarily at certain magnetic local times, they were observed more frequently at certain invariant latitudes than at others. Figure 16a shows that more FA events occurred (at all MLT's) in the interval

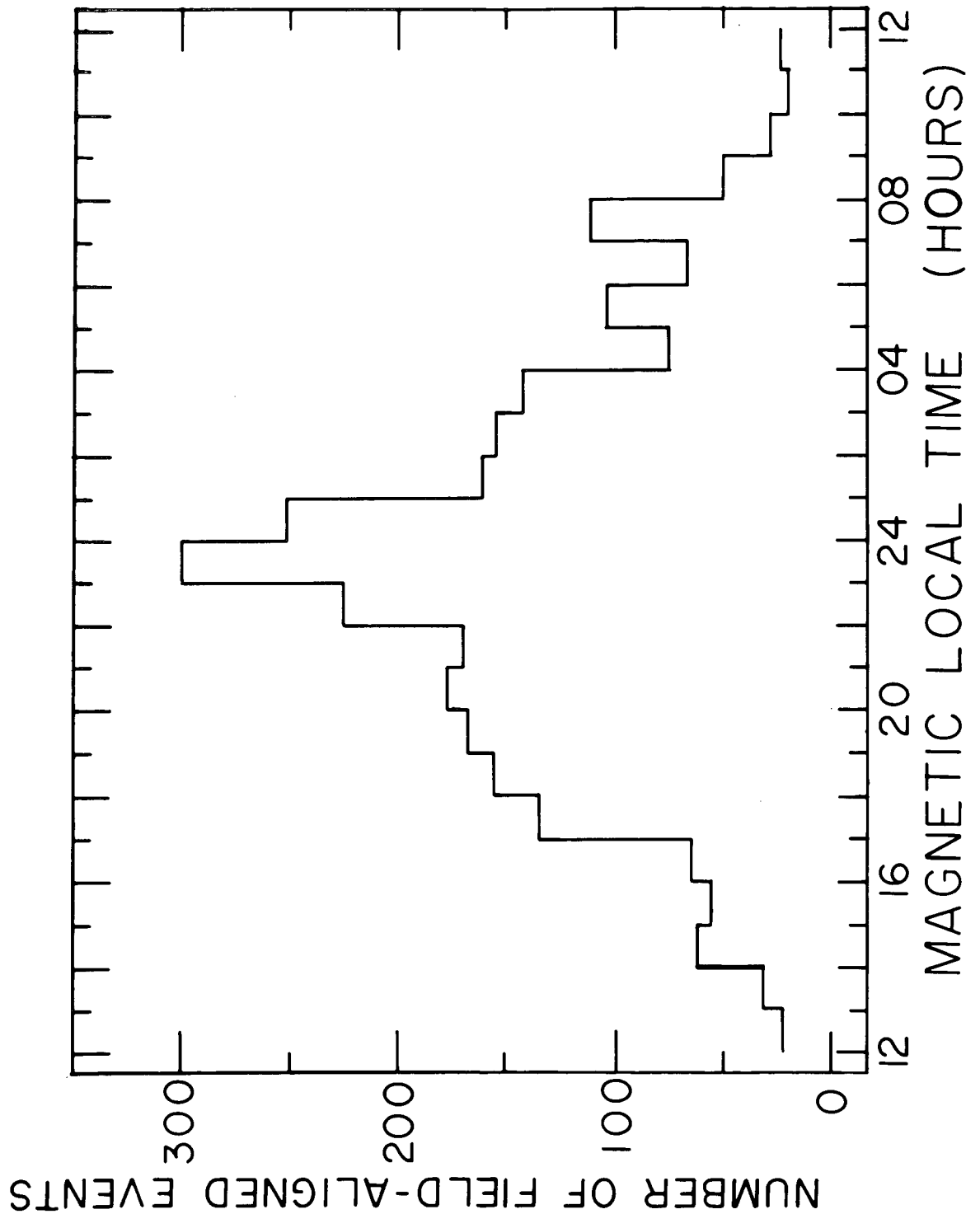

Figure 15. Distribution of field-aligned events as a function of magnetic local time.

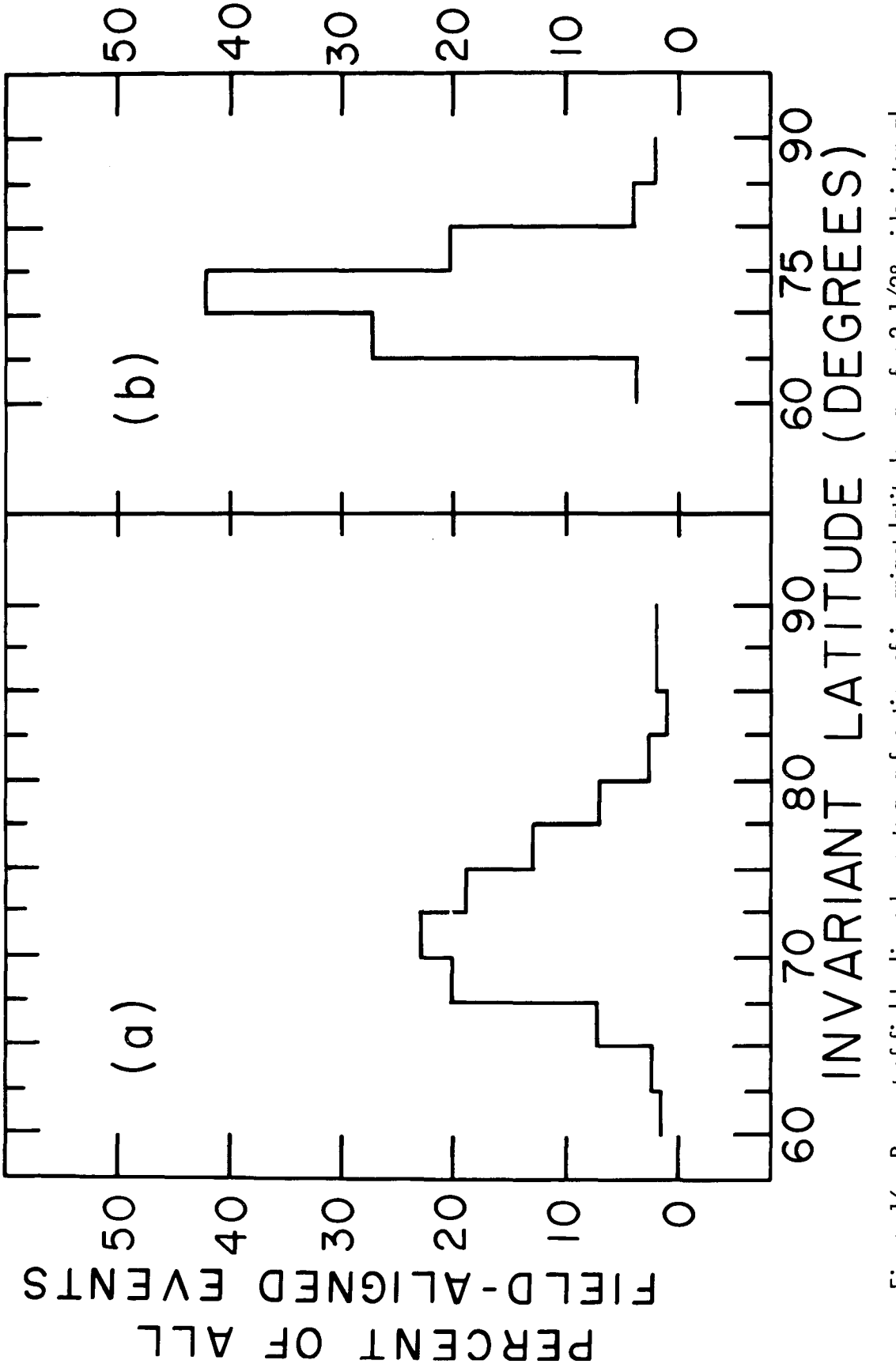

Figure 16. Percent of field-aligned events as a function of invariant latitude: a - for 2-1/2° wide intervals; b - for 5° wide intervals.

$70° \leq \Lambda < 72.5°$ than in any other interval, with 12% - 15% fewer events in the 2-1/2° wide intervals just equatorward and poleward of this "maximum" interval. At $\Lambda < 67.5°$ and $\Lambda > 77.5°$, the numbers of FA events in each of the 2-1/2° wide invariant latitude intervals drop to less than 1/3 of the number in the maximum interval. This peak in the invariant latitude distribution of field-aligned events becomes even more pronounced when the invariant latitude intervals are taken to be 5° wide, as in Figure 16b. The maximum number of FA events, 42.2% of the total, occurred in the interval $70° \leq \Lambda < 75°$. Less than 4% of the total number were observed (at all MLTs) at $\Lambda < 65°$, and only 6.1% were detected at $\Lambda \geq 80°$. Thus, considering all MLTs, 2.3 keV field-aligned precipitation is observed primarily at invariant latitudes between 67.5° and 75°.

VI. PHENOMENA INFLUENCING FIELD-ALIGNED PRECIPITATION

Particle Fluxes and Energies

In all the example passes presented (Figures 1 to 13), the periods of field-aligned precipitation are generally associated with periods of high 0° fluxes, both at 2.3 and 0.7 keV. Three-point energy spectrums of near 0° pitch angle electrons (for electron energies from 0.7 to 7.3 keV) have been constructed for several of the field-aligned and non-field-aligned portions of one of the near-midnight examples, Pass 4351 (Figure 4), and are presented in Figure 17.

Two of the spectrums shown were at times of approximate isotropy, as indicated by the ratio of 0° to 60° 2.3 keV flux (R) having a value near 1. At the time of peak anisotropy in this pass (1604:38), when R = 7.93, the flux of 2.3 keV electrons was more than an order of magnitude higher than during the non-field-aligned period at 1604:27. During the lower latitude portion of this midnight pass, both the isotropic and field-aligned spectrums (spectrums 4 and 1 in Figure 18) were considerably harder than the higher latitude spectrums. Spectrum 1 shows a 2.3 keV flux more than 20 times greater than that of spectrum 4, which is quite typical for isotropic periods during the low latitude portion of Pass 4351.

Averaging over all of the field-aligned and non-field-aligned precipitation events used in this study, average energy spectrums were computed and are presented in

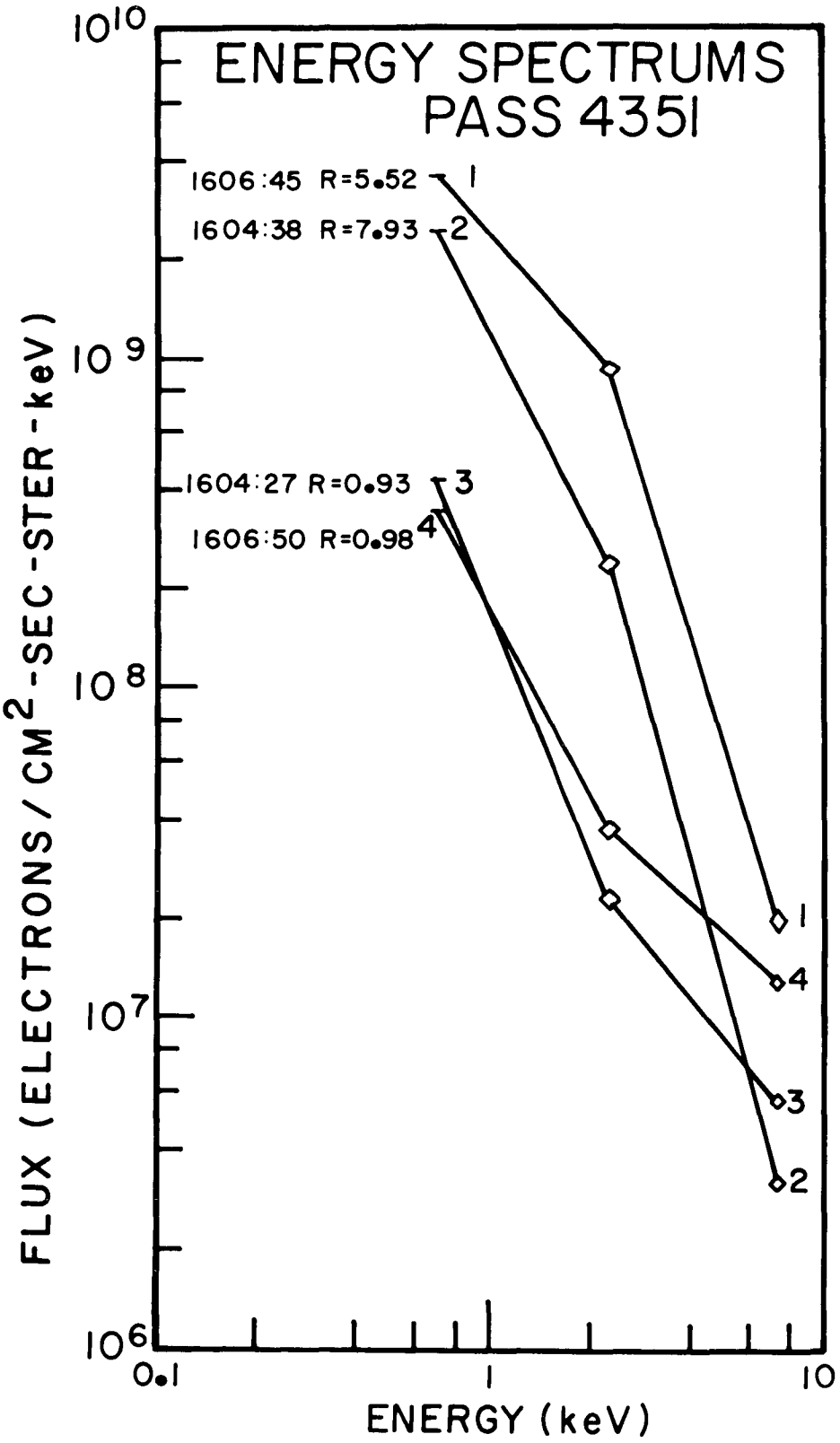

Figure 17. Energy spectrums for four periods during Pass 4351 (Figure 4). Spectrums 1 and 2 were obtained during field-aligned precipitation events. Spectrums 3 and 4 were obtained during times of isotropic fluxes.

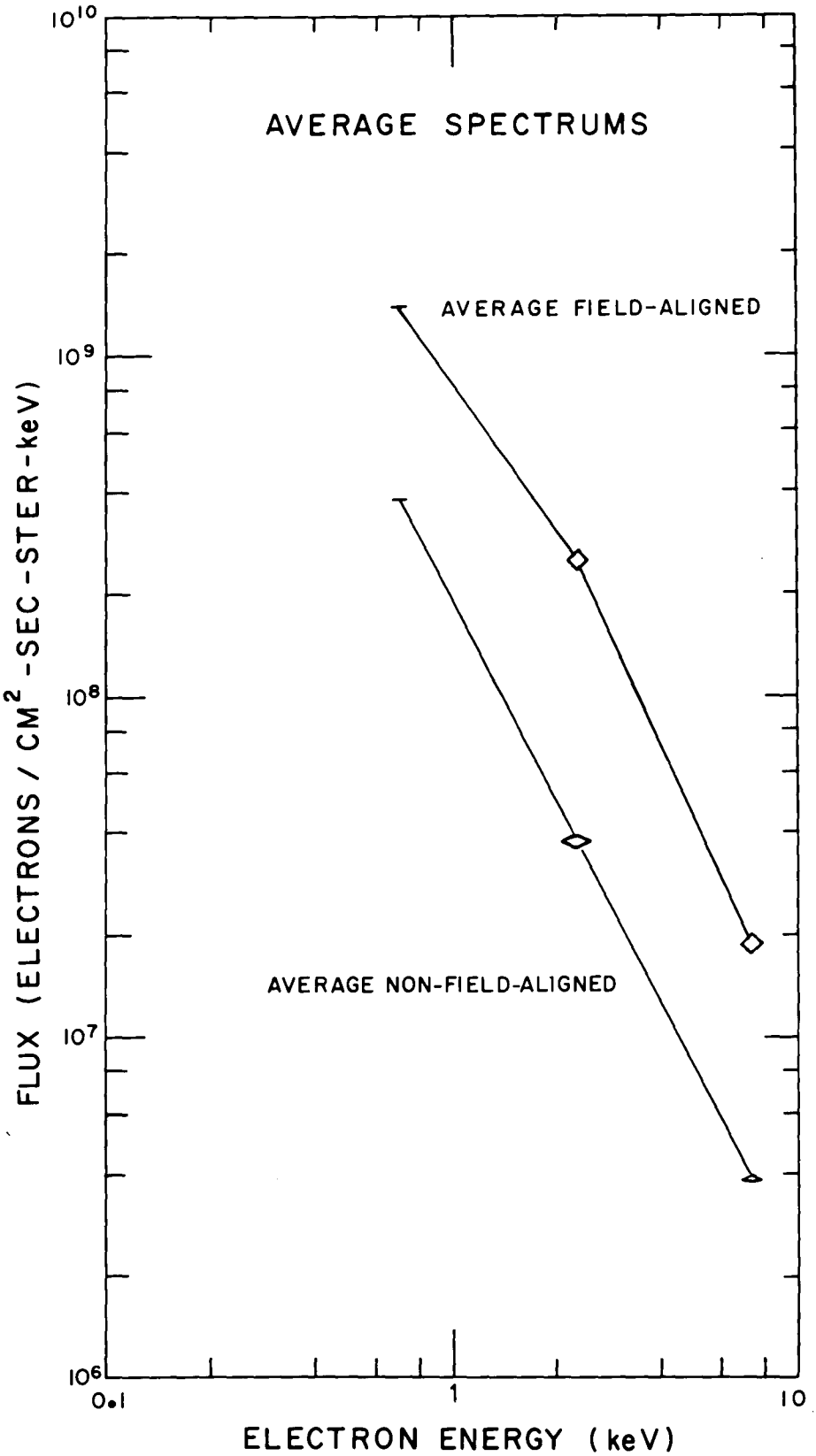

Figure 18. Average three point energy spectrums for all field-aligned and non-field-aligned precipitation events used in this study.

Figure 18. Clearly, the field-aligned precipitation is characterized by a slightly harder, much more intense energy spectrum. If we assume that no fine structure exists in these two energy spectrums, then we can calculate the average energy of the precipitating electrons between 0.7 and 7.3keV. The average energy during non-field-aligned precipitation is found to be 1.83keV, and the average energy during periods of field-aligned precipitation is 1.99keV.

Field-aligned 2.3keV electron precipitation is found to be strongly dependent on particle flux, as is evident from the several data examples presented. In Figure 19, we see that the probability of 2.3keV precipitation being field-aligned increases quite steadily with rising flux of 0° pitch angle electrons. The probability of precipitation being field-aligned increases very rapidly at 0° - 2.3keV fluxes above $\sim 10^9$ electrons/cm^2-sec-ster-keV. There is also a small but noticeable increase in the probability of 2.3keV electrons being field-aligned as the flux of 0° - 0.7 keV electrons rises, becoming significant at fluxes greater than 2×10^9 electrons/cm^2-sec-ster-keV.

In Figure 20, the (integral) percent of precipitation which was field-aligned above given 2.3keV fluxes is shown plotted as a function of the flux of 0° - 2.3keV electrons. Although only 20% of the precipitation was found to be field-aligned when the 2.3keV flux was greater than 10^8 electrons/cm^2-sec-ster-keV, 50% of all 2.3 keV precipitation at fluxes exceeding $\sim 7 \times 10^8$ was field-aligned. All of the precipitation was found to be field-aligned when the 0° - 2.3keV flux exceeded 1.8×10^9 electrons/cm^2-sec-ster-keV, and, conversely, none was field-aligned at fluxes below 2×10^7 electrons/cm^2-sec-ster-keV.

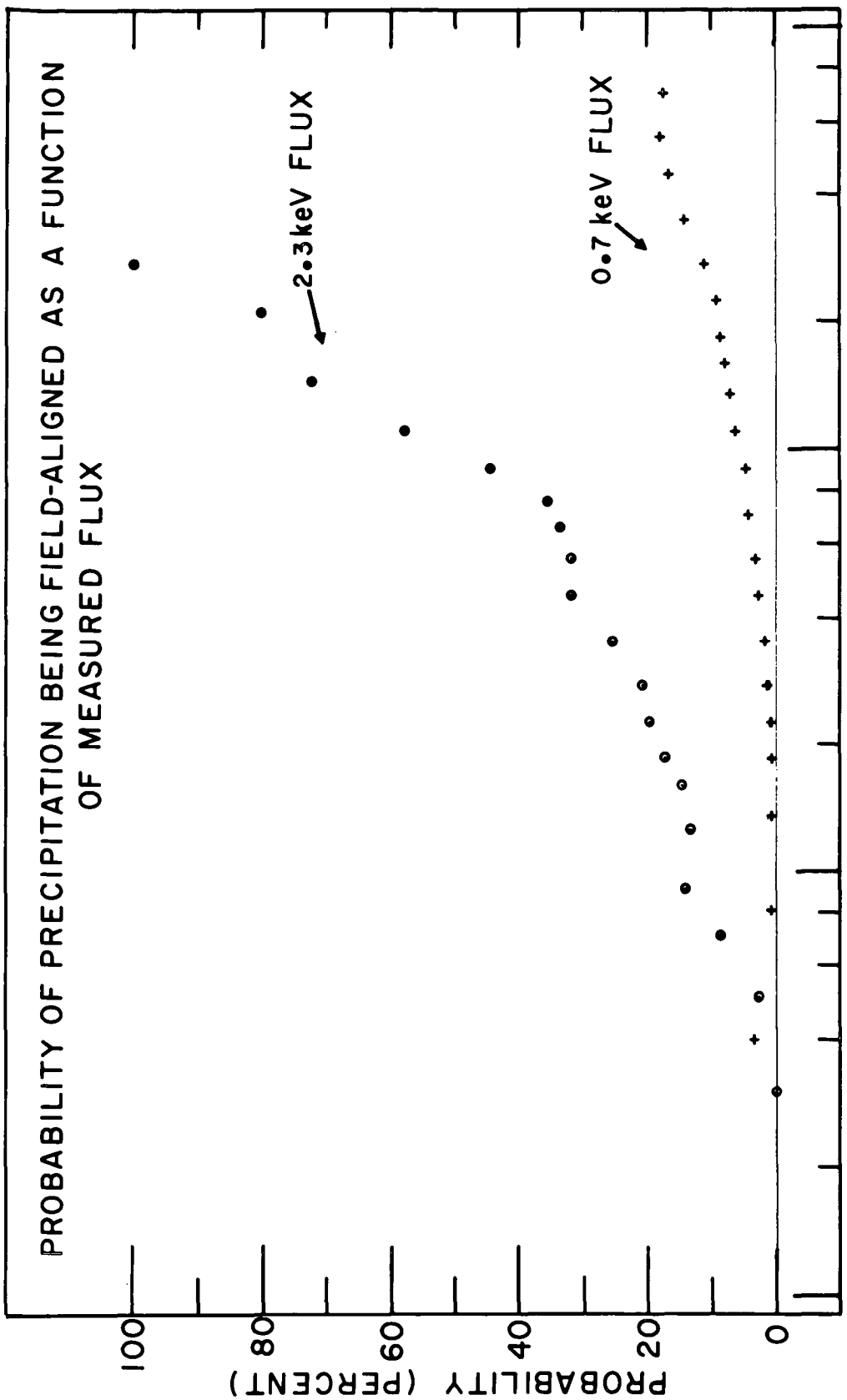

Figure 19. Probability of 2.3 keV precipitation being field-aligned as a function of 0° particle flux at 0.7 and 2.3 keV.

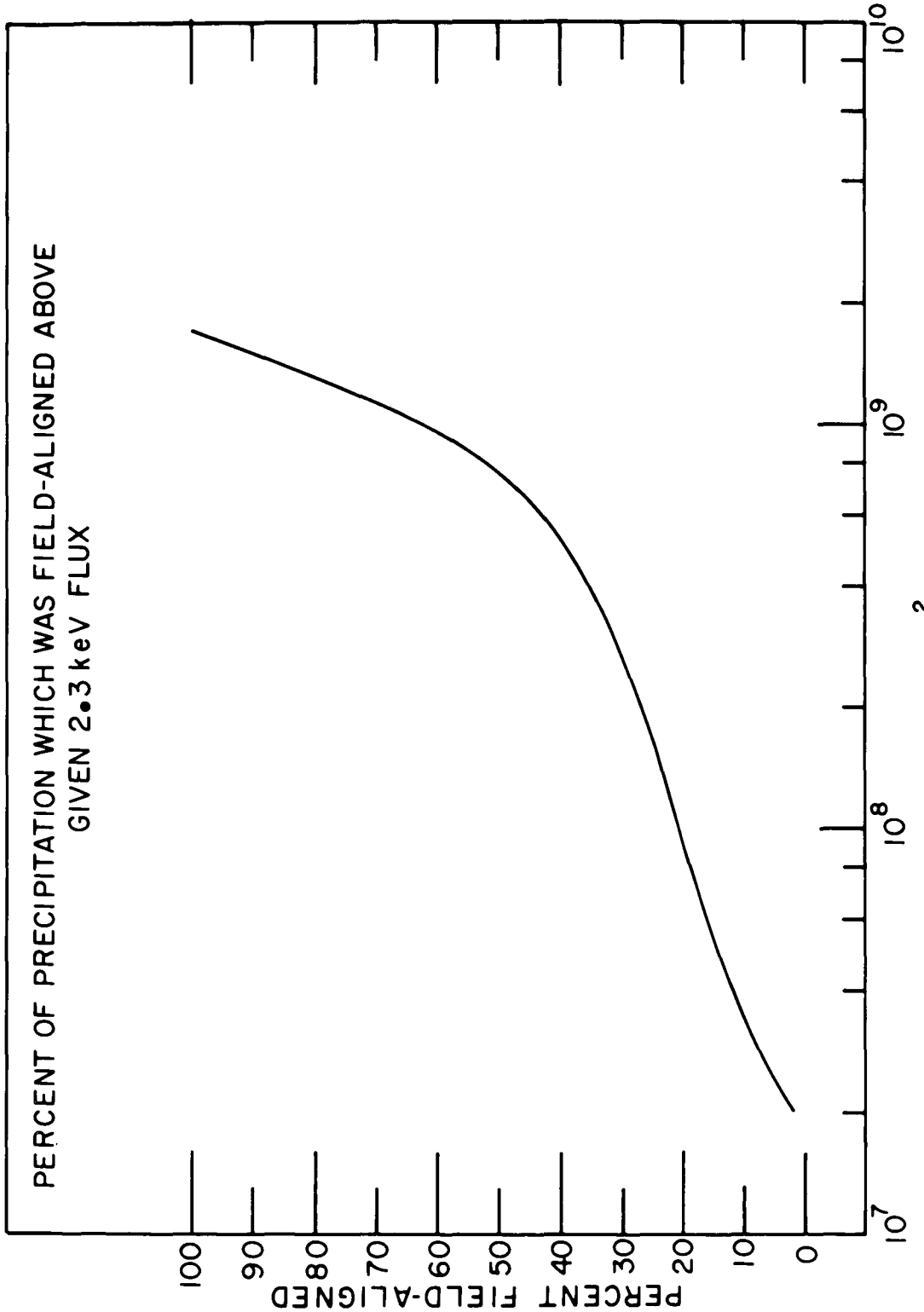

Figure 20. Percent of precipitation which was field-aligned above given 2.3keV fluxes, as a function of the 0° pitch angle 2.3keV flux.

It is also found that higher degrees of anisotropy occurred at higher levels of precipitated 2.3keV electron flux. Ratios of 0° to 60° fluxes greater than 4.0 occurred at 2.3keV fluxes which were, on the average, twice as high as the fluxes when the ratios were 2.0. Higher values of the ratio coincided with even higher 0° - 2.3keV fluxes, although the increase in average flux as the ratio increased to values greater than 4.0 was not as great as the factor of two increase in flux when the ratio increased from 2.0 to 4.0.

Magnetic Disturbances

Another physical parameter which showed a correlation with the occurrence of field-aligned precipitation is the magnetic activity during the periods of data accumulation. Among the several available indicators of magnetic activity are individual ground-station magnetograms, and the Kp and AE indexes derived from ground-station measurements. The Kp index of planetary or worldwide magnetic activity is derived from the mean standardized K-index from 12 stations lying between 48° and 63° northern or southern latitude, and is available in tables of 3-hour mean values for each day. AE, the auroral electrojet activity index (Davis and Sugiura, 1966), is derived as a measure of global electrojet activity.

To compile AE values, 2.5 minute average readings of the horizontal (H) component are tabulated from digitized magnetograms obtained at high latitude northern hemisphere ground stations, distributed as evenly as possible in longitude. The deviations of these H components from their baselines are superimposed on one another, and an upper (AU) and lower (AL) envelope to the superimposed ΔH values (in gammas) can be defined. These envelopes are then the loci of the maximum and minimum of ΔH for the ground stations used. The separation between the AU and

AL envelopes depends upon the maximum eastward and westward electrojet currents. Thus the AE index, defined by the equation

$$AE = AU - AL \quad ,$$

is a direct measure of the total maximum amplitude of east and west electrojet currents, and, consequently, of high-latitude geomagnetic perturbations.

The basic limitations on the use of the Kp index for this study are the latitude coverage of the stations, the inclusion of southern hemisphere stations, the influence of ring current effects, and the relatively long (three hour) time period over which the mean tabulated values are computed. There are also limitations on the values of the AE index, most notably a varying and largely incomplete longitudinal station coverage for the AE values available from the National Space Science Data Center (NSSDC) for the years 1965 - 1968 (Burch, 1972a). However, with its limitations kept in mind, AE hourly averages can be used as fairly good indicators of high latitude northern hemisphere magnetic activity.

Using the one-hour average AE values from the NSSDC, a tendency was found for field-aligned events to have occurred more often when AE was high. As shown in Figure 21, the probability of 2.3keV precipitation being field-aligned generally increases as the value of AE (in gammas) increases. The probability of observing field-aligned precipitation when AE was less than 50γ was about 0.5%, while 9.5% of all precipitation occurring when AE was greater than 800γ was field-aligned. One-half of all the field-aligned events which were included in the distribution of field-aligned precipitation occurred when AE exceeded 120γ, and 80% occurred when AE exceeded 50γ.

Magnetograms from ground-stations which were located approximately beneath the projected path of the satellite during periods of data acquisition are excellent

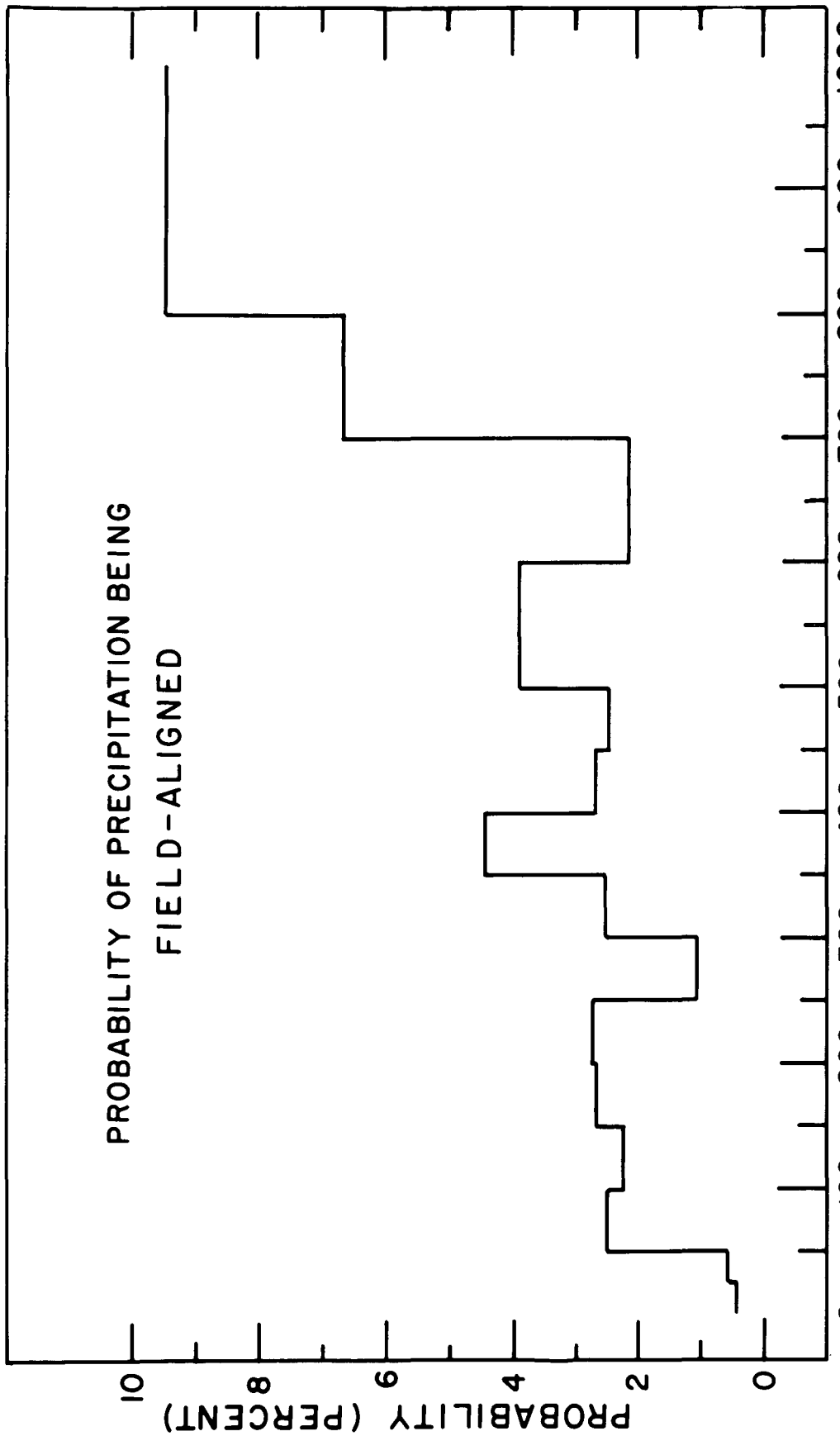

Figure 21. Probability of precipitation being field-aligned as a function of the one-hour average AE value.

indicators of the magnetic conditions which affected the measured precipitation. The top portion of Figure 22 presents the differential number fluxes of 0.7, 2.3, and 7.3keV electrons at 0° pitch angle, as well as the ratio of 0° to 60° fluxes of 2.3keV electrons during Pass 2590, a near-midnight pass. Magnetograms from Barrow, College, and Sitka are presented in the lower portion of the figure, with the time when each of these Alaskan stations passed through midnight indicated by a letter M. The time when Pass 2590 occurred is shown by a vertical line through the magnetometer traces, indicating that the data shown above were obtained during the expansion phase of a substorm. This substorm showed up as a 590γ bay at College, and a depression of over 650γ in the H component at the higher latitude Barrow station.

Experiment turn-on for Pass 2590 was at 1020:08, and particle fluxes are plotted from this time until the high-latitude boundary of 0.7keV electron precipitation was reached at 1023:19, when $\Lambda = 74.0°$. Similar boundaries for 2.3 and 7.3 keV electrons occurred at 1023:13, at $\Lambda = 73.6°$. The area under the 0° to 60° ratio histogram has been shaded where the 2.3keV precipitation was field-aligned. There are two fairly distinct regions of precipitation evident in this pass: a lower latitude region of fairly diffuse, very isotropic fluxes; and a higher latitude region of structured, often anisotropic precipitation (Hoffman and Berko, 1971b). Field-aligned fluxes occurred only during the latter portion of the pass, and the last field-aligned portion occurred at the high-latitude boundary of 2.3keV precipitation. From 1021:33 to 1022:03, the beginning of the first field-aligned period at $\Lambda = 69.8°$, the 7.3keV flux was less than 10^5 electrons/cm^2-sec-ster-keV.

A search through the OGO-4 data revealed 37 additional passes which traversed the dusk-to-midnight sector during periods of clearly quiet magnetic conditions, or

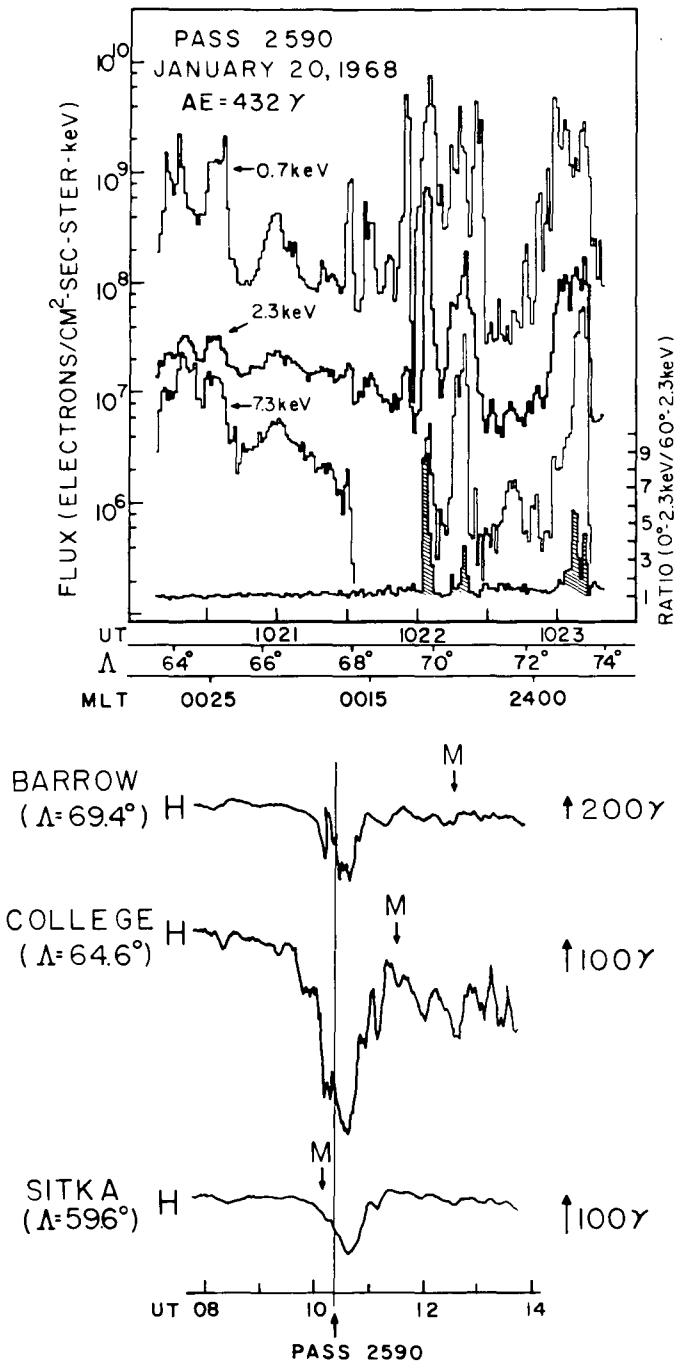

Figure 22. One-second average fluxes of 0.7, 2.3, and 7.3 keV near 0° pitch angle electrons, and the ratio of 0° - 2.3 keV to 60° - 2.3 keV electron fluxes, for a midnight pass during substorm expansion. Periods of field-aligned precipitation are indicated by cross hatching. Three magnetograms for the time period are shown with a heavy vertical line indicating the time when Pass 2590 occurred.

during substorm expansion, as determined from all available ground magnetograms. Each of these 38 passes also had well-defined high latitude particle cutoffs. The latitudinal distribution of near 0° pitch angle electron precipitation for three different energies is shown in Figure 23 for these passes, which are separated into three categories according to substorm activity and the direction of the interplanetary magnetic field (Burch, 1972b; Hoffman, 1972).

When the interplanetary magnetic field was directed north and the geomagnetic field was quiet, the high latitude particle cutoffs were at the highest latitudes, and the precipitation was generally isotropic. Only a few of the passes occurring under these "quiet-north" conditions had any appreciable field-aligned precipitation, and all of it was at high latitudes ($\Lambda > 72°$) and often at or near the high latitude boundary of 2.3keV precipitation.

Those passes shown in the lower left section of the figure occurred when the interplanetary magnetic field, (as observed by Explorers 33 and 35), was directed south, but ground station magnetograms indicated quiet magnetic conditions prior to breakup. No pitch angle anisotropies were observed during any of these pre-breakup passes, but the high latitude particle cutoffs were several degrees lower than the typical values of Hoffman (1969) and Burch (1968).

Passes occurring during the expansion phase of substorms all had field-aligned 2.3keV precipitation, indicated by a heavy vertical mark across the 2.3keV "precipitation line," the width of the mark corresponding to the latitudinal extent of the anisotropies. The field-aligned precipitation during these passes was generally at or near the high latitude boundary of auroral electron precipitation. This is especially evident in those passes which occurred during orbits 968, 2988, and 3247.

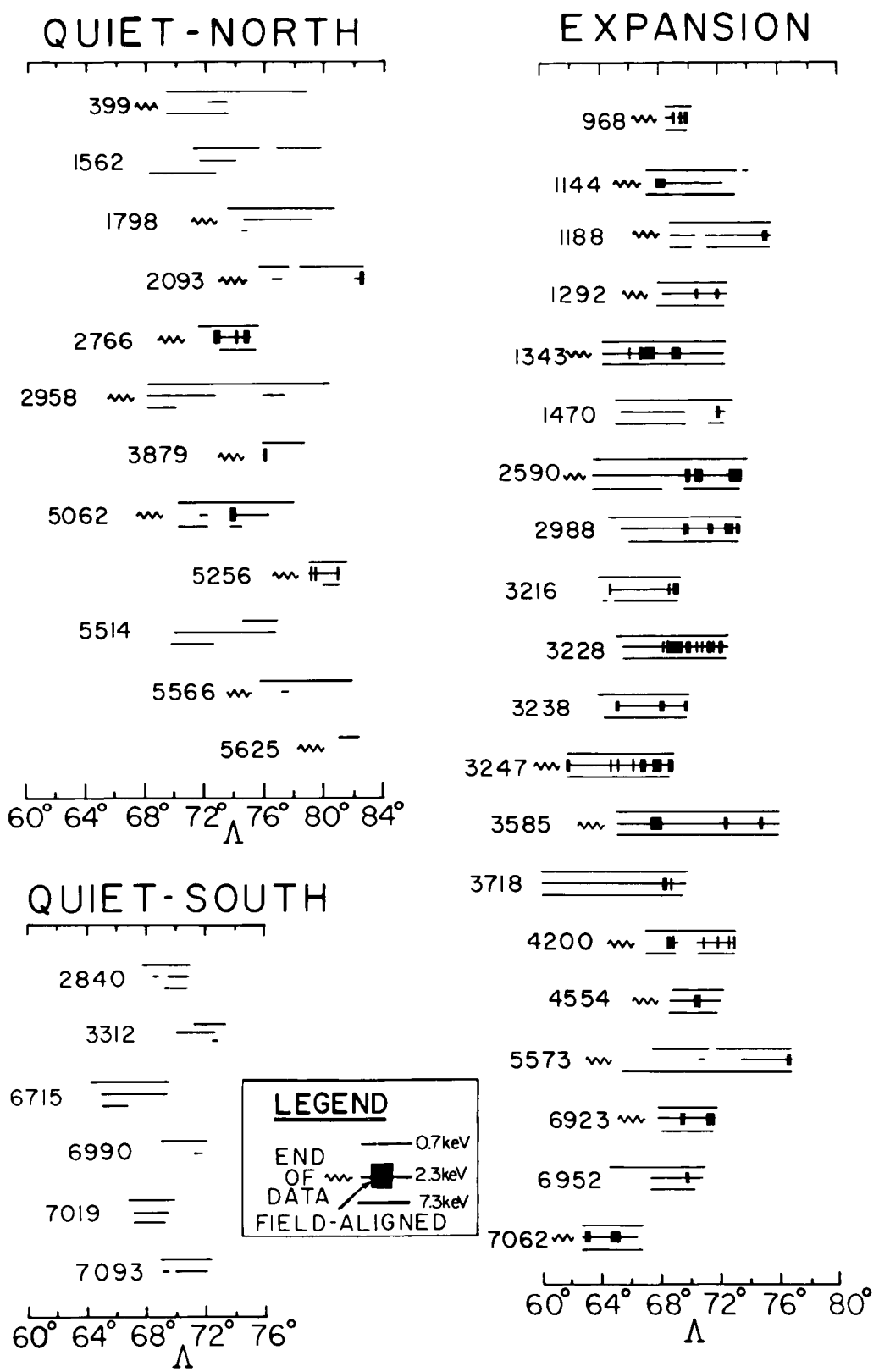

Figure 23. Latitudinal distribution of auroral electron precipitation at three energies for 38 passes in the dusk-to-midnight sector. The orbit number is given for each pass.

Thus, field-aligned 2.3keV electron precipitation, especially during times of magnetospheric substorms, is usually associated with the high latitude, or poleward portion of the auroral electron precipitation.

Universal Time and Seasonal Effects

The effects, if any, of universal time (UT) on field-aligned precipitation are not obvious or straightforward. While there is an apparent peak in the percent of field-aligned events per hour UT (normalized to account for uneven sampling in UT) at 9 to 10 hours, the percent of events fluctuates too much from hour to hour to be truly meaningful. If one considers only precipitation in the interval $67.5° \leq \Lambda \leq 75°$ and 22 hours $\leq$ MLT $\leq$ 1 hour, the percent of field-aligned events appears to be peaked in the UT intervals 9-10, 12-14, and 20-21 hours. Thus, even the precipitation in the region of maximum field-aligned events shows no clear UT dependence.

Seasonal effects do seem to influence the occurrence of field-aligned precipitation, and may be associated with possible UT effects. After normalizing the percent of field-aligned events in each season to account for uneven seasonal sampling of precipitation, a definite winter peak appears. As indicated in Table 6, almost half of the seasonally normalized field-aligned events occurred during the winter season, while only 12% were detected in the summer. Even taking into account that 42% of all the winter precipitation events occurred in the 21 hour to 03 hour MLT interval, but only 26.5% of the summer events were within 3 hours of local midnight, the MLT interval in which more than half of all field-aligned precipitation was observed, there is still a distinct peak in the winter months.

The combined seasonal and UT effects on field-aligned precipitation are illustrated in Figure 24 for the winter and summer months. During the winter months,

SEASONAL DIFFERENCES IN FIELD-ALIGNED PRECIPITATION FREQUENCY

Season	Percent of All Precipitation Events	Percent of Precipitation Events in MLT Interval 21 Hours-03 Hours	Number of Field-Aligned Events	Percent of All Field-Aligned Events Normalized to Even Seasonal Sampling
Winter	9.42	41.98	556	48.67
Spring	16.82	30.15	495	24.28
Summer	52.56	26.46	767	12.04
Autumn	21.20	23.61	386	15.01

TABLE 6

when the high-latitude northern hemisphere is receiving only minimal amounts of solar radiation, most of the field-aligned precipitation was observed between 9 and 15 hours UT. In the summer months, when solar heating is much greater in the northern hemisphere, almost 50% of the field-aligned events were observed between 15 and 21 hours UT. It is likely that sunlight effects on the ionosphere may be closely associated with the field-aligned electrons observed by OGO-4.

Variations with Altitude

The variation in the number of field-aligned events with satellite altitude is an effect which appears to be closely associated with seasonal effects. The percentages of field-aligned events and of the total number of 2.3keV precipitation events in each season at the highest and lowest altitudes attained by OGO-4 are listed in Table 7, as well as the totals for all seasons. From the tabulated values, we see that in the winter and autumn months, field-aligned precipitation occurred with much higher probability at altitudes greater than 800km than at low altitudes. In contrast, the

F

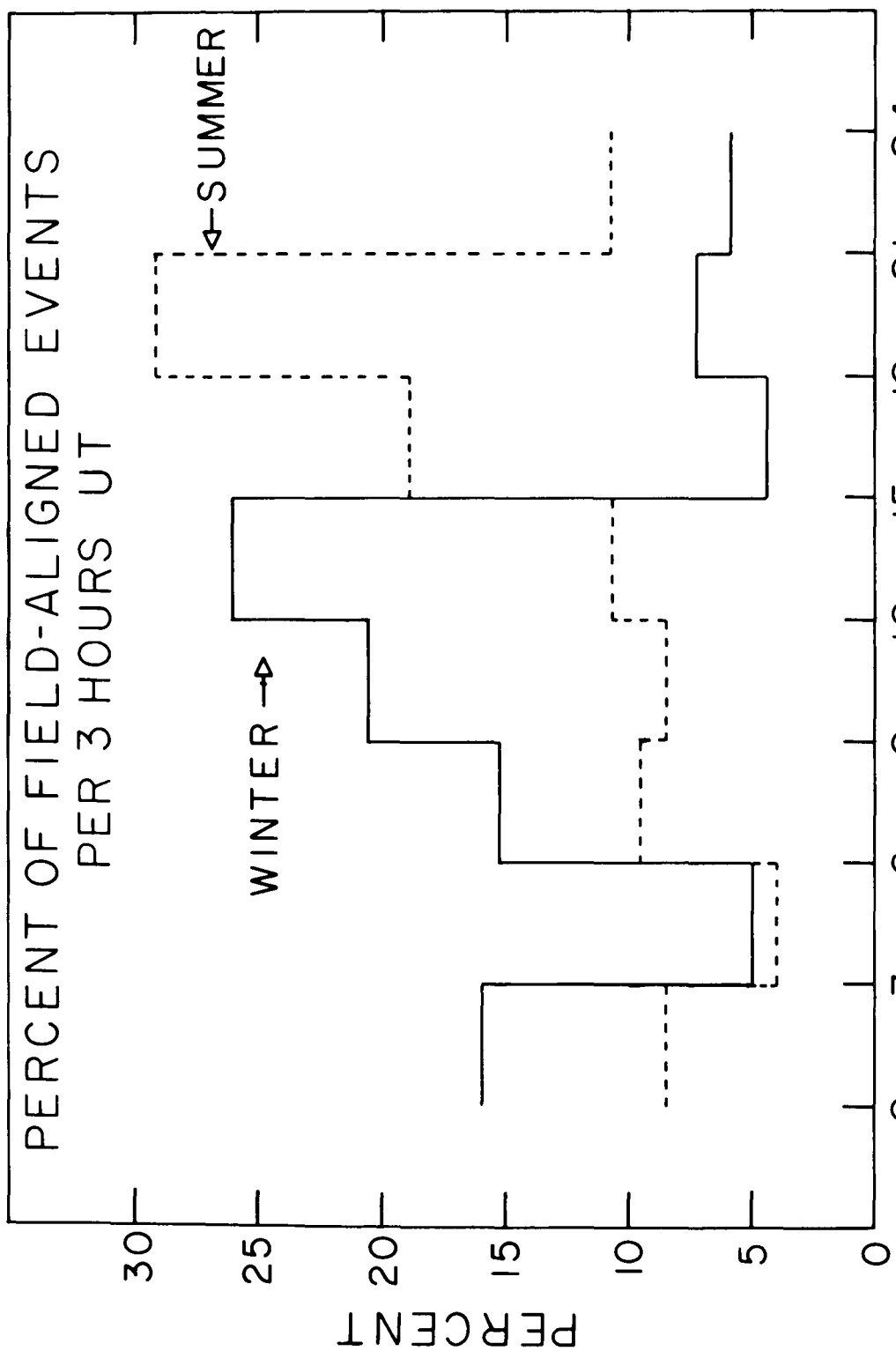

Figure 24. Winter and summer universal time modulation of field-aligned precipitation.

ALTITUDE VARIATION OF FIELD-ALIGNED PRECIPITATION

Season	Altitude Range (km)	Percent of All Events in That Season	Percent of All Field-Aligned Events in That Season	Probability of Event Being Field-Aligned in That Altitude Range in That Season
Winter	<500	34.6%	19.8%	2.85%
	>800	17.6	38.5	10.91
Spring	<600	22.5	24.3	2.67
	>800	25.7	38.4	3.70
Summer	<500	12.2	24.5	2.47
	>800	14.5	25.8	2.19
Autumn	<500	57.0	22.3	0.60
	>800	9.8	26.4	4.14
All Seasons	<500	22.7	21.1	1.72
	>800	15.7	31.9	3.79

TABLE 7

probabilities are about equal in the spring and summer months. Considering data from all seasons, the probability for field-aligned precipitation to occur is higher at the highest altitudes.

Since both the altitude and universal time variations are associated with seasonal differences, it is reasonable to seek some relationship between them. Solar heating of the ionosphere increases its conductivity and raises its density at higher altitudes. Only the very low density upper high latitude ionosphere is appreciably sunlit during the winter and for most of autumn. During the spring and summer months, the northern hemisphere ionosphere expands in altitude due to heating of

its lower layers by fairly direct sunlight, and the plasma density of the lower ionosphere increases due to electron heating (Coroniti and Kennel, 1972). The degree to which ionospheric scattering and conductivity changes might influence the altitude differences observed in the occurrence of field-aligned precipitation can be easily determined.

The angular spreading, or "de-focusing", of a beam of 2.3keV field-aligned electrons due to ionospheric scattering at high altitudes can be calculated fairly easily. Taylor et al., (1971) have reported high latitude H^+ number densities of 2-4 x $10^1/cm^3$ at 500-600km altitudes and 3-4 x $10^2/cm^3$ at 800-900km altitudes measured by OGO-4 at the autumnal equinox. Using the empirical relation given by Fermi (1950) for the angular spreading of a beam of electrons due to scattering, and normalizing the values of Taylor and co-workers to sea level atmospheric density, one computes that the angular spreading of an initially anisotropic (i.e., field-aligned) beam of 2.3keV electrons due to upper ionospheric scattering is less than $\sim 2 \times 10^{-7}$ degrees at altitudes greater than 500km. Thus, electron scattering in the ionosphere cannot account for an enhanced number of field-aligned precipitating electrons at higher altitudes than at lower altitudes.

Ionospheric conductivities are functions of density and collision frequency. As shown by Hanson (1965), the ionospheric conductivity in the direction of the magnetic field, often referred to as the ordinary or parallel conductivity, is given by:

$$\sigma_{\parallel} \cong n\ e^2 \left[\frac{1}{m_e \nu_e} + \frac{1}{m_i \nu_i} \right] ,$$

where n is the electron (or ion) number density, ν_e and ν_i are electron and ion collision frequencies, and m_e and m_i are the electron and ion masses. Using 1.6 x

10^{-20} emu for the electron charge, Hanson calculates that the parallel conductivity (in sunlight) varies from $\sim 5 \times 10^{-10}$ abmho/cm at 500km to $\sim 7.5 \times 10^{-10}$ abmho/cm at 900km. Nighttime values were found to be $\sim 3 \times 10^{-10}$ abmoho/cm at 500km and $\sim 8 \times 10^{-10}$ abmho/cm at 900km. The nighttime values should correspond roughly to a winter season ionosphere, while daytime values should approximate summer conditions. Neither Pederson nor Hall conductivities are usually appreciable at altitudes greater than $\sim$ 300km (Hanson, 1965). Although the high altitude winter (nighttime) conductivity is more than twice that at low altitudes, this difference cannot explain the enhanced winter high altitude occurrence of field-aligned precipitation, since if the precipitation were field-aligned at 900km, the conductivity would not prevent it from remaining so at 500km. Thus, sunlight ionospheric conductivity enhancement is not able to explain the higher probability of observing field-aligned precipitation at high altitudes during the winter months.

Magnetic field lines penetrating into the upper ionosphere cannot carry unlimited amounts of parallel current. Kindel and Kennel (1971) have shown that when fluxes of charged particles exceed certain threshold values, (comparable to those typically measured by OGO-4 during bursts of field-aligned electrons), the ionosphere is unstable to plasma growth, and electrostatic-wave instabilities will be generated in the topside ionosphere. The non-linear development of current driven instabilities leads to the appearance of 'anomalous' parallel resistivities in the ionosphere, and thus to the establishment of (localized) parallel electric fields. Kindel and Kennel show that the thresholds of current necessary to drive the ion-cyclotron or ion-acoustic instabilities responsible for the anomalous resitivities are proportional to the ionospheric density; i.e., the denser the ionosphere, the higher the critical current necessary to trigger an instability.

In examining the relationship of parallel electric fields to the observations of field-aligned electrons, certain physical constraints must be considered. Charged particles moving in the earth's magnetic field undergo motion governed by adiabatic constants of motion (Roederer, 1967). The first adiabatic invariant, μ, the magnetic moment, is defined by

$$\mu = \frac{W_\perp}{B} = \frac{W \sin^2 \alpha}{B} = \text{constant}, \tag{1}$$

where W is the energy of the particle, α is the pitch angle, and B is the magnetic field strength. For a particle moving between an initial and final location, equation 1 can be written in the equivalent form

$$\frac{W_i \sin^2 \alpha_i}{B_i} = \frac{W \sin^2 \alpha_f}{B_f}. \tag{2}$$

In addition to conserving the magnetic moment, particles moving through an electric potential V extending over a finite region of space must also satisfy energy conservation

$$W_f = W_i + eV, \tag{3}$$

where W_i is the initial kinetic energy and W_f is the kinetic energy of the particle with charge e after having passed through an electric field region with potential V.

Electrons traversing a region of parallel electric field will be accelerated by the amount given in equation 3. If the energy of the electron increases faster than the magnetic field (to conserve μ), then from equation 2 it follows that the pitch angle distribution at B_f (where the electron exits the accelerating field) will have an upper maximum less than 90°. Assuming that the electrons were fairly isotropic

when they entered the $E_{\parallel}$, then the pitch angle cutoff under the above conditions at B_f is given by

$$\sin^2 \alpha_{f_{max}} = \frac{B_f W_i}{B_i W_f} < 1. \tag{4}$$

Thus, the width of the pitch angle distribution at B_f will decrease with increasing ratio of energy increase to magnetic field increase between B_i and B_f. This parallel electric field acceleration process is therefore a focusing mechanism, leading to a pitch angle distribution cut-off at progressively smaller angles, i.e., eventually a field-aligned pitch angle distribution.

Liouville's theorem tells us that the ratio of the differential directional flux at energy W, j(W), to the energy W is a constant along the particle's trajectory. Thus, we have the additional condition that

$$\frac{j_i (W_i, B_i)}{W_i} = \frac{j_f (W_f, B_f)}{W_f} . \tag{5}$$

Equation 5 indicates that the flux change is independent of pitch angle, and hence, from the assumed isotropy at B_i, we see that the fluxes will be isotropic within the cone defined by equation 4. In addition, the fluxes will be increased by the energy ratio W_f/W_i.

In an attempt to explain the enhanced probability of observing field-aligned precipitation at high altitudes during the winter months, we now examine the relationship between seasonal ionospheric density variations and parallel electric fields. The ionospheric instabilities described by Kindel and Kennel (1971), which give rise to anomalous resistivities resulting in the creation of parallel electric fields, are dependent on density. Ionospheric density at high altitudes is appreciably greater

under sunlit, summer conditions than during winter conditions, due to thermal expansion of the ionosphere. Thus, parallel electric fields can exist at lower altitudes in winter than in summer.

Consider for example a possible summer situation. When the particle flux exceeds the critical instability value, anomalous resistivity will occur, creating a region of parallel electric field as indicated schematically in the top portion of Figure 25. Since the entire region of $E_{\parallel}$ exists at altitudes greater than satellite apogee, only those electrons initially in the shaded region where the potential is ~ 2.3 kV will be detected as field-aligned 2.3keV electrons at any satellite altitude from apogee to perigee. In this $E_{\parallel}$ configuration, approximately equal numbers of field-aligned 2.3keV electrons would be detected at altitudes < 500km and > 800km, which is the situation indicated for the summer months in Table 7.

In the winter months, the parallel electric field region can occur at considerably lower altitudes than in summer. Winter upper ionospheric densities are much less than summer values, especially at nighttime, and consequently, anomalous resistivities can be triggered at much lower altitudes. Consider the situation illustrated in the lower part of Figure 25, where a portion of the electric field region extends to altitudes below 900km. Under this situation, almost all of the (initially cold) electrons would be accelerated to the full value of the potential, exiting the lower portion of the electric field region with energies greater than 2.3keV. However, if the satellite-borne detectors should pass through the lower part of the $E_{\parallel}$ region, say at altitudes between 800km and 900km, then, depending on the maximum potential of the electric field region and its upper altitude, particles with small pitch angles, not accelerated through the full potential, could be measured

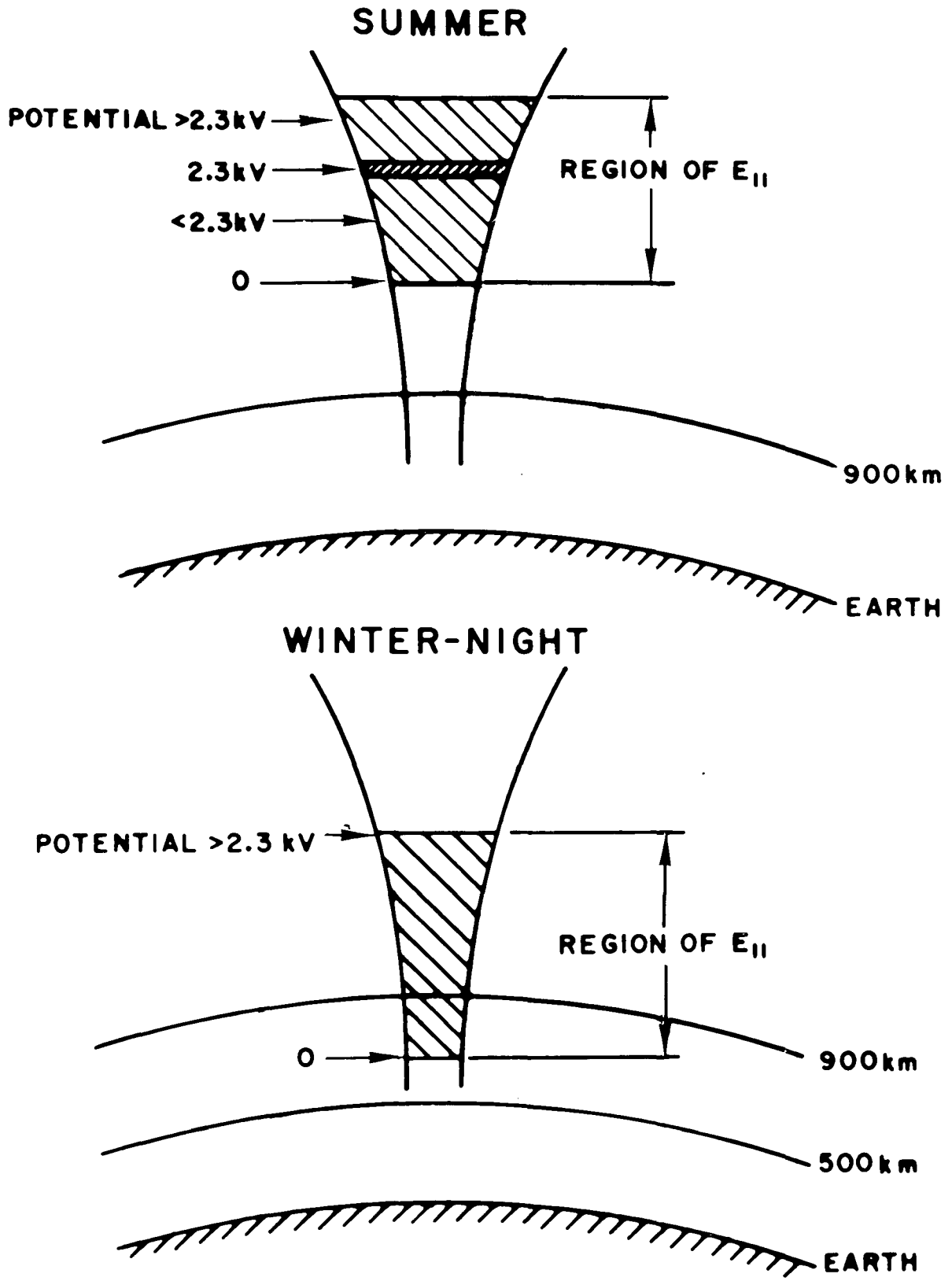

Figure 25. Schematic representation of two possible parallel electric field configurations: top - probable summer, fully sunlit situation; bottom - possible winter, nighttime situation.

within the bandpass of the 0° - 2.3keV detector. Hence, under these ideal conditions, the probability of observing field-aligned 2.3keV electrons would be much greater at altitudes > 800km than at altitudes < 500km.

In either the summer or winter field configurations, the electric field strengths necessary to perform the acceleration are of the order of several millivolts per meter. Parallel electric field strengths of about 10mV/m have been reported by Mozer and Fahleson (1970).

VII. COMPARISONS WITH OBSERVATIONS OF OTHER PHENOMENA

Auroral Optical Emissions

As has been noted previously, the field-aligned precipitation is found to occur most frequently in the nighttime hours when particle fluxes are fairly high. Accordingly, one may reasonably seek an association between field-aligned precipitation and optical aurora in the nighttime hours. To make a meaningful comparison, an optical study was sought which employed procedures most analogous to those used in determining the distribution of field-aligned precipitation presented in Figure 14. Thus, a suitable optical study should be synoptic in nature, have occurred during a similar epoch of the solar cycle, and have resolution in invariant latitude and local time comparable to the size of the elements in the distribution of field-aligned precipitation events.

Optical auroral frequency studies of Feldstein (1966), Lassen (1969), Sandford (1964, 1968), and Stringer and Belon (1967) were each considered. Of these four ground-based studies, the work of Stringer and Belon was the one which best conformed to the established criteria and is thus the most suitable for comparison with the satellite auroral particle observations.

Making use of data acquired by an all-sky camera network based in Alaska during the winter of 1964-65, Stringer and Belon (1967) produced contour maps showing

the probabilities of observing discrete, homogeneous, and all auroral forms in 15 minute intervals. It is their isoauroral diagram for all auroral forms which are compared to the distribution of field-aligned precipitation, since data obtained under all magnetic conditions were used in determining the regions of this type of precipitation.

In Figure 26 the shaded regions from 16 hours, through midnight, to 8 hours local time show where the probability of observing all auroral forms presented by Stringer and Belon (1967) was greater than 25%. The heavy lines in these same hours enclose the areas (from Figure 14) where more than at least 30 field-aligned precipitation events were observed. There is clearly a great deal of congruity of these two regions, especially during the 18 hour to 01 hour local time segment. However, at all local times, except near dawn, most of the field-aligned precipitation occurred poleward of the auroral optical emissions.

This spatial relationship is consistent with sounding rocket observations by Whalen and McDiarmid (1972), who observed auroral electron precipitation to be especially field-aligned as their rocket payload crossed the poleward edge of the visual aurora. Airplane studies of polar cap (i.e., very high latitude) aurora by Eather and Akasofu (1969) indicated that the field-aligned bursts of electrons reported by Hoffman and Evans (1968) would tend to excite the patches of northern high latitude auroral forms which they observed. Both of these findings are consistent with the results of the comparison made using Figure 26, and complement the pattern of field-aligned precipitation occurring at or near the high latitude boundary of auroral particle precipitation in the nightside hours noted in Section VI.

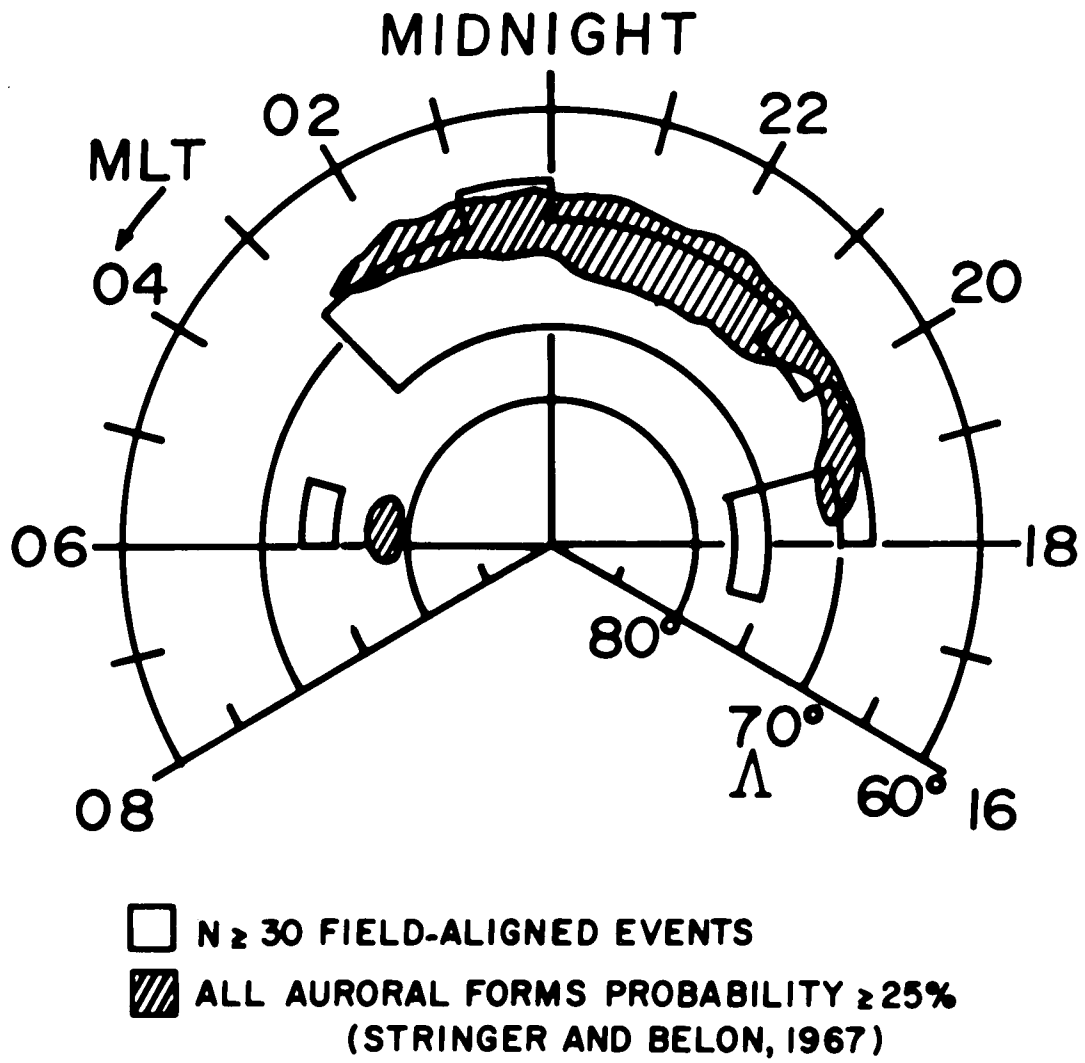

Figure 26. Polar projection of the regions of high numbers of field-aligned events in the nighttime hours in comparison with the region of high probability of all auroral forms (Stringer and Belon, 1967) during the same hours.

Auroral Hiss

Hoffman and Laaspere (1972) have recently shown an excellent correlation between the locations of the auroral hiss zone at 200 kHz and the region of soft electron precipitation. This comparison was made using particle data from OGO-4 (Hoffman and Berko, 1971a) and Very Low Frequency electromagnetic wave (VLF) data from OGO-6 (Laaspere et al., 1971), both sets of which were obtained under quiet magnetic conditions ($Kp \leq 2$). Additional comparisons made between data collected simultaneously by two OGO-4 experiments led them to conclude that VLF hiss correlates well with 0.7 keV electron precipitation events on the dayside, but generally poorly with higher energy (i.e., 2.3 keV and 7.3 keV) precipitation.

This latter result is not surprising, since it has already been shown that soft (e.g., ≤ 1 keV) electrons constitute the primary energy input to the dayside auroral oval (Hoffman and Berko, 1971a). However, it is still meaningful to attempt a comparison between the region of field-aligned 2.3 keV precipitation (from Figure 14) and the locations of the centers of the auroral hiss zone at 200 kHz from Laaspere et al. (1971). The superposition of these two sets of data is presented in Figure 27. More than two-thirds of the 200 kHz centers occurred in the regions where at least 10 field-aligned events were observed. A general pattern of field-aligned events and 200 kHz centers occurring at higher latitudes in the dayside than near midnight is clearly evident. Aside from the 200 kHz centers between 10 and 13 hours MLT, 77.5% of the centers are located in regions where 10 or more field-aligned events were detected. Both the auroral hiss and field-aligned fluxes are associated with structured precipitation. Thus, there appears to be a good correlation (except near

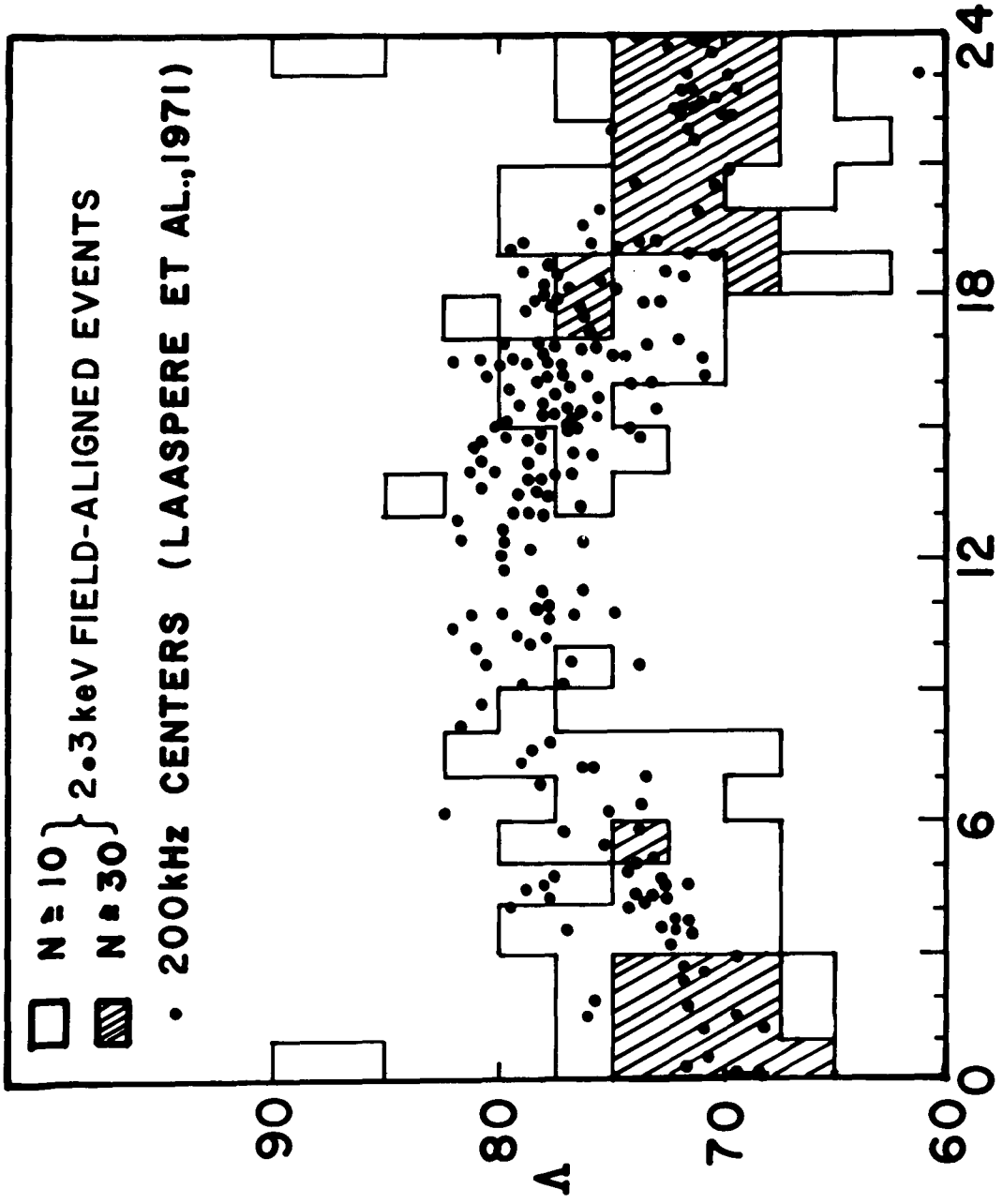

Figure 27. Comparison of the regions of observing field-aligned precipitation events with the location of 200 kHz centers (Laaspere et al., 1971).

local noon) between this particular VLF emission and 2.3 keV field-aligned electron precipitation at high latitudes.

Transverse Magnetic Disturbances

As mentioned in Section II, transverse magnetic disturbances have been observed at high latitudes by Zmuda et al. (1966) from the satellite 1963-38C. In later work, Zmuda et al. (1970) presented a statistical study indicating the spatial extent of transverse magnetic disturbances for different ranges of the magnetic activity index Kp. Although their data were primarily from the dayside because of the normal ground-station working hours and the solar-only mode capability of the satellite 1963-38C, their region of transverse magnetic disturbances, observed in the period February 1964 through May 1968, showed the same tendency of lying at higher latitudes in the dayside hours than near midnight as does the distribution of field-aligned precipitation shown in Figure 14. At midnight, under quiet magnetic conditions ($Kp \leq 2^+$), their region of transverse disturbances, which they associate with field-aligned currents, lay between 69° and 72° Λ, also in excellent agreement with the peak values of Figure 14.

A maximum, i.e., latitudinally widest, region of transverse magnetic disturbances has been arrived at from the regions for various Kp ranges presented by Zmuda et al. (1970). This region, indicated by the cross-hatched area in Figure 28, is superimposed on the regions of more than at least 10 field-aligned precipitation events (from Figure 14). General agreement in the location of these two regions is quite good, except between about 8 hours and 14 hours MLT, where very few 2.3 keV field-aligned precipitation events were detected. However, electron precipitation

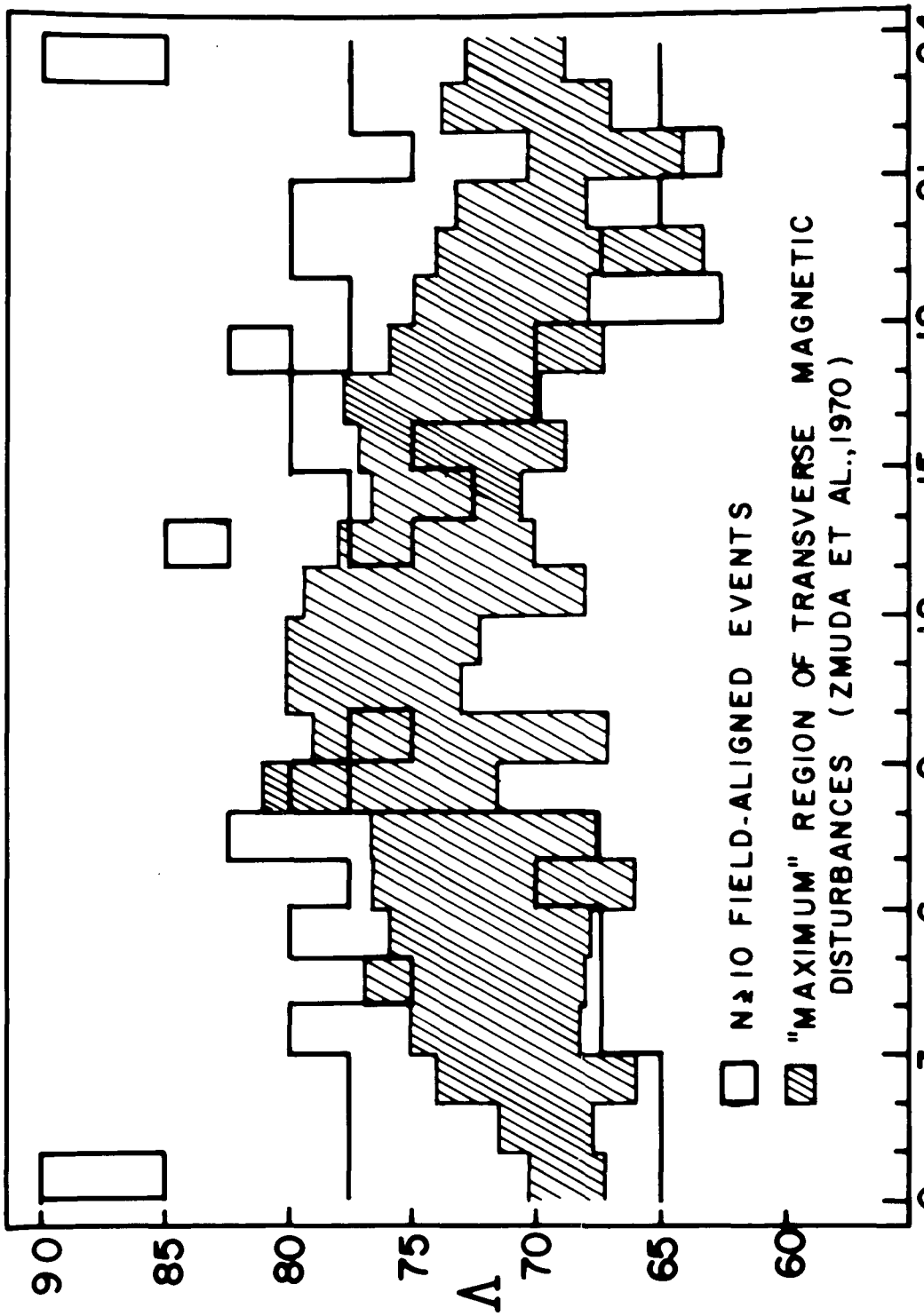

Figure 28. Comparison of the regions of observing field-aligned precipitation events with the "maximum" region of transverse magnetic disturbances (Zmuda et al., 1970).

at these local times has been shown to consist primarily of electrons with energies in the hundreds of electron volts (Hoffman and Berko, 1971b).

To estimate some properties of the currents producing the magnetic perturbations, Zmuda et al. (1970) used an infinite-sheet current approximation which required a particle flux of $0.12 - 3.5 \times 10^9$ particles/cm^2-sec. Electron fluxes of this magnitude have frequently been observed at 0.7keV in the dayside hours by the OGO-4 Auroral Particles Experiment (Hoffman and Berko, 1971a), and at lower energies by Heikkila and Winningham (1971) and Frank (1971), which implies that the (dayside) field-aligned currents of Zmuda et al. are due to particles with energies less than 2.3keV.

VIII. FIELD-ALIGNED PARTICLES AND FIELD-ALIGNED CURRENTS

The particle data from OGO-4 and other observations of particles and magnetic fields cited in Section II demonstrate that both field-aligned particles and field-aligned currents do exist. Those 2.3 keV field-aligned electrons measured by OGO-4 were found in only $\sim 2\%$ of all precipitation events, but they were concentrated in the nighttime hours, in an oval-shaped region coincident with and extending poleward of the optically defined auroral oval. Field-aligned double sheet currents were observed more than 90% of the time, primarily in the daytime hours, by Zmuda et al. (1970), also in an oval-shaped region (see e.g. Figure 28). In this section, an attempt will be made to show how the various particle and field measurements can be interpreted to form a cohesive pattern of current flow in the magnetosphere, and how they support or tend to refute several of the more prevalent theories and models involving magnetospheric currents.

The double sheet current system proposed by Armstrong and Zmuda (1970) to explain a larger (800γ), clear transverse magnetic disturbance is in good qualitative agreement with a model current system proposed by Boström (1964). Perturbations in the declination of the magnetic field observed on Heos I by Haerendel et al. (1971) have been interpreted as indicating a net earthward field-aligned current flow, in agreement with the model of Akasofu and Meng (1969).

The two basic types of magnetospheric field-aligned current systems are illustrated schematically in Figure 29. In the top portion of the figure, current flows inward and outward along field lines connecting with the auroral zone. Such currents extending over a finite longitudinal range constitute single sheet currents. Their circuits would close in the ionosphere and the magnetosphere through a path perpendicular to the field-aligned current flow. The longitudes of current flow and their paths in the magnetosphere and ionosphere are the main differences between the major proposed current systems of this type, the Boström (1968) model 1 and that of Akasofu and Meng (1969). The Boström model has all its current flow confined to the near midnight region, while the model of Akasofu and Meng has field-aligned currents flowing into the ionosphere on the dawn side and out on the dusk side, with a closing current flowing in the equatorial plane from dusk to dawn on the dayside of the earth.

The current system illustrated in the lower portion of Figure 29 is made up of two anti-parallel current sheets flowing simultaneously along field lines. These current sheets complete their circuit in the magnetosphere by radial current flow, and in the ionosphere via short north-south (Pedersen) currents. The current system has the important feature that perturbation vectors from the currents add between the sheets and cancel outside the sheets. The direction of the current flow in the sheets is the most frequent difference between different versions of this double sheet current model.

Magnetic effects of a current system similar to that of Akasofu and Meng, but which closes in a west to east direction in the nighttime equatorial plane have been calculated by Bonnevier et al. (1970). By spreading their currents over a finite

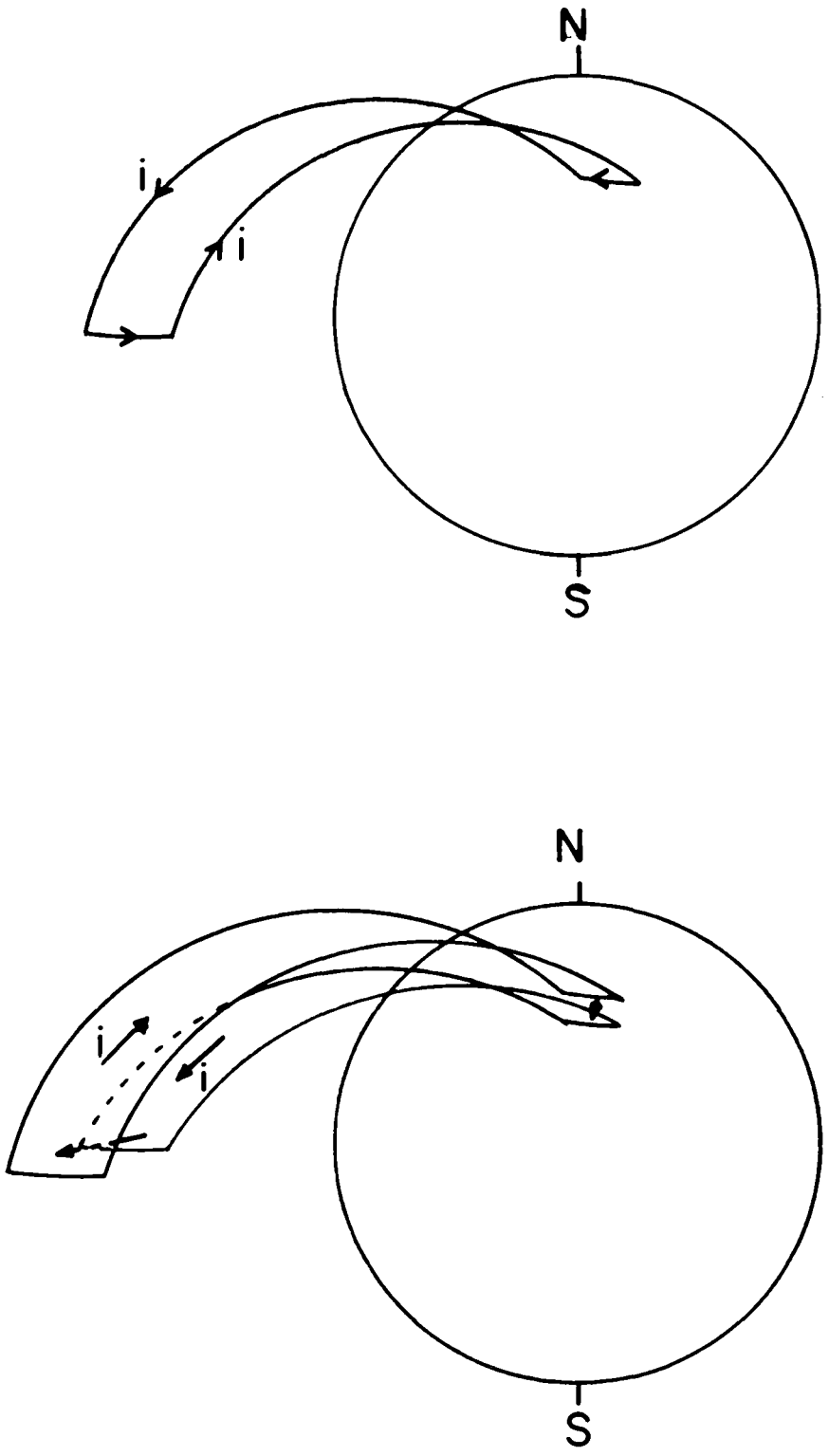

Figure 29. Representation of two models of magnetospheric field-aligned current systems: top - line current model; bottom - double sheet current system.

range of latitudes and reducing the longitudinal separation between inward and outward field-aligned currents, they obtained very good agreement with high latitude ground measurements, whereas Akasofu and Meng had good agreement only at fairly low latitudes. Further examples which confirmed the essential features of their current system and demonstrated its variability, implying a closer longitudinal placement of inward and outward currents were presented by Meng and Akasofu (1969). In discussing similar field-aligned current flow, Atkinson (1967) suggested that the outward current is associated with the westward traveling surge, and the inward flow with the eastward portion of the northward expanding auroral bulge, implying an association with the collapsing dipole field of the tail and its outward expansion into the tail.

Dayside currents similar to those reported by Armstrong and Zmuda have been detected in the outer magnetosphere by Fairfield and Ness (1972). They observed magnetic perturbations confined to a limited latitude range, as did Armstrong and Zmuda. Sheets of precipitating electrons and protons have been reported on the dayside by Frank (1971), with the protons appearing at the higher latitudes. However, measurements of even lower energy particles by Heikkila and Winningham (1971) do not confirm the existence of Frank's particle sheets at lower altitudes. Gurnett and Frank (1972) infer a field-aligned current configuration similar to Frank's from VLF observations on the Injun 5 satellite, almost identical to the current configuration observed by Cloutier et al. (1970) with rocket-borne magnetometers and particle detectors.

Various measurements, aside from the OGO-4 data discussed in this study, are seen to support some type of magnetospheric field-aligned current flow. To varying

degrees they support the existence of double sheet currents, single sheet currents, or field-aligned line current flows in the magnetosphere and ionosphere. The measured or inferred existence of double sheet currents does not preclude the possible existence of the Akosofu-Meng type currents, which are harder to detect and could be present along with double sheet currents. Measured, inferred and theoretical values of field-aligned currents are presented in Table 8.

FIELD-ALIGNED CURRENT VALUES

Author(s)	Current (A)	Current Density (A/M^2)
Akasofu and Meng (1969)[3]	10^6	
Armstrong and Zmuda (1970)[2]	6.4×10^5 /sheet	
Boström (1968)[3]	1.5×10^6 /sheet	7.5×10^{-6}
Cummings and Dessler (1967)[2]	10^5	
Haerendel et al. (1971)[2]	5×10^5	
Zmuda et al. (1970)[2]		$0.2 - 6.0 \times 10^{-6}$
Choy et al. (1971)[1]		$5 \times 10^{-6} - 5 \times 10^{-7}$
Cloutier et al. (1970)[1]		2×10^{-5}
Frank (1971)[1]		3×10^{-7}
Park and Cloutier (1971)[2]		2×10^{-5}
Vondrak et al. (1971)[1]		1.5×10^{-5} *
Whalen and McDiarmid (1972)[1]		2×10^{-4} *

*These were maximum values.

1 = measured 2 = inferred 3 = theoretical

TABLE 8

An indication of the magnitude of field-aligned currents observed by OGO-4 can be obtained from the average field-aligned spectrum shown in Figure 18. From these plotted fluxes, the average field-aligned current density in the bandpasses of the OGO-4 detectors can be calculated if we assume an average pitch angle distribution strongly peaked near 0° and azimuthal isotropy about magnetic field lines, since the particles' mean free paths are much greater than their gyroradii. The field-aligned current is calculated using:

$$J_{\parallel} = \int_{\Omega} nev_{\parallel}\, d\Omega = \int_{\Omega} j(\alpha) \sin\alpha\, d\Omega = \pi \int_{0}^{\pi/2} j(\alpha) \sin\alpha\cos\alpha\, d\alpha,$$

where n is number density, e is the electronic charge, $v_{\parallel}$ is the particles' velocity parallel to the direction of the magnetic field, Ω is the solid angle, α is the pitch angle, and j (α) is the pitch angle dependent directional current density of charged particles. One can express j (α) as a power series:

$$j(\alpha) = I_0 \sum_{n=1}^{11} C_n \alpha^{n-1},$$

where I_0 is the current density in the bandpasses of the 0° pitch angle detectors. The coefficients C_n obtained by fitting a 10th order power series to the average field-aligned pitch angle distribution shown in Figure 30 were:

$C_1 = 4.00$; $C_2 = 8.918 \times 10^{-2}$; $C_3 = -2.476 \times 10^{-2}$; $C_4 = 1.621 \times 10^{-3}$; $C_5 = -4.797 \times 10^{-5}$;

$C_6 = 2.554 \times 10^{-7}$; $C_7 = 2.398 \times 10^{-8}$; $C_8 = -7.369 \times 10^{-10}$; $C_9 = 9.754 \times 10^{-12}$;

$C_{10} = -6.359 \times 10^{-14}$; $C_{11} = 1.665 \times 10^{-16}$.

The current density I_0 was calculated using:

$$I_0 = I_{0.7} + I_{2.3} + I_{7.3} = 8.14 \times 10^{-7}\ A/m^2\text{-ster},$$

where I_E (A/m^2-ster), the current density at energy E (keV), is given by:

I_E = flux$_E$ (electrons/cm^2-sec-ster-keV) x (E x 0.3 keV) x (1.6×10^{-19} coul/electron) x (10^4 cm^2/m^2).

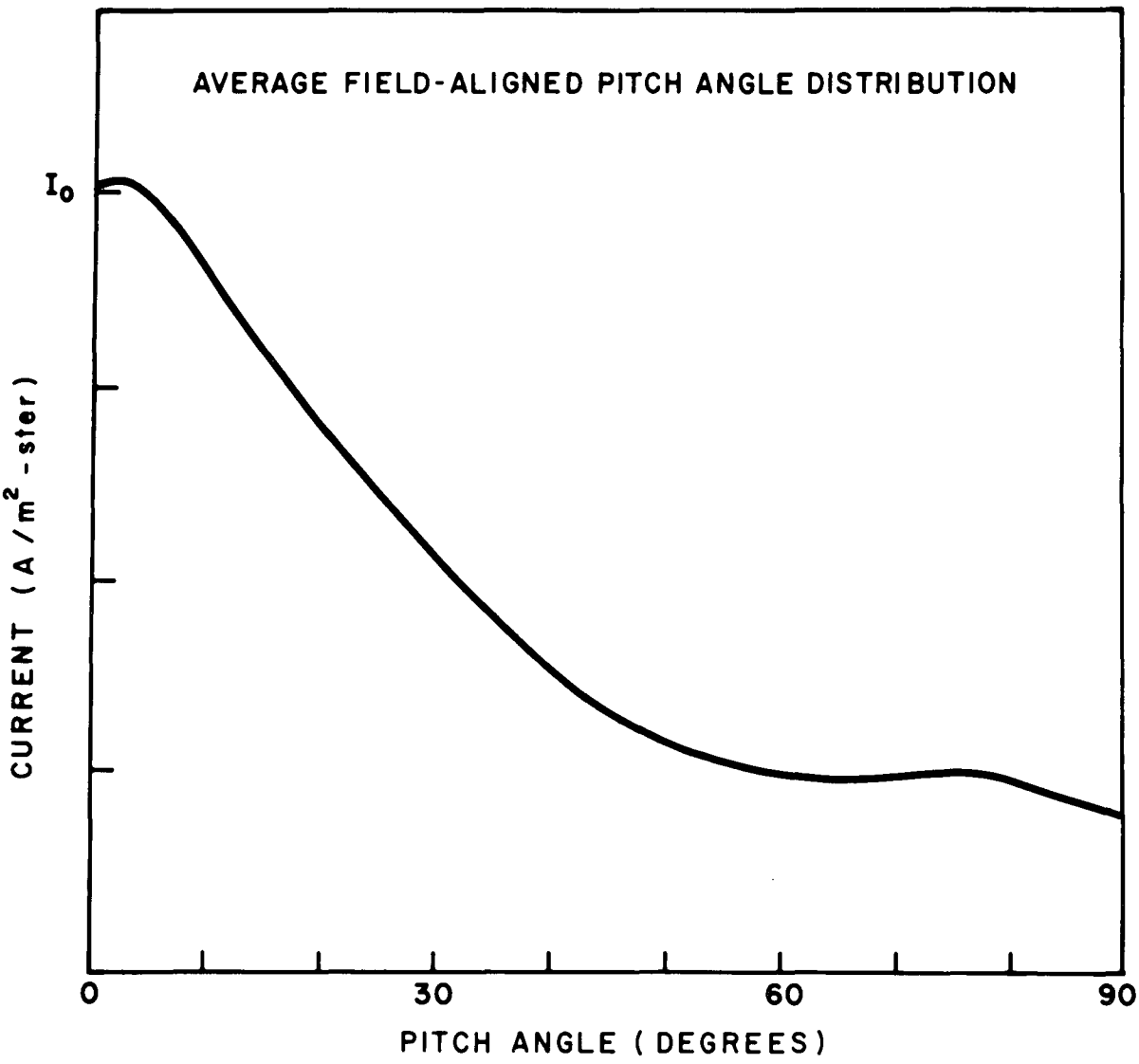

Figure 30. Average field-aligned pitch angle distribution.

Substituting these quantities and the coefficients C_n into the first equations, the field-aligned current density, $J_{\parallel}$, is found to be $J_{\parallel} = 1.03 \times 10^{-5}$ A/m^2. Note that average field-aligned pitch angle distributions and fluxes were used in the calculation, and the maximum field-aligned current density could be as much as 50% greater (1.55×10^{-5} A/m^2).

A comparison with the values listed in Table 8 indicates that this calculated average current density falls well within the range of published values. Assuming further that the field-aligned precipitation is seen by OGO-4 for an average duration of 5 seconds, and that the field-aligned current sheet at satellite altitudes has a longitudinal extent of 1000km (Boström, 1968), the field-aligned current corresponding to the above calculated current density is then 3.4×10^5 A, in excellent agreement with the values given in Table 8.

It has been shown in Sections VI and VII that the region of field-aligned 2.3keV electron precipitation generally coincides with and extends poleward of the optically defined auroral region. Additionally, it was shown that field-aligned precipitation is often associated with the high latitude, poleward portion of auroral electron precipitation. Thus, the data from the OGO-4 auroral particles experiment imply that the arrows indicating the direction of current flow (the direction a positive test charge would flow) should be reversed in the lower portion of Figure 29. Indeed, the observation of large field-aligned electron intensities at 19 hours MLT above the 45keV trapping boundary (located at $\Lambda = 69.5°$) by Ackerson and Frank (1972) on Injun 5, with simultaneous observations of precipitating protons at latitudes below the trapping boundary, tends to further support this latter current flow orientation.

As previously mentioned, field-aligned double sheet currents extend over a fairly wide region of longitude in the nightside magnetosphere. Such currents, or

more precisely one of the sheets of current, would lie poleward of the commonly accepted statistically defined auroral ovals, such as that of Feldstein (1966). Field-aligned line currents, flowing into and out of the ionosphere at local times several hours away from midnight, close in the ionosphere by flowing largely along the electrojet in the midnight hours (see for example Akasofu and Meng, 1969). The statistical distribution of field-aligned 2.3keV electron precipitation presented in this dissertation is thus generally consistent with a model field-aligned double sheet current system similar to that sketched in the lower portion of Figure 29.

It is therefore reasonable to associate the field-aligned electrons first reported by Hoffman and Evans (1968), and analyzed in this dissertation, with a field-aligned portion of the magnetospheric current system. Such a field-aligned current system would most likely be of the double sheet current type, which, with the average current densities calculated above, Armstrong and Zmuda (1970) have shown would be capable of producing magnetic disturbances of at least 800γ. Hence, a field-aligned current system consonant with the patterns and characteristics of field-aligned precipitation presented in this study would be significant, since the magnitude of the magnetic effects it is likely to produce would be certainly observed by both ground based and satellite or rocket borne magnetometers.

In addition to magnetospheric field-aligned current systems, parallel electric fields not far above the altitude of the satellite must also be considered. Magnetic field lines penetrating into the low density winter upper ionosphere cannot carry unlimited parallel currents. Kindel and Kennel (1971) have shown that under these ionospheric density conditions, and with fairly high particle fluxes comparable to those typically measured during bursts of field-aligned particles, electrostatic-wave

instabilities will be generated in the topside ionosphere, at sunlight-dependent altitudes. The non-linear saturation of current driven instabilities leads to an 'anomalous' parallel resistance, and thus to the development of (localized) parallel electric fields.

The increased probability of observing high altitude field-aligned electrons during the winter months argues in support of the Kindel and Kennel theory of localized parallel electric fields in the ionosphere as a mechanism for producing field-aligned particle precipitation. Since this mechanism is seasonally dependent, while magnetospheric current systems are independent of seasonal variations, it seems reasonable to conclude that field-aligned electron precipitation is associated with both magnetospheric current systems and fairly localized parallel electric fields.

IX. SUMMARY AND CONCLUSIONS

Sixteen months of data collected by the OGO-4 Auroral Particles Experiment have been surveyed for the presence of field-aligned 2.3keV electron precipitation. This type of precipitation was found in about 2% of all the high latitude electron data. It was determined that field-aligned 2.3keV electron precipitation at high latitudes is found to occur in a roughly oval-shaped region, with the greatest number of field-aligned events observed at about 70° invariant latitude near local midnight.

Field-aligned 2.3keV electron precipitation is characterized by electron energy spectrums which are harder and considerably more intense than energy spectrums of typical isotropic precipitation. The anisotropies in pitch-angle are found to occur preferentially when fluxes of 0° pitch-angle 2.3keV electrons, and to a lesser extent 0.7keV electrons, are high. Magnetically disturbed conditions are found to coincide with the occurrence of pitch angle anisotropies, which were also observed to appear in association with the post-breakup phases of magnetospheric substorms. Field-aligned precipitation appeared considerably more frequently during the winter months than during the summer months, and more often at higher altitudes than at lower altitudes.

In the nighttime hours, the region of field-aligned electron precipitation generally coincides with and extends poleward of the optically defined auroral region.

It was found that field-aligned precipitation occurred at or near the high latitude boundary of auroral precipitation in these hours. A comparison between the regions where field-aligned precipitation was observed and the location of 200kHz auroral hiss centers revealed that both phenomena are observed in similar high latitude locations. Another comparison with the regions of "maximum" transverse disturbance showed similar features in the distributions, notably a tendency for both to occur at higher latitudes in the dayside than in the nightside hours.

The magnitudes of field-aligned currents calculated from average field-aligned particle fluxes, and the agreement with other calculated, measured, and postulated field-aligned currents indicate that the field-aligned electrons observed by OGO-4 are manifestations of a magnetospheric current system. This field-aligned current system is most likely to be of the double sheet current type, but may also contain single sheet currents or line currents. Localized parallel electric field acceleration also plays a major role in producing the observed field-aligned particles.

Field-aligned precipitation as seen by OGO-4 appears as a generally short-time-duration phenomenon, seldom appearing continuously for more than 5 to 10 seconds in the satellite data. Whether this is really a temporal effect (Hoffman and Evans, 1968; Chase, 1970; O'Brien and Reasoner, 1971), or a spatial effect (Eather and Akasofu, 1969; Cloutier et al., 1970; Choy et al., 1971; Whalen and McDiarmid, 1972), or some combination of spatial and time varying effects (D. S. Evans, private communication, 1972), cannot easily be determined using data obtained from a satellite moving at ~ 7.5km/sec. Determination of the mechanism responsible for field-aligned auroral zone precipitation is strongly dependent on whether spatial or temporal processes are dominant.

APPENDIX A

The reasons for considering an event to be field-aligned only if the 0° - 2.3 keV flux exceeded $\sim 2 \times 10^7$ electrons/cm^2-sec-ster-keV and the ratio of 0° to 60° 2.3 keV flux was greater than or equal to 2.0 are as follows. Fluxes less than 2×10^7 represented as few as 7 counts per second (N). At this counting rate, the statistical uncertainty ($\sqrt{N}/N$) is 38%, and equal 0° and 60° counting rates of 7 counts per second would then yield a combined uncertainty of ±53% in the ratio, giving a 0° to 60° flux ratio of 1.0 ±0.53. Therefore, choosing ratios greater than or equal to 2.0 insures that only statistically significant field-aligned events were included in the distribution for all fluxes greater than $\sim 2 \times 10^7$.

REFERENCES

Ackerson, K. L., and L. A. Frank, Correlated satellite measurements of low-energy electron precipitation and ground-based observations of a visible auroral arc, J. Geophys. Res., 77, 1128-1136, 1972.

Akasofu, S. -I., and C. -I. Meng, A study of polar magnetic substorms, J. Geophys. Res., 74, 293-313, 1969.

Albert, R. D., and P. J. Lindstrom, Auroral-particle precipitation and trapping caused by electrostatic double layers in the ionosphere, Science, 170, 1398-1401, 1970.

Alfvén, H., A theory of magnetic storms and aurorae, 2 and 3, Kungl. Sv. Vetenskapskad. Hundl., 18, 1, 1940.

Armstrong, J. C., and A. J. Zmuda, Field-aligned current at 1100km in the auroral region measured by satellite, J. Geophys. Res., 75, 7122-7127, 1970.

Atkinson, G., The current system of geomagnetic bays, J. Geophys. Res., 72, 6063-6067, 1967.

Axford, W. I., and C. O. Hines, A unifying theory of high latitude geophysical phenomena and geomagnetic storms, Can. J. Physics, 39, 1433-1464, 1961.

Birkeland, K., Norwegian aurora polaris expedition, 1902-3, Part I, H. Aschehong and Co., Christiania, 1908.

Bonnevier, B., R. Boström, and G. Rostoker, A three-dimensional model current system for polar magnetic substorms, J. Geophys. Res., 75, 107-122, 1970.

Boström, R., A model of the auroral electrojet, J. Geophys. Res., 69, 4983-4999, 1964.

Boström, R., Currents in the ionosphere and magnetosphere, Ann. Geophys., 24, 681-694, 1968.

Burch, J. L., Low-energy electron fluxes at latitudes above the auroral zone, J. Geophys. Res., 73, 3585-3590, 1968.

Burch, J. L., Effects of interplanetary magnetic field azimuth on auroral zone and polar cap magnetic activity, submitted to J. Geophys. Res., 1972a.

Burch, J. L., Precipitation of low-energy electrons at high latitudes: Effects of substorms, interplanetary magnetic field and dipole tilt angle, submitted to J. Geophys. Res., 1972b.

Carlqvist, P., and R. Boström, Space charge regions above the aurora, J. Geophys. Res., 75, 7140-7146, 1970.

Chamberlain, J. W., Theory of auroral bombardment, Astrophys. J., 134, 401-424, 1961.

Chamberlain, J. W., Electric acceleration of auroral particles, Rev. Geophys., 7, 461-482, 1969.

Chase, L. M., Evidence that the plasma sheet is the source of auroral electrons, J. Geophys. Res., 74, 348-350, 1969.

Chase, L. M., Energy spectra of auroral zone particles, J. Geophys. Res., 75, 7128-7139, 1970.

Choy, L. W., R. L. Arnoldy, W. Potter, P. Kintner, and L. J. Cahill, Jr., Field-aligned particle currents near an auroral arc, J. Geophys. Res., 76, 8279-8298, 1971.

Cloutier, P. A., H. R. Anderson, R. J. Park, R. R. Vondrak, R. J. Spiger, and B. R. Sandel, Detection of geomagnetically aligned currents associated with an auroral arc, J. Geophys. Res., 75, 2595-2600, 1970.

Coroniti, F. V., and C. F. Kennel, Polarization of the auroral electrojet, J. Geophys. Res., 77, 2835-2850, 1972.

Cummings, W. D., and A. J. Dessler, Field aligned currents in the magnetosphere, J. Geophys. Res., 72, 1007-1013, 1967.

Davis, T. N., and M. Sugiura, Auroral electrojet activity index AE and its universal time variations, J. Geophys. Res., 71, 785-802, 1966.

Eather, R. H., and S. -I. Akasofu, Characteristics of polar-cap auroras, J. Geophys. Res., 74, 4794-4798, 1969.

Evans, D. S., Low-energy charged-particle detection using the continuous-channel electron multiplier, Rev. Sci. Instr., 36, 375-382, 1965.

Fairfield, D. H., and N. F. Ness, Imp 5 magnetic-field measurements in the high-latitude outer magnetosphere near the noon meridian, J. Geophys. Res., 77, 611-623, 1972.

Feldstein, Y.I., Peculiarities in the auroral distribution and magnetic disturbance distribution in high latitudes caused by the asymmetrical form of the magnetosphere, Planet. Space Sci., 14, 121-130, 1966.

Fermi, E., Nuclear Physics, p. 37, University of Chicago Press, Chicago, 1950.

Frank, L. A., Plasma in the earth's polar magnetosphere, J. Geophys. Res., 76, 5202-5219, 1971.

Frank, L. A., and K. L. Ackerson, Observation of charged particle precipitation into the auroral zone, J. Geophys. Res., 76, 3612-3643, 1971.

Gurnett, D. A., and L. A. Frank, VLF Hiss and related plasma observations in the polar magnetosphere, J. Geophys. Res., 77, 172-190, 1972.

Haerendel, G., P. C. Hedgecock, and S. -I. Akasofu, Evidence for magnetic field aligned currents during the substorms of March 18, 1969, J. Geophys. Res., 76, 2382-2395, 1971.

Hanson, W. B., Structure of the ionosphere, in Satellite Environment Handbook, ed. F. S. Johnson, pp. 40-47, Stanford University Press, Stanford, Cal., 1965.

Heikkila, W. J., and J. D. Winningham, Penetration of magnetosheath plasma to low altitudes through the dayside magnetospheric cusps, J. Geophys. Res., 76, 883-891, 1971.

Hoffman, R. A., Low-energy electron precipitation at high latitudes, J. Geophys. Res., 74, 2425-2432, 1969.

Hoffman, R. A., Electron precipitation patterns and substorm morphology, EOS, Trans. AGU, 53, 360, 1972.

Hoffman, R. A., and F. W. Berko, Primary electron influx to dayside auroral oval, J. Geophys. Res., 76, 2967-2976, 1971a.

Hoffman, R. A., and F. W. Berko, On the dual nature of the auroral oval, EOS, Trans. AGU, 52, 325, 1971b.

Hoffman, R. A., and D. S. Evans, OGO-4 auroral particles experiment and calibrations, preprint X-611-67-632, GSFC, Greenbelt, Md., 1967.

Hoffman, R. A., and D. S. Evans, Field-aligned electron bursts at high latitudes observed by OGO 4, J. Geophys. Res., 73, 6201-6214, 1968.

Hoffman, R. A., and T. Laaspere, Comparison of Very-Low-Frequency auroral hiss with precipitating low-energy electrons by the use of simultaneous data from two OGO-4 experiments, J. Geophys. Res., 77, 640-650, 1972.

Kern, J. W., A charge separation mechanism for the production of polar auroras and electrojets, J. Geophys. Res., 67, 2649-2665, 1962.

Kindel, J. M., and C. F. Kennel, Topside current instabilities, J. Geophys. Res., 76, 3055-3078, 1971.

Laaspere, T., W. C. Johnson, and L. C. Semprebon, Observations of auroral hiss, LHR noise, and other phenomena in the frequency range 20 Hz - 540 kHz on OGO 6, J. Geophys. Res., 76, 4477-4493, 1971.

Lassen, K., Polar cap emissions, in Atmospheric Emissions, ed. B. M. McCormac and A. Omholt, p. 63, Van Nostrand Reinhold Co., New York, 1969.

Meng, C. -I., and S. -I. Akasofu, A study of polar magnetic substorms, 2. Three dimensional current system, J. Geophys. Res., 74, 4035-4053, 1969.

Mozer, F. S., and U. V. Fahleson, Parallel and perpendicular electric fields in an aurora, Planet. Space Sci., 18, 1563-1571, 1970.

O'Brien, B. J., Considerations that the source of energetic auroral particles is not a parallel electrostatic field, Planet. Space Sci., 18, 1821-1827, 1970.

O'Brien, B. J., and D. L. Reasoner, Measurements of highly collimated short-duration bursts of auroral electrons and comparison with existing auroral models, J. Geophys. Res., 76, 8258-8278, 1971.

Park, R. J., and P. A. Cloutier, Rocket-based magnetometer measurements of birkeland currents related to an auroral arc and electrojet, J. Geophys. Res., 76, 7714-7733, 1971.

Perkins, F. W., Plasma wave instabilities in the ionosphere over the aurora, J. Geophys. Res., 73, 6631-6648, 1968.

Reasoner, D. L., R. H. Eather, and B. J. O'Brien, Detection of alpha particles in auroral phenomena, J. Geophys. Res., 73, 4185-4198, 1968.

Roederer, J. G., On the adiabatic motion of energetic particles in a model magnetosphere, J. Geophys. Res., 72, 981-992, 1967.

Sandford, B. P., Aurora and airglow intensity variations with time and magnetic activity at southern high latitudes, J. Atmos. Terr. Phys., 26, 749, 1964.

Sandford, B. P., Variations of auroral emissions with time, magnetic activity, and the solar cycle, J. Atmos. Terr. Phys., 30, 1921, 1968.

Schield, M. A., J. W. Freeman, and A. J. Dessler, A source of field aligned currents at auroral latitudes, J. Geophys. Res., 74, 247-256, 1969.

Stringer, W. J., and A. E. Belon, The morphology of the IQSY auroral oval, 1, Interpretation of isoauroral diagrams, J. Geophys. Res., 72, 4415-4422, 1967.

Taylor, H. A., Jr., J. M. Grebowsky, and W. J. Walsh, Structured variations of the plasmapause: Evidence of a corotating plasma tail, J. Geophys. Res., 76, 6806-6814, 1971.

Vasyliunas, V. M., A study of low-energy electrons in the evening sector of the magnetosphere with OGO 1 and OGO 3, J. Geophys. Res., 73, 2839-2884, 1968.

Vondrak, R. R., H. R. Anderson, and R. J. Spiger, Rocket-based measurement of particle fluxes and currents in an auroral arc, J. Geophys. Res., 76, 7701-7713, 1971.

Whalen, B. A., and I. B. McDiarmid, Observations of magnetic-field-aligned auroral-electron precipitation, J. Geophys. Res., 77, 191-202, 1972.

Zmuda, A. J., J. H. Martin, and F. T. Heuring, Transverse magnetic disturbances at 1100 kilometers in the auroral regions, J. Geophys. Res., 71, 5033-5054, 1966.

Zmuda, A. J., F. T. Heuring, and J. H. Martin, Dayside magnetic disturbances at 1100km in the auroral oval, J. Geophys. Res., 72, 1115-1117, 1967.

Zmuda, A. J., J. C. Armstrong, and F. T. Heuring, Characteristics of transverse magnetic disturbances observed at 1100 kilometers in the auroral oval, J. Geophys. Res., 75, 4757-4762, 1970.

* U.S. GOVERNMENT PRINTING OFFICE: 1972—735-962/143

NASA—GSFC